A DISSERTATION FOR THE DEGREE OF DOCTOR OF PHILOSOPHY

Identification and Characterization of Two Immune Receptors Required for the Recognition of *Ralstonia pseudosolanacearum* Effectors in *Nicotiana benthamiana*

풋마름병균의 이펙터 단백질을 인식하는 *Nicotiana benthamiana*의 면역수용체 발굴 및 활성화 기작 구명

AUGUST, 2023

BOYOUNG KIM

MAJOR IN HORTICULTURAL SCIENCE AND BIOTECHNOLOGY

DEPARTMENT OF AGRICULTURE, FORESTRY AND BIORESOURCES

COLLEGE OF AGRICULTURE AND LIFE SCIENCES

THE GRADUATE SCHOOL OF SEOUL NATIONAL UNIVERSITY

Identification and Characterization of Two Immune Receptors Required for the Recognition of *Ralstonia pseudosolanacearum* Effectors in *Nicotiana benthamiana*

UNDER THE DIRECTION OF DR. CECILE SEGONZAC
SUBMITTED TO THE FACULTY OF THE GRADUATE SCHOOL OF SEOUL NATIONAL UNIVERSITY

BY
BOYOUNG KIM

MAJOR IN HORTICULTURAL SCIENCE AND BIOTECHNOLOGY
DEPARTMENT OF AGRICULTURE, FORESTRY AND BIORESOURCES

AUGUST, 2023

APPROVED AS A QUALIFIED DISSERTATION OF BOYOUNG KIM
FOR THE DEGREE OF DOCTOR OF PHILOSOPHY
BY THE COMMITTEE MEMBERS

CHAIRMAN	**Doil Choi, Ph.D.**
VICE-CHAIRMAN	**Cécile Segonzac, Ph.D.**
MEMBER	**Byoung-Cheorl Kang, Ph.D.**
MEMBER	**Chang-Sik Oh, Ph.D.**
MEMBER	**Eui-Hwan Chung, Ph.D.**

Identification and Characterization of Two Immune Receptors Required for the Recognition of *Ralstonia pseudosolanacearum* Effectors in *Nicotiana benthamiana*

BOYOUNG KIM

Department of Agricultural, Forestry and Bioresources

The Graduate School of Seoul National University

ABSTRACT

Bacterial wilt caused by *Ralstonia pseudosolanacearum* (*Rps*) has a severe impact on numerous crop species, particularly economically valuable Solanaceae crops. Although several resistance genes have been discovered in plants, developing crop varieties with durable resistance against *Rps* is still a challenge due to the pathogen genetic diversity. To achieve durable resistance, stacking multiple resistances from diverse germplasm is required. *Rps* delivers a large repertoire of effector proteins into host cells to promote infection, some of which are recognized by intracellular nucleotide-binding leucine-rich repeat receptors (NLRs) that activate plant defense responses culminating in the hypersensitive response (HR), a form of programmed

cell death. The solanaceous model plant *Nicotiana benthamiana* is suitable for identifying resistance genes coding NLRs due to its amenability for functional genetic studies as well as availability of genome-wide annotated NLR genes. Here, an integrative approach that combines multiple gene-silencing and transient expression assay was used to identify new NLRs that mediate immune responses against *Rps*.

In chapter 1, 39 *Rps* effectors from multiple Korean *Rps* isolates were cloned and transiently expressed in the leaves of *N. benthamiana* and *N. tabacum*. Multiple *Rps* effectors induced NLR-associated cell death in *N. benthamiana*. Notably, RipE1 and RipY induced effector-triggered immunity (ETI) responses upon the recognition by *N. benthamiana* immune system. In addition, genetic components involved in immune signaling were not required for both RipE1 and RipY-induced cell death. Using reverse-genetic approach, hundreds of NLRs were systematically screened. We identified the *N. benthamiana* homolog of PSEUDOMONAS TOMATO RACE 1 (NbPtr1) and RESISTANCE TO RALSTONIA SOLANACEARUM RIPY (RRS-Y) that recognize RipE1 and RipY, respectively, in *N. benthamiana*.

In chapter 2, a series of genetic complementation assays demonstrated the genetic requirement of NbPtr1 for RipE1 recognition in *N. benthamiana*. NbPtr1-mediated immunity restricted pathogenic *Rps* strain growth in *N. benthamiana* in the presence of RipE1, indicating that NbPtr1 contributes to resistance against *Rps*. Furthermore, the association of RipE1 on the plasma membrane was required for the recognition by NbPtr1. The activation of NbPtr1 is initiated by the proteolytic

activity of *Pseudomonas syringae* effector AvrRpt2 on the plasma membrane protein RIN4. In accordance, RIN4 proteins from different plants were degraded in the presence of RipE1 *in planta*. These findings suggest that NbPtr1 recognizes RipE1 at the plasma membrane by monitoring the degradation of RIN4 proteins by RipE1 in *N. benthamiana*.

In chapter 3, RRS-Y was shown to be genetically required for the recognition of RipY in *N. benthamiana*. In addition, we demonstrated that RRS-Y was a functional NLR that recognizes RipY and mediates immunity to *Rps* in *N. benthamiana*. RRS-Y and RipY are both localized at the plasma membrane *in planta*. Coiled-coil domain of RRS-Y plays an important role in mediating the association of RRS-Y with plasma membrane, which is critical for immune signaling. Moreover, RRS-Y has ability to form the self-association in plant cells in a RipY-independent manner. It is noteworthy that RRS-Y can recognize polymorphic RipY alleles across different *Ralstonia* species, and that the C-terminus of RipY is crucial for RRS-Y recognition. Therefore, the RRS-Y/RipY system provides a novel framework for exploring the underlying molecular mechanism of NLR activation in plants.

Altogether, this work has led to the identification of two immune receptors contributing to resistance against *Rps* in the model *N. benthamiana*, thus expanding the pool of available genetic resources to improve crop protection against bacterial wilt disease. Furthermore, this work provides solid basis for the elucidation of the activation mechanisms of coiled-coil NLR in plants.

Key words: Bacterial wilt disease, *Ralstonia pseudosolanacearum*, type III effectors (T3Es), disease resistance, nucleotide-binding leucine-rich repeat receptors (NLRs), *Nicotiana benthamiana*

Student number: 2018-31228

CONTENTS

LIST OF TABLES

CHAPTER 1

CHAPTER 2

CHAPTER 3

LIST OF FIGURES

CHAPTER 1

CHAPTER 2

CHAPTER 3

LIST OF ABBREVIATIONS

ADR1	ACTIVATED DISEASE RESISTANCE 1
ANK	Ankyrin
CAPS	Cleaved amplified polymorphic sequence
Cas9	CRISPR-associated protein 9
CC	Coiled-coil
CHD	Cysteine-histidine-aspartate
CNL	Coiled-coil NLR
CRISPR	Clustered regularly interspaced short palindromic repeats
DAMPs	Damage-associated molecular patterns
EDS1	ENHANCED DISEASE SUSCEPTIBILITY 1
EF1α	*ELONGATION FACTOR-1 α*
ETI	Effector-triggered immunity
FLS2	FLAGELLIN SENSING 2
GLPL	Glycine-leucine-proline-leucine
HAMPs	Herbivore-associated molecular patterns
HIN1	*HARPIN-INDUCED 1*
Hop	Hrp-dependent outer protein
HR	Hypersensitive response
Hsr203J	*HYPERSENSITIVE-RELATED203J*
InDel	Insertion and deletion
JA	Jasmonic acid
JAZ	JASMONATE ZIM DOMAIN
LRR	Leucine-rich repeat
MAMPs	Microbe-associated molecular patterns
MAPK	Mitogen-activated protein kinase

MHD	Methionine-histidine-aspartate
MLA1	MILDEW RESISTANCE LOCUS A 1
NB-ARC	Nucleotide-binding adaptor shared by APAF-1, R proteins, and CED-4
$NbPtr1^{syn}$	Synthetic NbPtr1
NLR	Nucleotide-binding leucine-rich repeat receptor
NRC	NB-LRR REQUIRED FOR HR-ASSOCIATED CELL DEATH
PAMPs	Pathogen-associated molecular patterns
PEPC	Phosphoenolpyruvate carboxylase
P-loop	Phosphate-binding loop
Pst	*Pseudomonas syringae* pv. *tomato* DC3000
PTI	Pattern-triggered immunity
Pto	RESISTANCE TO PSEUDOMONAS SYRINGAE PV. TOMATO
Ptr1	PSEUDOMONAS TOMATO RACE 1
QY	Quantum yield
R protein	Resistance protein
RACE	Rapid amplification of cDNA ends
RIN4	RPM1-INTERACTING PROTEIN 4
Rips	*Ralstonia*-injected proteins
RLCK	Receptor-like cytoplasmic kinase
RLK	Receptor-like kinase
RLP	Receptor-like protein
RNAi	RNA interference
RNL	RPW8-like NLR
Roq1	RECOGNITION OF XOPQ 1
ROS	Reactive oxygen species
Rpi-blb2	Resistance to *Phytophthora infestans* from *Solanum bulbocastanum*

RPM1	PSEUDOMONAS SYRINGAE PV. MACULICOLA 1
Rps	*Ralstonia pseudosolanacearum*
RPS4	RESISTANCE TO PSEUDOMONAS SYRINGAE 4
RPS5	RESISTANCE TO PSEUDOMONAS SYRINGAE 5
RPW8	RESISTANCE TO POWDERY MILDEW 8
RRS1	RESISTANCE TO RALSTONIA SOLANACEARUM 1
RRS-Y	RESISTANCE TO RALSTONIA SOLANACEARUM RIPY
RRS-Y^{syn}	Synthetic RRS-Y
RSSC	*Ralstonia solanacearum* species complex
sgRNA	Single guide RNA
SGT1	SUPPRESSOR OF THE G2 ALLELE OF SKP1
SNP	Single nucleotide polymorphisms
Sr50	STEM RUST RESISTANCE 50
T3E	Type III effector
T3SS	Type III secretion system
TIR	Toll/Interleukin-1 receptor/Resistance
TNL	TIR-NLR
TRV	Tobacco rattle virus
v-cADPR	Variant-cyclic-ADP-ribose
VIGS	Virus-induced gene silencing
WT	Wild type
Xop	*Xanthomonas* outer protein
ZAR1	HOPZ-ACTIVATED RESISTANCE 1

GENERAL INTRODUCTION

Disease outbreaks and importance of resistance in plant

Plant crop diseases pose a significant threat to food security. Estimated crop yield losses ranges from 11 % to 30 % in important crops (Oerke, 2006; Savary et al., 2019). Contributing factors, including shifts in biogeography response to climate change, intensive monocultures, and the emergence of new pathogens, accelerate the outbreaks and epidemics in agriculture (Corredor-Moreno and Saunders, 2020). To manage plant pathogens, an integrated approach that combines cultural controls, chemical treatment, and breeding resistant crops is necessary (van Esse et al., 2020). Although chemical pesticides are widely used, caution must be taken due to their potential side effects, such as toxicity to other organisms in the environment and loss of effectiveness from emergence of pathogen resistance. Host plant resistance is generally considered the most favorable control method for environmental, economic, and social reasons (Mundt, 2014). However, a challenge arises in that resistance conferred by a single gene can be only effective in the short term, as new pathogen strains evolve to overcome it (Nelson et al., 2018; Schultink and Steinbrenner, 2021). Therefore, it is necessary to stack multiple resistances from diverse germplasms to achieve durable resistance (Schultink and Steinbrenner, 2021; Kim et al., 2022).

Plant immune system

Multicellular organisms have immune systems to defend against diverse pathogens. While animals have both adaptive and innate immunity, plants rely solely on innate immunity. Nevertheless, most plants resist to diverse pathogens, including fungi, oomycetes, viruses, bacteria, herbivores, and parasitic plants. Plant immune receptors detect the pathogen and trigger immune response. Conversely, in order to cause disease, pathogens must avoid the detection by the plant and/or suppress immune responses. Cell-surface pattern recognition receptors (PRRs) detect the pathogen-/microbe-/damage-/herbivore-associated molecular patterns (PAMPs/MAMPs/DAMPs/HAMPs) and activate pattern-triggered immunity (PTI), which restricts pathogen growth (Boutrot and Zipfel, 2017). Pathogens have evolved virulence molecules known as effectors that suppress PTI or modify host physiological responses. In plants, some effectors are directly or indirectly recognized by intracellular nucleotide-binding leucine-rich repeat receptors (NLRs), resulting in effector-triggered immunity (ETI) that includes the hypersensitive response (HR), a type of programmed cell death (Ngou et al., 2022). Under natural selection, pathogens may evolve to evade ETI by losing, diversifying, or acquiring effectors that suppress ETI. These interactions between the plant immune system and pathogens are described by the "zig-zag" model (Jones and Dangl, 2006).

Pattern-triggered immunity

PRRs are either receptor-like kinase (RLKs) or receptor-like protein (RLPs). RLKs consist of an extracellular domain, a transmembrane domain, and an intracellular

kinase domain, but RLPs lack cytoplasmic kinase domain (Boutrot and Zipfel, 2017). PRRs typically recognize pathogen derived non-self (PAMPs/MAMPs/HAMPs, hereafter referred to as PAMPs) or self-molecules (DAMPs) via their extracellular domains. PAMPs are highly conserved molecules within pathogen species, such as flagellin, peptidoglycans from bacteria, or chitin from fungi. The perception of PAMPs by PRRs induces heterodimeric complex between PRRs and their co-receptors to activate downstream immune signals. This phosphorylates multiple receptor-like cytoplasmic kinases (RLCKs) and mitogen-activated protein kinases (MAPKs). The phosphorylation cascades induce cytosolic calcium influx, burst of reactive oxygen species (ROS) production, and transcriptional reprogramming, resulting in biosynthesis of antimicrobial compounds and callose deposition (Boutrot and Zipfel, 2017; Ngou et al., 2022).

Effector-triggered immunity

NLRs are classified into three subgroups depending on their N-terminal domains: Toll/Interleukin-1 receptor/Resistance (TIR) NLRs (TNLs), coiled-coil (CC) NLRs (CNLs), and Resistance to Powedery mildew 8-like CC (RPW8) NLRs (RNLs) (Jones et al., 2016). NLRs contain a central nucleotide-binding adaptor shared by APAF-1, R proteins, and CED-4 (NB-ARC, hereafter NB) domain, and a C-terminal leucine-rich repeat (LRR) domain. The NB domain functions as a molecular switch that regulates NLR activation by binding ATP and ATP hydrolysis (Wang et al., 2019). The function of each domain in NLRs varies depending on NLRs. The LRR

domain is typically associated with the recognition of effectors (Krasileva et al., 2010; Ma et al., 2020; Martin et al., 2020). The TIR, CC, and RPW8 domains serve as signaling domains that initiate downstream defense responses (Adachi et al., 2019; Duxbury et al., 2021; Bi et al., 2021; Jacob et al., 2021). Upon activation, most TNLs form oligomeric complexes that allow the association of TIR domains, which has NADase activity and produces variant-cyclic-ADP-ribose (v-cADPR) considered as signaling molecule for downstream responses (Ma et al., 2020; Martin et al., 2020). The oligomerization of CNLs/RNLs results in the formation of CC/RPW8 domains into a funnel-shaped structure at the plasma membrane that acts as a calcium channel, leading to cytosolic calcium influx to induce cell death (Wang et al., 2019; Bi et al., 2021; Jacob et al., 2021; Ahn et al., 2023; Contreras et al., 2023).

NLR network in plant immunity

Plants carry diverse repertoires of NLRs that are interconnected in the complex networks (Wu et al., 2018). NLRs detect pathogen effectors either by direct physical interaction or by indirectly monitoring the modification of host proteins (guardee/decoy) targeted by effectors (Kourelis and van der Hoorn, 2018). Some NLRs function as pairs that a sensor NLR detects effector, while a helper NLR activates immune response at the downstream of sensor NLRs. Two NLRs in pair are genetically linked and transcript levels are controlled under same promoter. For example, two TNLs RESISTANCE TO RALSTONIA SOLANACEARUM 1 (RRS1) and RESISTANCE TO PSEUDOMONAS SYRINGAE 4 (RPS4) from

Arabidopsis are paired to translate the signaling (Gao et al., 2021). RRS1 senses two unrelated effectors AvrRps4 from *Pseudomonas syringae* and RipP2 (formerly, PopP2) from *Ralstonia pseudosolanacearum* via an integrated WRKY transcription factor domain that mimics the host targets of effectors and activates immune responses, while RPS4 functions to translate immune signaling upon effector recognition (Narusaka et al., 2009; Le Roux et al., 2015; Sarris et al., 2015). Multiple sensor NLRs form the complex network with multiple helper NLRs in plant immunity. In Solanaceae, a distinct phylogenetic clade of CNLs NB-LRR REQUIRED FOR HR-ASSOCIATED CELL DEATH (NRC) proteins (NRCs) functions as a helper NLR for multiple sensor NLRs to translate signals (Wu et al., 2017). Solanaceae sensor NLRs, such as Rx from potato, Rpi-blb2 from potato, and Prf from tomato, require NRC network to confer resistance to a virus Potato Virus X, an oomycete *Phytophthora infestans*, and a *Pseudomonas syringae*, respectively (Wu et al., 2017). Most TNLs or some CNLs associate with the helper RNLs ACTIVATED DISEASE RESISTANCE 1 (ADR1s) and N REQUIREMENT GENE 1 (NRG1s) in *Arabidopsis* (Bonardi et al., 2011; Castel et al., 2019; Saile et al., 2020). Following the activation of TNLs, the lipase-like proteins, such as ENHANCED DISEASE SUSCEPTIBILITY 1 (EDS1), associate with RNLs to mediate HR and resistance (Parker et al., 1996; Dongus and Parker, 2021). Conversely, some NLRs can function both sensor and helper and are called a singleton (Adachi et al., 2019a). For example, Arabidopsis CNL HOPZ-ACTIVATED RESISTANCE 1 (ZAR1) perceives the modification of receptor-like cytoplasmic kinases by multiple effectors

and forms pentamers called resistosome (Wang et al., 2019). The ZAR1-resistosome acts as a calcium channel at the plasma membrane to initiate HR (Bi et al., 2021). Both TNL-and CNL-dependent signaling require the SUPPRESSOR OF THE G2 ALLELE OF SKP1 (SGT1), which is a component of molecular chaperone contributing to NLR protein stability with HEAT SHOCK PROTEIN 90 (HSP90) and REQUIRED FOR MLA12 RESISTANCE 1 (RAR1) (Azevedo et al., 2002; Peart et al., 2002; Shirasu, 2009).

Bacterial wilt disease

Ralstonia species are Gram-negative and soil-borne pathogens causing bacterial wilt disease of over 250 hosts (Hayward, 1991; Mansfield et al., 2012). This bacterium colonizes xylem vessels through natural openings or wounds of roots. Rapid proliferation and biofilm production block water flow, leading to wilting and cell death (Genin and Denny, 2012; Lowe-Power et al., 2018). The disease outbreaks caused by *Ralstonia* species have economic impact on important crops, including banana, potato, tomato, and pepper (Hayward, 1991; Mansfield et al., 2012). These bacteria form a heterogeneous group referred to as "*Ralstonia solanacearum* species complex (RSSC)" that were commonly classified into four phylotypes reflecting geographical origins (Fegan and Prior, 2005). Phylotype I is present in Asia, phylotype IIA and IIB in America, phylotype III in Africa, and phylotype IV in Indonesia, Australia, and Japan (Fegan and Prior, 2005). Combinational analysis of genomics and proteomics has proposed to reclassify the RSSC into three species, *R.*

pseudosolanacearum (*Rps*) (phylotype I and III), *R. solanacearum* (phylotype II), and *R. syzygii* (phylotype IV) (Prior et al., 2016).

Type III secretion system

For successful infection, RSSC relies on virulence determinants, such as exopolysaccharides, plant cell wall-degrading enzymes, and bacterial motility (Genin and Denny, 2012; Peeters et al., 2013a). However, the major virulence determinant of RSSC is the type III secretion system, a molecular syringe-like apparatus that directly delivers type III effectors (T3Es) into host cells (Coll and Valls, 2013). The RSSC has a large T3E repertoire, ranging from 40-70 T3Es, which is considerably more than other plant pathogenic bacteria like *Xanthomonas* spp. (30 T3Es) and *Pseudomonas* spp. (30-40 T3Es) (Schwartz et al., 2015; Wei et al., 2015). These T3Es, also referred to as *Ralstonia*-injected proteins (Rips), play a crucial role in virulence by suppressing immune responses and manipulating physiological processes in the hosts (Peeters et al., 2013b; Sabbagh et al., 2019; Landry et al., 2020). Conversely, some T3Es are perceived by immune receptors, leading to immune responses that often result in HR (Landry et al., 2020). These T3Es function as avirulence factors in host and could potentially be suitable targets for mining disease resistance.

Effectors as tools to identify disease resistance in Solanaceae model plant

Effector-assisted breeding is one of approaches used for mapping resistance loci (Vleeshouwers and Oliver, 2014; Jayaraman et al., 2016). Pathogen effectors are used to screen plant germplasm carrying resistance genes (Jayaraman et al., 2016). The resistance proteins encoded by these genes recognize pathogen effectors, leading to a visible and quantifiable HR that can be used as a proxy for disease resistance. Phenotypic screenings can be achieved through a simple pathogen or agrobacterium infiltration assays, thereby replacing the need for laborious and time-consuming disease infection assays in large populations. This approach enhances the accuracy of the genetic analysis by simplifying complex interactions between the environment, host, and pathogen to the presence or absence of a single resistance gene. Core effectors, which are essential for full virulence of pathogens, are particularly suitable targets for identifying corresponding resistance proteins that recognize them.

Nicotiana benthamiana, a solanaceous species native to Australia, is commonly used model plant in plant biology research (Goodin et al., 2008; Bally et al., 2018). *N. benthamiana* is amenable to various functional genetics methods, including virus-induced gene silencing (VIGS), RNA interference (RNAi), clustered regularly interspaced short palindromic repeats (CRISPR)-mediated genome editing, or agroinfiltration in laboratories (Derevnina et al., 2019). Moreover, advanced sequencing technologies have led to the genome-wide annotation of NLR (307 NLR genes) in *N. benthamiana* genome (Seong et al., 2020). The combination of systematic silencing and transient expression assay enable to rapidly identify one-to-one relationships between pathogen effectors and NLR genes in *N. benthamiana*.

This study describes the identification of two *N. benthamiana* NLRs using *Rps* T3Es, and provides insights into the molecular mechanism by which these NLRs are activated. The dissertation is composed of three chapters.

Chapter 1: Recognition of RipE1 and RipY by *Nicotiana benthamiana* immune system

Chapter 2: NbPtr1 mediates the recognition of the *Ralstonia pseudosolanacearum* effector RipE1 at plasma membrane in *Nicotiana benthamiana*

Chapter 3: The plasma membrane-associated RRS-Y mediates the recognition of the *Ralstonia pseudosolanacearum* effector RipY in *Nicotiana benthamiana*

REFERENCES

Adachi, H., Derevnina, L., and Kamoun, S. (2019a). NLR singletons, pairs, and networks: evolution, assembly, and regulation of the intracellular immunoreceptor circuitry of plants. *Curr. Opin. Plant Biol.* **50**:121–131.

Adachi, H., Contreras, M.P., Harant, A., Wu, C., Derevnina, L., Sakai, T., Duggan, C., Moratto, E., Bozkurt, T.O., Maqbool, A., et al. (2019b). An N-terminal motif in NLR immune receptors is functionally conserved across distantly related plant species. *eLife* **8**:e49956.

Ahn, H.-K., Lin, X., Olave-Achury, A.C., Derevnina, L., Contreras, M.P., Kourelis, J., Wu, C.-H., Kamoun, S., and Jones, J.D.G. (2023). Effector-dependent activation and oligomerization of plant NRC class helper NLRs by sensor NLR immune receptors Rpi-amr3 and Rpi-amr1. *EMBO J.* **42**:e111484.

Azevedo, C., Sadanandom, A., Kitagawa, K., Freialdenhoven, A., Shirasu, K., and Schulze-Lefert, P. (2002). The RAR1 interactor SGT1, an essential component of *R* gene-triggered disease resistance. *Science* **295**:2073–2076.

Bally, J., Jung, H., Mortimer, C., Naim, F., Philips, J. G., Hellens, R., Bombarely, A., Goodin, M.M., and Waterhouse, P.M. (2018). The rise and rise of *Nicotiana benthamiana*: a plant for all reasons. *Annu. Rev. Phytopathol.* **56**:405–426.

Bi, G., Su, M., Li, N., Liang, Y., Dang, S., Xu, J., Hu, M., Wang, J., Zou, M., Deng, Y., et al. (2021). The ZAR1 resistosome is a calcium-permeable channel triggering plant immune signaling. *Cell* **184**:3528–3541.

Bonardi, V., Tang, S., Stallmann, A., Roberts, M., Cherkis, K., and Dangl, J.L. (2011). Expanded functions for a family of plant intracellular immune receptors beyond specific recognition of pathogen effectors. *Proc. Natl. Acad. Sci. U.S.A.* **108**:16463–16468.

Boutrot, F., and Zipfel, C. (2017). Function, discovery, and exploitation of plant pattern recognition receptors for broad-spectrum disease resistance. *Annu. Rev. Phytopathol.* **55**:257–286.

Castel, B., Ngou, P.-M., Cevik, V., Redkar, A., Kim, D.-S., Yang, Y., Ding, P., and Jones, J.D.G. (2019). Diverse NLR immune receptors activate defence via the RPW8-NLR NRG1. *New Phytol.* **222**:966–980.

Coll, N.S., and Valls, M. (2013). Current knowledge on the *Ralstonia solanacearum* type III secretion system. *Microb. Biotechnol.* **6**:614–620.

Contreras, M.P., Pai, H., Tumtas, Y., Duggan, C., Yuen, E.L.H., Cruces, A.V., Kourelis, J., Ahn, H.-K., Lee, K.-T., Wu, C.-H., et al. (2023). Sensor NLR immune proteins activate oligomerization of their NRC helpers in response to plant pathogens. *EMBO J.* **42**:e111519.

Corredor-Moreno, P., and Saunders, D.G.O. (2020). Expecting the unexpected: factors influencing the emergence of fungal and oomycete plant pathogens. *New Phytol.* **225**:118–125.

Derevnina, L., Kamoun, S., and Wu, C. (2019). Dude, where is my mutant? *Nicotiana benthamiana* meets forward genetics. *New Phytol.* **221**:607–610.

Dongus, J.A., and Parker, J.E. (2021). EDS1 signalling: At the nexus of intracellular and surface receptor immunity. *Curr. Opin. Plant Biol.* **62**:102039.

Duxbury, Z., Wu, C., and Ding, P. (2021). A comparative overview of the intracellular guardians of plants and animals: NLRs in innate immunity and beyond. *Annu. Rev. Plant Biol.* **72**:155–184.

Fegan, M., and Prior, P. (2005). How complex is the *Ralstonia solanacearum* species complex. *Bacterial wilt disease and the Ralstonia solanacearum species complex* **1**:449–461.

Genin, S., and Denny, T.P. (2012). Pathogenomics of the *Ralstonia solanacearum* species complex. *Annu. Rev. Phytopathol.* **50**:67–89.

Goodin, M.M., Zaitlin, D., Naidu, R.A., and Lommel, S.A. (2008). *Nicotiana benthamiana*: its history and future as a model for plant-pathogen

interactions. *Mol. Plant Microbe Interact.* **21**:1015–1026.

Hayward, A.C. (1991). Biology and epidemiology of bacterial wilt caused by *Pseudomonas solanacearum*. *Annu. Rev. Phytopathol.* **29**:65–87.

Jacob, P., Kim, N.H., Wu, F., El Kasmi, F., Chi, Y., Walton, W.G., Furzer, O.J., Lietzan, A.D., Sunil, S., Kempthorn, K., et al. (2021). Plant "helper" immune receptors are Ca^{2+}-permeable nonselective cation channels. *Science* **373**:420–425.

Jayaraman, J., Segonzac, C., Cho, H., Jung, G., and Sohn, K.H. (2016). Effector-assisted breeding for bacterial wilt resistance in horticultural crops. *Hortic. Environ. Biotechnol.* **57**:415–423.

Jones, J.D.G., Vance, R.E., and Dangl, J.L. (2016). Intracellular innate immune surveillance devices in plants and animals. *Science* **354**:aaf6395.

Kim, B., Choi, J., and Segonzac, C. (2022). Tackling multiple bacterial diseases of Solanaceae with a handful of immune receptors. *Hortic. Environ. Biotechnol.* **63**:149–160.

Kourelis, J., and van der Hoorn, R.A.L. (2018). Defended to the nines: 25 years of resistance gene cloning identifies nine mechanisms for R protein function. *Plant Cell* **30**:285–299.

Krasileva, K.V., Dahlbeck, D., and Staskawicz, B.J. (2010). Activation of an *Arabidopsis* resistance protein is specified by the in planta association of its leucine-rich repeat domain with the cognate oomycete effector. *Plant Cell* **22**:2444–2458.

Landry, D., González-Fuente, M., Deslandes, L., and Peeters, N. (2020). The large, diverse, and robust arsenal of *Ralstonia solanacearum* type III effectors and their in planta functions. *Mol. Plant Pathol.* **21**:1377–1388.

Le Roux, C., Huet, G., Jauneau, A., Camborde, L., Trémousaygue, D., Kraut, A., Zhou, B., Levaillant, M., Adachi, H., Yoshioka, H., et al. (2015). A receptor pair with an integrated decoy converts pathogen disabling of transcription factors to immunity. *Cell* **161**:1074–1088.

Lowe-Power, T.M., Khokhani, D., and Allen, C. (2018). How *Ralstonia*

solanacearum exploits and thrives in the flowing plant xylem environment. *Trends Microbiol.* **26**:929–942.

Ma, S., Lapin, D., Liu, L., Sun, Y., Song, W., Zhang, X., Logemann, E., Yu, D., Wang, J., Jirschitzka, J., et al. (2020). Direct pathogen-induced assembly of an NLR immune receptor complex to form a holoenzyme. *Science* **370**:eabe3069.

Mansfield, J., Genin, S., Magori, S., Citovsky, V., Sriariyanum, M., Ronald, P., Dow, M., Verdier, V., Beer, S.V., Machado, M.A., et al. (2012). Top 10 plant pathogenic bacteria in molecular plant pathology. *Mol. Plant Pathol.* **13**:614–629.

Martin, R., Qi, T., Zhang, H., Liu, F., King, M., Toth, C., Nogales, E., and Staskawicz, B.J. (2020). Structure of the activated ROQ1 resistosome directly recognizing the pathogen effector XopQ. *Science* **370**:eabd9993.

Narusaka, M., Shirasu, K., Noutoshi, Y., Kubo, Y., Shiraishi, T., Iwabuchi, M., and Narusaka, Y. (2009). *RRS1* and *RPS4* provide a dual *Resistance*-gene system against fungal and bacterial pathogens. *Plant J.* **60**:218–226.

Nelson, R., Wiesner-Hanks, T., Wisser, R., and Balint-Kurti, P. (2018). Navigating complexity to breed disease-resistant crops. *Nat. Rev. Genet.* **19**:21–33.

Ngou, B.P.M., Ding, P., and Jones, J.D.G. (2022). Thirty years of resistance: Zig-zag through the plant immune system. *Plant Cell* **34**:1447–1478.

Oerke, E.-C. (2006). Crop losses to pests. *J. Agric. Sci.***144**:31–43.

Parker, J.E., Holub, E.B., Frost, L.N., Falk, A., Gunn, N.D., and Daniels, M.J. (1996). Characterization of *eds1*, a mutation in Arabidopsis suppressing resistance to *Peronospora parasitica* specified by several different *RPP* genes. *Plant Cell* **8**:2033–2046.

Peart, J. R., Lu, R., Sadanandom, A., Malcuit, I., Moffett, P., Brice, D.C., Schauser, L., Jaggard, D.A.W., Xiao, S., Coleman, M.J., et al. (2002). Ubiquitin ligase-associated protein SGT1 is required for host and nonhost disease resistance in plants. *Proc. Natl. Acad. Sci. U.S.A.* **99**:10865–10869.

Peeters, N., Guidot, A., Vailleau, F., and Valls, M. (2013a). *Ralstonia solanacearum*, a widespread bacterial plant pathogen in the post-genomic era. *Mol. Plant Pathol.* **14**:651–662.

Peeters, N., Carrère, S., Anisimova, M., Plener, L., Cazalé, A.-C., and Genin, S. (2013b). Repertoire, unified nomenclature and evolution of the type III effector gene set in the *Ralstonia solanacearum* species complex. *BMC Genom.* **14**:859.

Prior, P., Ailloud, F., Dalsing, B. L., Remenant, B., Sanchez, B., and Allen, C. (2016). Genomic and proteomic evidence supporting the division of the plant pathogen *Ralstonia solanacearum* into three species. *BMC Genom.***17**:90.

Sabbagh, C.R.R., Carrere, S., Lonjon, F., Vailleau, F., Macho, A.P., Genin, S., and Peeters, N. (2019). Pangenomic type III effector database of the plant pathogenic *Ralstonia* spp. *PeerJ* **7**:e7346.

Saile, S.C., Jacob, P., Castel, B., Jubic, L.M., Salas-Gonzáles, I., Bäcker, M., Jones, J.D.G., Dangl, J.L., and El Kasmi, F. (2020). Two unequally redundant "helper" immune receptor families mediate *Arabidopsis thaliana* intracellular "sensor" immune receptor functions. *PLoS Biol.* **18**:e3000783.

Sarris, P.F., Duxbury, Z., Huh, S.U., Ma, Y., Segonzac, C., Sklenar, J., Derbyshire, P., Cevik, V., Rallapalli, G., Saucet, S.B., et al. (2015). A plant immune receptor detects pathogen effectors that target WRKY transcription factors. *Cell* **161**:1089–1100.

Savary, S., Willocquet, L., Pethybridge, S.J., Esker, P., McRoberts, N., and Nelson, A. (2019). The global burden of pathogens and pests on major food crops. *Nat. Ecol. Evol.* **3**:430–439.

Schultink, A., and Steinbrenner, A.D. (2021). A playbook for developing disease-resistant crops through immune receptor identification and transfer. *Curr. Opin. Plant Biol.* **62**:102089.

Schwartz, A.R., Potnis, N., Timilsina, S., Wilson, M., Patané, J., Martins, J., Minsavage, G.V., Dahlbeck, D., Akhunova, A., Almeida, N., et al. (2015).

Phylogenomics of *Xanthomonas* field strains infecting pepper and tomato reveals diversity in effector repertoires and identifies determinants of host specificity. *Front. Microbiol.* **6**:535.

Seong, K., Seo, E., Witek, K., Li, M., and Staskawicz, B.J. (2020). Evolution of NLR resistance genes with noncanonical N-terminal domains in wild tomato species. *New Phytol.* **227**:1530–1543.

Shirasu, K. (2009). The HSP90-SGT1 chaperone complex for NLR immune sensors. *Annu. Rev. Plant Biol.* **60**:139–164.

van Esse, H.P., Reuber, T.L., and van der Does, D. (2020). Genetic modification to improve disease resistance in crops. *New Phytol.* **225**:70–86.

Vleeshouwers, V.G.A.A., and Oliver, R.P. (2014). Effectors as tools in disease resistance breeding against biotrophic, hemibiotrophic, and necrotrophic plant pathogens. *Mol. Plant Microbe Interact.* **27**:196–206.

Wang, J., Hu, M., Wang, J., Qi, J., Han, Z., Wang, G., Qi, Y., Wang, H.-W., Zhou, J.-M., and Chai, J. (2019). Reconstitution and structure of a plant NLR resistosome conferring immunity. *Science* **364**:eaav5870.

Wei, H.-L., Chakravarthy, S., Mathieu, J., Helmann, T.C., Stodghill, P., Swingle, B., Martin, G.B., and Collmer, A. (2015). *Pseudomonas syringae* pv. *tomato* DC3000 type III secretion effector polymutants reveal an interplay between HopAD1 and AvrPtoB. *Cell Host Microbe* **17**:752–762.

Wu, C.-H., Abd-El-Haliem, A., Bozkurt, T.O., Belhaj, K., Terauchi, R., Vossen, J.H., and Kamoun, S. (2017). NLR network mediates immunity to diverse plant pathogens. *Proc. Natl. Acad. Sci. U.S.A.* **114**:8113–8118.

Wu, C.-H., Derevnina, L., and Kamoun, S. (2018). Receptor networks underpin plant immunity. *Science* **360**:1300–1301.

CHAPTER 1

Recognition of RipE1 and RipY by *Nicotiana benthamiana* immune system

I acknowledge that some parts in this chapter either quote or alter my work reported in "A plasma membrane nucleotide-binding leucine-rich repeat receptor mediates the recognition of the *Ralstonia pseudosolanacearum* effector RipY in *Nicotiana benthamiana*" published online in Plant Communications (DOI: https://doi.org/10.1016/j.xplc.2023.100640).

ABSTRACT

Bacterial wilt disease caused by *Ralstonia pseudosolanacearum* (*Rps*) leads to economic losses of Solanaceae crops. In plants, intracellular nucleotide-binding leucine-rich repeats receptors (NLRs) activate immune responses upon recognition of pathogens and have potential as genetic resources to develop disease resistant crops. However, only a few NLRs that confer resistance to *Ralstonia* species have been identified so far. Here, RipE1 and RipY, which are type III effectors of *Rps*, were recognized by *Nicotiana benthamiana* immune system. The recognition of these effectors induced cell death and significantly restricted pathogen growth. Silencing of immune signaling components revealed that putative *N. benthamiana* NLRs are involved in the recognition of RipE1 and RipY, and that ENHANCED DISEASE SUSCEPTIBILITY 1 (EDS1) or helper NLRs were not required for these recognition events. Screening of a multiplexed NbNLR-VIGS library identified two NLRs that mediate the recognition of RipE1 and RipY in *N. benthamiana*. Therefore, these NLRs could potentially improve the pool of available genetic resources for bacterial wilt disease resistance.

INTRODUCTION

Ralstonia species cause bacterial wilt disease in Solanaceae crops (Hayward, 1991; Mansfield et al., 2012). The *Ralstonia solanacearum* species complex (RSSC) has been classified into three species *R. solanacearum* (englobing phylotype II strains), *R. pseudosolanacearum* (*Rps*, phylotype I and III strains), and *R. syzygii* (phylotype IV strains) (Prior et al., 2016). The RSSC employs the type III secretion system (T3SS) for pathogenicity and injects approximately 70 type III effectors (T3Es) called *Ralstonia*-injected protein (Rip) into the host cell (Peeters et al., 2013; Sabbagh et al., 2019).

While several *Rps* T3Es activate effector-triggered immunity (ETI) in different plant species, only a few nucleotide-binding leucine-rich repeats receptors (NLRs) responsible for *Rps* T3E recognition have been cloned so far (Landry et al., 2020; Kim et al., 2022). In *Arabidopsis thaliana*, the paired TNLs RESISTANCE TO RALSTONIA SOLANACEARUM 1 (RRS1) and RESISTANCE TO PSEUDOMONAS SYRINGAE 4 (RPS4) recognize the acetyltransferase effector RipP2 (Deslandes et al., 1998; Deslandes et al., 2002; Narusaka et al., 2009). In Solanaceous plants, the TNL RECOGNITION OF XOPQ 1 (Roq1) and the CNL PSEUDOMONAS TOMATO RACE 1 (Ptr1) were identified (Schultink et al., 2017; Mazo-Molina et al., 2020). Roq1, from *Nicotiana benthamiana*, recognizes RipB as well as RipB homologs HopQ1-1 and XopQ from *P. syringae* and *Xanthomonas* spp., respectively (Schultink et al., 2017; Nakano and Mukaihara, 2019; Thomas et al.,

2020). Accordingly, transgenic tomato plants expressing *Roq1* are resistant to multiple bacterial pathogens carrying RipB homologs (Thomas et al., 2020). The *Ptr1* gene from the *Solanum lycopersicoides*, as well as its homologs from *N. benthamiana* and *S. tuberosum*, is required for the recognition of RipBN, a *Rps* homolog of the cysteine protease effector AvrRpt2 from *P. syringae* (Mazo-Molina et al., 2019; Mazo-Molina et al., 2020).

The identification of NLRs is still challenging and time-consuming. Recent findings, however, have facilitated the identification of novel NLRs required for the recognition of *Rps* T3Es in *N. benthamiana*. The effector repertoire of 30 *Rps* strains isolated from tomato and pepper across the Republic of Korea was recently determined from whole-genome based approach (Prokchorchik et al., 2020). Furthermore, Ahn et al (2023) developed a reverse genetic tool to screen most *N. benthamiana* NLRs via multiple virus-induced gene silencing (VIGS) (Seong et al., 2020; Ahn et al., 2023). This chapter reports the identification of two candidate NLRs that mediate immunity upon recognition of RipE1 and RipY in *N. benthamiana*. Two large-scale screenings were conducted to identify new NLRs in *N. benthamiana*. The *Rps* T3Es repertoire was screened, and multiple *Rps* T3Es that induced cell death dependent on the NLR chaperone SUPPRESSOR OF THE G2 ALLELE OF SKP1 (SGT1) in *N. benthamiana* were identified. In particular, RipE1 or RipY expression activated the *N. benthamiana* immune system as well as induced cell death. The NLR-signaling components, such as lipase-like protein ENHANCED DISEASE SUSCEPTIBILITY 1 (EDS1) and helper NLRs, were not associated with

RipE1- or RipY-triggered immunity. Finally, the NbNLR-VIGS library was used to identify the NLRs required for the recognition of RipE1 and RipY.

MATERIALS AND METHODS

Plant growth conditions

Nicotiana benthamiana and *N. tabacum* plants were grown in a growth chamber under long-day conditions with 16 h: 8 h, light: dark at 24-26°C for 4-5 weeks before bacterial infiltration.

Bacterial strains

Bacterial strains used in this study were *Escherichia coli* DH5α, *A. tumefaciens* AGL1 and GV3101, *P. syringae* pv. *tomato* DC3000 wild-type (*Pst*) and *Pst* lacking the recognized effector *HopQ1-1* (*Pst* Δ*hopQ1-1*) (Wei et al., 2007; Wei et al., 2015). *Escherichia coli* DH5α, and *A. tumefaciens* strains were grown on Low-salt Luria-Bertani medium at 37°C and 28°C, respectively. *Pst* strains were grown on King's B medium at 28°C. All bacteria were grown on solid medium for 2 days (1 day for *E. coli*) with appropriate antibiotics. Single colonies were inoculated on liquid medium overnight in a shaker at 200 rpm. Bacterial suspensions were harvested by centrifugation for subsequent experiments.

Plasmid vectors and constructs

All the *Rps* T3Es commonly found in Korean isolates of *Rps* were synthesized by Twist Bioscience (USA) and cloned into the entry vector pICH41021 for Golden Gate cloning (Engler et al., 2008) (Table 1-1). For *Agrobacterium*-mediated

expression, the modules of *Rps* T3Es were assembled into the binary vectors pICH86988 or pICH86966 to generate full-length *Rps* T3E alleles in fusion with 3xFLAG C-terminal epitope tag under the control of the 35S cauliflower mosaic virus promoter. Binary vectors were mobilized into *A. tumefaciens* AGL1 using electroporation. For *Pseudomonas*-mediated effector delivery, the modules were assembled into the broad host range vector pEDV3 carrying AvrRps4N (408-bp) under the control of AvrRps4 native promoter (128-bp) (Sohn et al., 2007). The final constructs were mobilized into *Pst* or *Pst* Δ*hopQ1-1* by triparental conjugation with *E. coli* HB1-1 (pRK2013), as described previously (Jayaraman et al., 2017). For subcloning of individual silencing fragments from TRV:Com1 and TRV:Com3 constructs, each silencing fragments were amplified using PCR, and ligated into TRV2 between *Eco*RI and *Bam*HI sites (Table 1-2).

Hypersensitive response cell death assay and quantification

Agrobacteria cells grown in liquid culture were centrifuged at 8,000 rpm and resuspended in infiltration buffer (10 mM $MgCl_2$, 10 mM MES-KOH pH5.6). Cell suspensions were adjusted to OD_{600} of 0.4 ~ 0.5 and infiltrated into leaf tissues of 4 to 5-week old *N. benthamiana* or *N. tabacum* using a needless syringe. Cell death occurrence was observed and photographed in visible or LED light (red-orange 617 nm and cool white 6500 K) at 3 or 4 days post infiltration (dpi). The extent of cell death was estimated by the quantum yield of chlorophyll fluorescence ($F_v/F_{m,}$ QY) using a closed FluorCam (Photon Systems Instruments, Czech Republic). The

default F_v/F_m protocol from FluorCam 7.0 software was used to determine minimum fluorescence (F_0), maximum fluorescence (F_m) and maximum quantum yield of photosystem II (F_v/F_m). The F_v/F_m value was around 0.7 in healthy leaves (Jones et al., 2001; Lee et al., 2021). All the experiments were repeated at least three times independently and merged values were analyzed with ANOVA and appropriate multiple comparison tests using the GraphPad Prism9 software.

Virus-induced gene silencing

Gene-silencing in *N. benthamiana* was conducted using the tobacco rattle virus (TRV)-based vectors pTRV1 and pTRV2 (Liu et al., 2002). Two week-old *N. benthamiana* seedlings were infiltrated with a 1 : 1 ratio mixture of *A. tumefaciens* carrying pTRV1 and pTRV2 at OD_{600} of 0.5 into cotyledons. The plants were grown for 4 to 5 weeks before *A. tumefaciens* carrying constructs were infiltrated for transient expression of gene of interest. For VIGS of genetic components required for NLR-mediated immune responses, TRV:*NbSGT1* was provided by Dr. Sera Choi (Choi et al., 2017). Other TRV constructs (TRV:*NbEDS1*, TRV:*NbADR1/NbNRG1*, TRV:*NbNRC2/3/4*) were obtained from Dr. Hye-Young Lee (Lee et al., 2021).

Gene expression

A. tumefaciens carrying effector constructs were infiltrated in leaf tissues of *N. benthamiana,* and leaf discs were harvested before tissue collapse (~36 h post-infiltration). Total RNA was extracted using Trizol reagent (Invitrogen, USA) and

cDNA was synthesized from 2 µg RNA using Maxima First Strands cDNA Synthesis kit (Thermo Fisher Scientific, USA) according to the manufacturer's instructions. cDNA was analyzed by semi-quantitative PCR or qRT-PCR. The housekeeping gene *NbEF1α* was used as reference. For semi-qPCR, cDNA was amplified by PCR using Prime Taq Premix (Genetbio, Republic of Korea). The amplicons were analyzed using agarose gel electrophoresis. For qRT-PCR, cDNA was amplified using GoTaq qPCR Master Mix (Promega, USA) in the CFX96 Thermal Cycler (Bio-rad, USA). The relative expression was determined using the comparative 2(-Delta Delta C(t)) method (Livak and Schmittgen, 2001). Primers used in semi qRT-PCR or semi-qPCR are listed in Table 1-2. All the experiments were repeated at least three times independently and merged values were analyzed with ANOVA and appropriate multiple comparison tests using the GraphPad Prism9 software.

Bacterial growth assay

Pst strains grown in liquid culture were centrifuged at 8,000 rpm and resuspended in 10 mM $MgCl_2$. The cell suspensions were adjusted to 10^5 CFU. ml^{-1} before infiltration in leaf tissues of 4 to 5-week old *N. benthamiana* using a needless syringe. Three or four leaf discs were harvested at 0, 3, and 6 dpi using 8 mm puncher, ground in 10 mM $MgCl_2$ and serially diluted before plating on KB solid medium with appropriate antibiotics. Bacterial colonies were enumerated after 2 days incubation at 28°C.

Sequencing analysis and molecular markers

The amplicons from *N. benthamiana* cDNA were sequenced using Sanger's sequencing analysis by Macrogen Co., Ltd. (Republic of Korea). The nucleotide sequences were then aligned and analyzed using Geneious Prime (Biomatters, New Zealand). To perform the cleaved amplified polymorphic sequence (CAPS) assays, the amplicons carrying single nucleotide polymorphisms (SNPs) were treated with either *Hin*dIII or *Eco*RI restriction enzyme (New England Biolabs, USA), and the resulting fragments were then analyzed using agarose gel electrophoresis. For the insertion and deletion (InDel) assay, the amplicon carrying a deletion was analyzed using gel electrophoresis to determine its size. All amplicons were generated by PCR using Phusion High-Fidelity DNA polymerase (New England Biolabs, USA). Primer sequences are listed in Table 1-2.

Table 1-1. Information of *Rps* T3Es used in this study

Gene	Reprentative strain[a]	References
RipA1	GMI1000[b]	Jeon et al., (2020)
RipA3	Pe_1[c]	Prokchorchik et al., (2020)[d]
RipB	Pe_9	Prokchorchik et al., (2020)
RipC1	Pe_2	Prokchorchik et al., (2020)
RipD	Pe_1	Prokchorchik et al., (2020)
RipE1	GMI1000	Jeon et al., (2020)
RipF1	GMI1000	Prokchorchik et al., (2020)
RipG1	Pe_1	Prokchorchik et al., (2020)
RipG2	Pe_1	Prokchorchik et al., (2020)
RipG4	Pe_4	Prokchorchik et al., (2020)
RipG5	Pe_2	Prokchorchik et al., (2020)
RipG6	Pe_1	Prokchorchik et al., (2020)
RipG7	To_7	Prokchorchik et al., (2020)
RipH1	Pe_1	Prokchorchik et al., (2020)
RipI	Pe_1	Prokchorchik et al., (2020)
RipJ	Pe_1	Prokchorchik et al., (2020)
RipN	Pe_1	Prokchorchik et al., (2020)
RipP1	Pe_9	Prokchorchik et al., (2020)
RipT	Pe_42	Prokchorchik et al., (2020)
RipU	Pe_1	Prokchorchik et al., (2020)
RipV1	Pe_1	Prokchorchik et al., (2020)
RipW	Pe_2	Prokchorchik et al., (2020)
RipY	Pe_1	Prokchorchik et al., (2020)
RipAB	Pe_1	Prokchorchik et al., (2020)
RipAC	Pe_1	Prokchorchik et al., (2020)

RipAG	Pe_4	Prokchorchik et al., (2020)
RipAH	Pe_9	Prokchorchik et al., (2020)
RipAI	Pe_1	Prokchorchik et al., (2020)
RipAN	Pe_1	Prokchorchik et al., (2020)
RipAP	Pe_1	Prokchorchik et al., (2020)
RipAR	Pe_2	Prokchorchik et al., (2020)
RipAX1	Pe_9	Prokchorchik et al., (2020)
RipAX2	Pe_9	Prokchorchik et al., (2020)
RipAY	Pe_1	Prokchorchik et al., (2020)
RipAZ1	Pe_9	Prokchorchik et al., (2020)
RipBA	Pe_9	Prokchorchik et al., (2020)
RipTAL	Pe_1	Prokchorchik et al., (2020)
RS_T3E_Hyp6	Pe_1	Prokchorchik et al., (2020)
RS_T3E_Hyp18	To_7	Prokchorchik et al., (2020)

[a]This strain represents multiple Korean *R. pseudosolanacearum* strains that carry the effector (Prokchorchik et al., 2020).

[b]*R. pseudosolanacearum* reference strain

[c]Pe_XX indicates the strain isolated from pepper; To_XX strain from tomato.

[d]The cloning was conducted in collaboration with Prof. Kee Hoon Sohn's laboratory (Seoul National University, Korea).

Table 1-2. Primers used in this study

Name	Sequences (5' to 3')	Purpose	References
NbEF1α_F	AGAAGGAAGCTGCTGAGATGA	Semi-qPCR, qRT-PCR	In this study
NbEF1α_R	CTTGGGGGTGGTAGCATCC	Semi-qPCR, qRT-PCR	In this study
NbSGT1_F	TAATGTGTCATCAGATGCCC	Semi-qPCR, qRT-PCR	Choi et al., (2017)
NbSGT1_R	ACTTCTTTCCAGTTTGTCGAC	Semi-qPCR, qRT-PCR	Choi et al., (2017)
NbHin1_F	GCTTGGTTTTATTGGGAGAT	qRT-PCR	In this study
NbHin1_R	ATGATCTGCCATTAGACCCT	qRT-PCR	In this study
NbHsr203J_F	GGAGGAGCTTAAATTGCCGC	qRT-PCR	In this study
NbHsr203J_R	TTCAGAACCAGTTACAGGGT	qRT-PCR	In this study
NbNRC2a/b_F	AGTGGATGAGAGTGTGGGTG	qRT-PCR	Wu et al., (2015)
NbNRC2a/b_R	AAGCAGGGATCTCAAAGCCT	qRT-PCR	Wu et al., (2015)
NbNRC2c_F	TCAAAACATGCCGTGTTCAT	qRT-PCR	Wu et al., (2015)
NbNRC2c_R	CCTGCGGGTTTTGTACTGAT	qRT-PCR	Wu et al., (2015)
NbNRC3_F	CCTCGAAAAGCTGAAGTTGG	qRT-PCR	Wu et al., (2015)
NbNRC3_R	TGTCCCCTAAACGCATTTTC	qRT-PCR	Wu et al., (2015)
NbNRC4_F	AAACAAATCTGCGGGTTGAC	qRT-PCR	Wu et al., (2015)
NbNRC4_R	GGATGGCATTGAAGTCACCT	qRT-PCR	Wu et al., (2015)
NbEDS1_F	TGTTGGCACAGATGAGGTAGCCA	qRT-PCR	Tran et al., (2016)
NbEDS1_R	CCCGACGAGTGCCCTGCAAA	qRT-PCR	Tran et al., (2016)
NbADR1_F	TGGTCGCTCTCTGTGCTAGA	qRT-PCR	Qi et al., (2018)
NbADR1_R	GAACTTAATGCGCGACACAA	qRT-PCR	Qi et al., (2018)
NbNRG1_F	AAGAGAATCAGCCTGGAACG	qRT-PCR	Qi et al., (2018)
NbNRG1_R	CAAATGCCTCACCAATTTCA	qRT-PCR	Qi et al., (2018)
Com1-1_F	GAATTCAAATTCCGAGAGAGGACTTCA	Subcloning	In this study

Com1-1_R	GGATCCCAAATGCTTGTACCAC ATC	Subcloning	In this study
Com1-2_F	GAATTCCAACTAATGCACATAT GGGTCGCC	Subcloning	In this study
Com1-2_R	GGATCCAACTCTGTCATCTGCT CT	Subcloning	In this study
Com1-3_F	GAATTCTGAGAAGGGGGTCTC T	Subcloning	In this study
Com1-3_R	GGATCCGATTTCTTCCACAACT TG	Subcloning	In this study
Com1-4_F	GAATTCTGCCTAGATATAATAG AATTGA	Subcloning	In this study
Com1-4_R	GGATCCCAACCACGCCAACTTT GAG	Subcloning	In this study
Com1-5_F	GAATTCCTCTCAAATGTGCATT	Subcloning	In this study
Com1-5_R	GGATCCAAGGCTTCAAATTAT AA	Subcloning	In this study
Com1-6_F	GAATTCAATGGTGTAACATTTT ACTCTAGAG	Subcloning	In this study
Com1-6_R	GGATCCCAACCACCTCAAATC AGCAG	Subcloning	In this study
Com3-1_F	GAATTCAAGTCCTGCAAGATT ATGATCAC	Subcloning	In this study
Com3-1_R	GGATCCAATTTAGCATTTGTCC TGA	Subcloning	In this study
Com3-2_F	GAATTCGTTCTTCCTTCAGGTC AG	Subcloning	In this study
Com3-2_R	GGATCCATTTGTAACTAAAGTG GCC	Subcloning	In this study
Com3-3_F	GAATTCACGACACTTGCTAAA AAAG	Subcloning	In this study
Com3-3_R	GGATCCACAGACGAGGCTTA	Subcloning	In this study
Com3-4_F	GAATTCTTCAATCCAAGCTGTA CTAAT	Subcloning	In this study
Com3-4_R	GGATCCAAGTCATCCAAGAGA TCAT	Subcloning	In this study
Com3-5_F	GAATTCAATCTAAACTATCTGA TCCGAA	Subcloning	In this study
Com3-5_R	GGATCCCGCACAAATGGC	Subcloning	In this study
Com3-6_F	GAATTCGCAACAGCAGGAAAC AAA	Subcloning	In this study
Com3-6_R	GGATCCGGAGTCGTGAGA	Subcloning	In this study
GeneA/B_F	ATGAAAACAGACGAAAATGAA TGG	Polymorphism analaysis	In this study
GeneA/B_R	CTGCCACTGACTGTGCAAGATC	Polymorphism analaysis	In this study

GeneC/D_F	ACTCTCTGAGAAGAAAATACTTG	Polymorphism analaysis	In this study
GeneC/D_R	GTGCTGCTGTCCACTCTATT	Polymorphism analaysis	In this study
GeneD_F	GTTCTGGCCCTCGTGAATTTCTTCCT	3'RACE-PCR	In this study

RESULTS

HR-like cell death triggered by various *R. pseudosolanacearum* T3Es in *Nicotiana* species.

Some T3Es of *Ralstonia* species have been reported to induce cell death or even resistance in different plant species, including *Nicotiana* spp. (Landry et al., 2020). Effector-induced cell death is used as a proxy to identify potential T3Es activating plant immune responses. In order to identify *Rps* T3Es that trigger cell death in *N. benthamiana* and *N. tabacum*, 39 *Rps* effectors commonly found in multiple Korean *Rps* isolates were cloned from strains GMI1000, Pe_1, Pe_2, Pe_4, Pe_9, Pe_42, and To_7, in collaboration with Prof. Sohn laboratory (Seoul National University, Korea) (Table 1-1) (Prokchorchik et al., 2020). Using agroinfiltration, 39 *Rps* T3Es were transiently expressed under the 35S promoter in leaves of *N. benthamiana* and *N. tabacum* (Figure 1-1). RipE1 from *Rps* GMI1000 (hereafter referred to as RipE1) and GFP were used as a positive and negative controls for cell death, respectively (Jeon et al., 2020; Sang et al., 2020; Prokchorchik et al., 2020). As expected, RipE1 expression induced cell death in both *N. benthamiana* and *N. tabacum* (Jeon et al., 2020; Sang et al., 2020; Prokchorchik et al., 2020). 13 out of 39 Korean *Rps* T3Es (RipA1, RipD, RipE1, RipH1, RipI, RipP1, RipT, RipV1, RipY, RipAB, RipAI, RipAN, and RipAP) induced cell death in *N. benthamiana* leaves, and six of them (RipE1, RipI, RipP1, RipT, RipV1, and RipAN) also triggered cell death in *N. tabacum* (Figure 1-1). One *Rps* T3E (RipB) triggered cell death only in *N. tabacum*

(Figure 1-1). The HR-like cell death-inducing 13 *Rps* T3Es were selected as candidates that are recognized by *N. benthamiana* immune system.

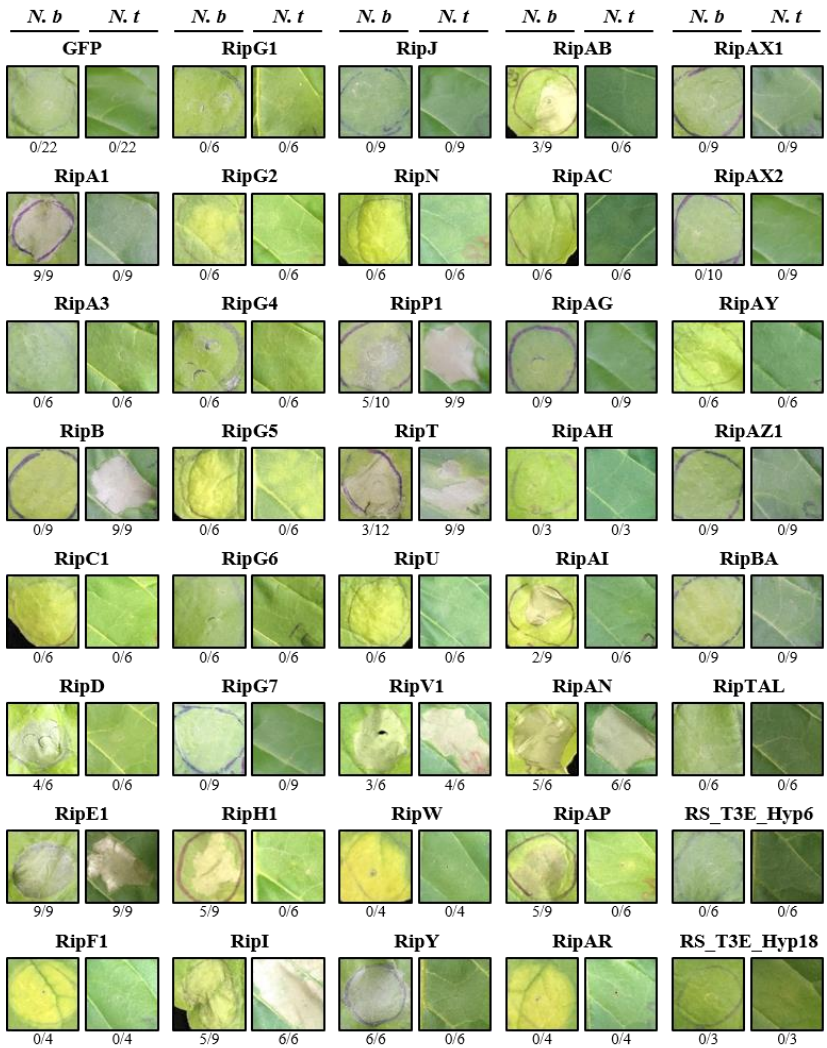

Figure 1-1. Multiple *Rps* T3Es induce HR-like cell death in the leaves of *Nicotiana* spp.

Agrobacterium-mediated transient expression of *Rps* T3Es in *N. benthamiana* (*N. b*) and *N. tabacum* (*N. t*). *Agrobacterium* strains carrying GFP or *Rps* T3E constructs (OD_{600}=0.4) were infiltrated in *N. b* or *N. t* leaves. Pictures were taken 6 days after infiltration (dpi) under a bright field. Numbers indicate patches with cell death out of total infiltrated patches.

NbSGT1-dependent cell death triggered by multiple T3Es in *N. benthamiana*

To investigate whether NLRs are involved in *Rps* T3E-induced cell death, the SUPPRESSOR OF G2 ALLELE OF SKP1 (SGT1), a key component of molecular chaperone complexes required for NLR functions, was silenced using virus-induced gene silencing (VIGS) (Azevedo et al., 2002; Shirasu, 2009). RipE1 and RipA1 were used as positive and negative controls for *NbSGT1*-dependent cell death, respectively (Jeon et al., 2020; Sang et al., 2020). As expected, RipE1-induced cell death was abolished in the *NbSGT1*-silenced plants. Similarly, the cell death induced by RipD, RipH1, RipP1, RipT, RipV1, RipY, or RipAP was compromised in the *NbSGT1*-silenced plants (Figure 1-2A). Semi-qPCR analysis of *NbSGT1* expression confirmed silencing efficiency (Figure 1-2B). These results suggest that *N. benthamiana* NLRs are associated with the cell death triggered by RipE1, RipD, RipH1, RipP1, RipT, RipV1, RipY, or RipAP. Given that RipE1 is a core effector with a putative catalytic triad (Peeters et al., 2013; Sabbagh et al., 2019; Sang et al., 2020), and that RipY consistently induced strong cell death but plays a role in bacterial fitness in other Solanaceae (Macho et al., 2010), further investigations were focused on RipE1 and RipY.

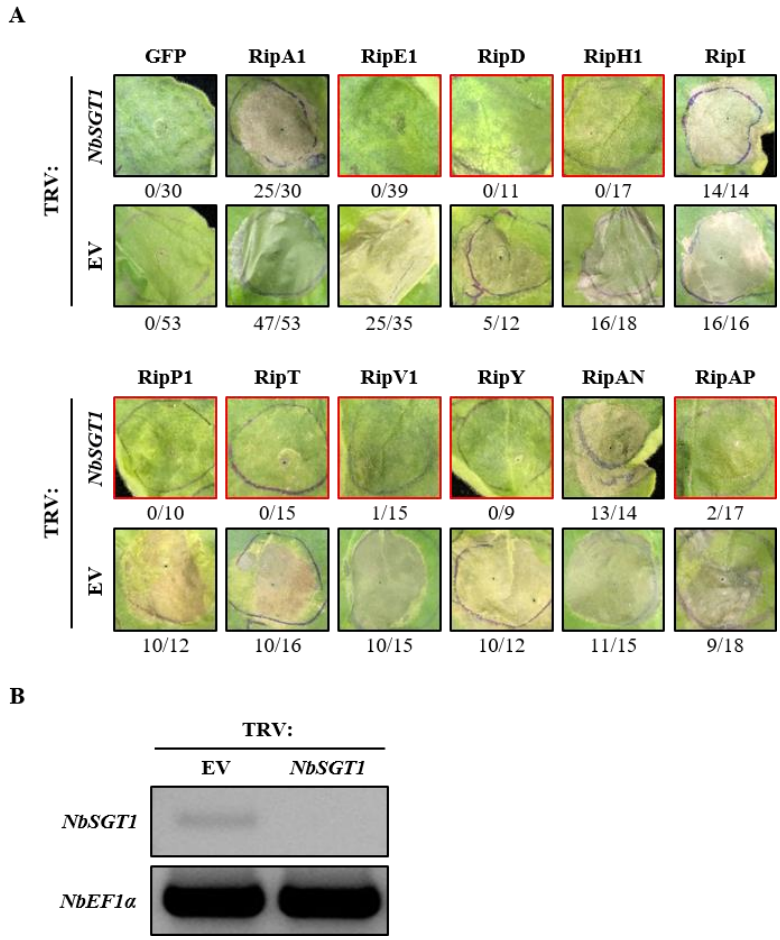

Figure 1-2. Several *Rps* T3Es induce *NbSGT1*-dependent cell death in *N. benthamiana*.

(A) Cell death induced by eight *Rps* T3Es was suppressed in *NbSGT1*-silenced plants. *Agrobacterium* strains carrying GFP or *Rps* T3Es (OD_{600}=0.4) were infiltrated in TRV:EV or TRV:*NbSGT1* plants. Pictures were taken 6 dpi under a bright field. The pictures labeled in red indicate the suppression of cell death induced by *Rps* T3Es in *NbSGT1*-silenced plants. Numbers indicate patches with cell death out of total infiltrated patches. (B) Semi-quantitative PCR of *NbSGT1* transcript in TRV:EV and TRV:*NbSGT1* plants. *NbEF1α* was used as a control.

Immune response activation by RipE1 and RipY in *N. benthamiana*

To confirm that the observed cell death is not due to the cell toxicity by pathogen effector expression, the physiological responses associated with plant immunity, including transcription regulation and restriction of pathogen growth, were examined in *N. benthamiana* leaves transiently expressing RipE1 or RipY. The activation of *HARPIN-INDUCED 1* (*HIN1*) and *HYPERSENSITIVE-RELATED* (*Hsr203J*) genes, which are activated during hypersensitive response (HR) in tobacco were monitored in *N. benthamiana* (Pontier et al., 1994; Gopalan et al., 1996). In accordance with cell death observation, RipE1 and RipY expression enhanced the accumulation of *HIN1* and *Hsr203J* transcripts in *N. benthamiana* (Figure 1-3A).

Next, it was investigated whether RipE1 and RipY could activate *N. benthamiana* immune responses that restrict pathogen growth. Chimeric constructs of RipE1 and RipY under the control of the AvrRps4 promoter and the AvrRps4 secretion signal peptide to deliver RipE1 and RipY through *Pseudomonas syringae* type III secretion system were generated (Sohn et al., 2007). Each construct was mobilized in the pathogenic *P. syringae* pv. *tomato* DC3000 strain lacking the recognized effector *HopQ1-1* (hereafter, *Pst* Δ*hopQ1-1*) (Wei et al., 2007; Wei et al., 2015). *P. syringae* effector HopQ1 activates *N. benthamiana* NLR Roq1, leading to bacterial growth restriction (Schultink et al., 2017; Mazo-Molina et al., 2020; Ahn et al., 2023). Therefore, *Pst*+EV was used as positive control for activation of immune responses. As expected, *Pst*+EV grew less than *Pst* Δ*hopQ1-1*+EV due to HopQ1 recognition by Roq1 (Figure 1-3B). Similarly, at both 3 and 6 dpi, *Pst* Δ*hopQ1-*

1+RipE1 and *Pst* Δ*hopQ1-1*+RipY reached growth levels about 10-fold and 100-fold lower than *Pst* Δ*hopQ1-1*+EV, respectively. This result indicates that T3SS-mediated delivery of RipE1 and RipY restricted the growth of *Pst* Δ*hopQ1-1* to a similar extent as the delivery of HopQ1. Altogether these results suggest that RipE1 and RipY are recognized by NLRs in *N. benthamiana*.

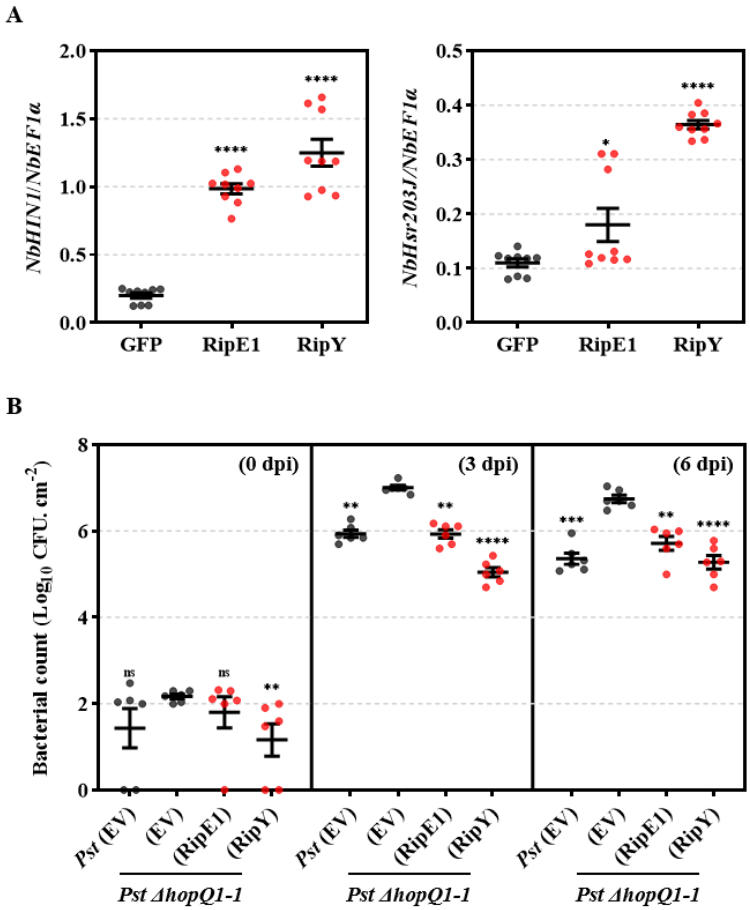

Figure 1-3. RipE1 and RipY activate *N. benthamiana* immune responses.

(A) Relative expression of the hypersensitive response marker genes, *NbHIN1* and *NbHsr203J*, was determined by quantitative RT-PCR and normalized by *NbEF1α*. Individual values from independent experiments are indicated as dots. Data were analyzed by one-way ANOVA followed by Dunnett's multiple comparison test. Asterisks indicate statistically significant differences with GFP (*, P<0.05; ****, P<0.0001). Bars represent mean ± SEM (n=9). (B) RipE1 and RipY recognition inhibits the growth of virulent bacteria in *N. benthamiana*. *Pseudomonas syringae* pv. *tomato* DC3000 (*Pst*) carrying empty vector (EV) and *Pst hopQ1-1* mutants (Δ*hopQ1-1*) carrying EV, RipE1, or RipY constructs were infiltrated at 10^5 CFU. ml^{-}

[1] in *N. benthamiana* leaves. Bacterial populations were counted at 0, 3, and 6 dpi. Individual values from independent experiments are indicated as dots. Data were analyzed with two-way ANOVA followed by Dunnett's multiple comparison test. Asterisks indicate statistically significant differences with Δ*hopQ1-1*+EV (**, $P<0.01$; ***, $P<0.001$; ****, $P<0.0001$; ns, not significant). Bars represent mean ± SEM (n=6).

Cell death induced by RipE1 and RipY is independent of EDS1 and helper NLRs.

The lipase-like protein EDS1 and the helper RNLs ADR1 and NRG1 are required for most TNL-mediated signaling pathways, whereas helper CNLs, NRC2a/b/c, NRC3, and NRC4, are required for multiple sensor CNLs from Solanaceae to activate immune responses (Parker et al., 1996; Peart et al., 2005; Collier et al., 2011; Wu et al., 2017; Qi et al., 2018; Dongus and Parker, 2021). To test whether the immune responses activated by RipE1 and RipY require these known regulators of NLR-mediated pathways, multiple VIGS was conducted to silence the immune signaling components in *N. benthamiana*.

The suppression of cell death triggered by RipE1 or RipY in *NbSGT1*-silenced plants was observed, which is consistent with Figure 1-2, was used as the silencing positive control (Figure 1-4A). Silencing of *NbEDS1* or *NbADR1*/*NbNRG1* did not impair RipE1- and RipY-induced cell death, while it abolished the cell death mediated by co-expression of the tobacco TNL N with tobacco mosaic virus protein p50 as previously reported (Figure 1-4A) (Peart et al., 2005; Qi et al., 2018). The combined silencing of *NbNRC2a/b/c*, *NbNRC3* and *NbNRC4* compromised the cell death mediated by immune receptors Pto and Rpi-blb2 when the corresponding effectors AvrPto from *P. syringae* and Avrblb2 from *P. infestans* were co-expressed, respectively (Wu et al., 2017) (Figure 1-4A). In contrast, RipE1 and RipY expression still induced cell death in TRV:*NbNRC2/3/4* plants. The cell death intensity was estimated by the measurement of the QY values. Consistent with occurrence of cell

death, RipY- or RipE1-expressing tissues displayed lower QY values than GFP-expressing tissues in the TRV:*NbEDS1*, TRV:*NbADR1*/*NbNRG1*, or TRV:*NbNRC2/3/4*-mediated silencing plants (Figure 1-4B). Silencing efficiency was confirmed by qRT-PCR analysis of each gene expression (Figure 1-4C). Altogether, these results indicate that cell death induced by RipE1 and RipY is independent on EDS1 and helper NLRs in *N. benthamiana*.

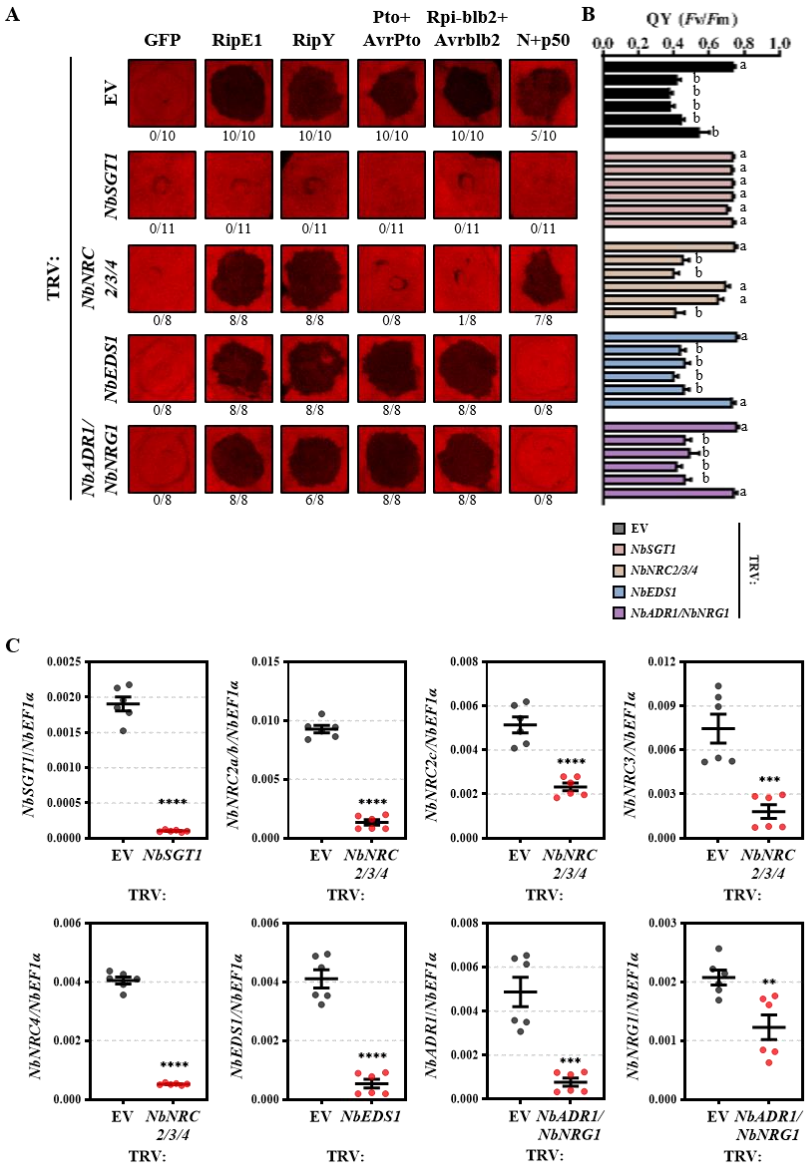

Figure 1-4. RipE1 and RipY-induced cell death is neither dependent on NbEDS1 nor helper NbNLRs.

(A) RipE1 and RipY-induced cell death was not suppressed in TRV:*NbNRC2*/*3*/*4*, TRV:*NbEDS1*, and TRV:*NbADR1/NbNRG1* plants. *Agrobacterium* strains carrying GFP, RipE1, RipY, or different combinations of immune receptor and effector (Pto

and AvrPto, Rpi-blb2 and Avrblb2, N and p50) were infiltrated (OD_{600}=0.5) in TRV:EV, TRV:*NbSGT1*, TRV:*NbNRC2/3/4*, TRV:*NbEDS1,* or TRV:*NbADR1/NbNRG1* plants. TRV:*NbSGT1* was used as a VIGS control. Pto/AvrPto and Rpi-blb2/Avrblb2 were used as controls for NRC2/3/4-dependent cell death. N and p50 were used as a control for TNL-mediated cell death. Pictures were taken at 4 dpi. Numbers indicate patches with cell death out of total infiltrated patches. (B) Quantum yield (QY, *F*v/*F*m) was measured in the infiltrated patches. Individual values from independent experiments are indicated as dots. Data were analyzed with two-way ANOVA followed by Dunnett's multiple comparisons test. Different letters indicate statistically significant differences (P<0.0001). Bars represent mean ± SEM (n=8-11). (C) Relative expression of the characterized signaling components *NbSGT1*, *NbNRC2/3/4, NbEDS1*, *NbADR1*, and *NbNRG1* was determined by quantitative RT-PCR and normalized by *NbEF1α*. Individual values from independent experiments are indicated as dots. Data were analyzed by *t*-test. Asterisks indicate statistically significant differences (**, P<0.01; ***, P<0.001; ****, P<0.0001). Bars represent mean ± SEM (n=6).

Identification of NLR candidates using a multiplexed NbNLR-VIGS library

To pinpoint the NLRs responsible for RipE1- and RipY-induced cell death from the NLR repertoire of *N. benthamiana* (Seong et al., 2020), an early version of the recently developed TRV-based NbNLR-VIGS library was used (Ahn et al., 2023). The NbNLR-VIGS library was composed of 47 constructs targeting approximately 345 putative NLRs in *N. benthamiana*. Out of the 47 TRV:Com constructs, TRV:Com1 and TRV:Com3-silenced plants showed the complete suppression of cell death induced by RipE1 or RipY expression, respectively (Figure 1-5).

As six fragments are concatenated in Com1 construct, different VIGS constructs (TRV:Com1-1 to Com1-6) were subcloned to narrow down NLR candidates. RipE1-induced cell death was specifically compromised in TRV:Com1-1 plants (Figure 1-6A). The Com1-1 fragment targets two NLR genes referred to as Gene A and Gene B (Figure 1-6B). To determine the NLR gene involved in RipE1 recognition, the sequence polymorphisms within candidates Gene A and Gene B were investigated (Figure 1-6B). Sanger's sequencing analysis confirmed the presence of Gene A type of polymorphism in the amplicon obtained from *N. benthamiana* cDNA (Figure 1-6C). Furthermore, CAPS assay demonstrated that the *Hin*dIII enzyme did not digest the amplicon from cDNA but did that from gDNA (Figure 1-6C). These findings suggest that both Gene A and Gene B are present in *N. benthamiana* genome, but only Gene A is expressed. As Gene A gene was a homolog of tomato *Ptr1* gene with 89% amino acid identity (Mazo-Molina et al., 2020), it was named *NbPtr1*.

Experiments similar to those described above were carried out to identify the

NLR candidate responsible for RipY recognition. The subcloned VIGS constructs (TRV:Com3-1 to Com3-6) were used to silence NLR candidates. RipY-induced cell death was specifically suppressed in TRV:Com3-1 plants (Figure 1-7A). The Com3-1 fragment targets two NLR genes named Gene C and Gene D (Figure 1-7B). Two sequence polymorphisms present in Gene C and Gene D (a SNP and a 57-bp deletion) were investigated (Figure 1-7B). Sanger's sequencing analysis confirmed the presence of Gene D type of polymorphism and the 57-bp deletion in the amplicon obtained from *N. benthamiana* cDNA (Figure 1-7C). Moreover, the amplicon from cDNA of *N. benthamiana* was digested by *Eco*RI treatment, and further an amplicon of less than 400-bp was generated from cDNA and gDNA in the InDel assay (Figure 1-7D). These data indicate that only Gene D was present in the *N. benthamiana* genome and expressed. As different annotations were predicted for Gene D gene structure, the full coding region of Gene D gene was determined by 3' rapid amplification of cDNA ends (RACE) PCR. Gene D gene identified here was named *RESISTANCE TO RALSTONIA SOLANACEARUM RIPY* (*RRS-Y*).

The expression of *Rps* T3E repertoire by agroinfiltration revealed that six *Rps* T3Es (RipD, RipH1, RipT, RipV1, RipY, and RipAP) were newly identified to induce SGT1-dependent cell death in *N. benthamiana*. These findings suggest that *N. benthamiana* immune system can detect diverse *Rps* T3Es in addition to RipB, RipE1, RipP1, RipAA, and RipBN, which are known avirulent effectors that activate immune responses in *N. benthamiana* (Carney and Denny, 1990; Poueymiro et al., 2009; Mazo-Molina et al., 2019; Nakano and Mukaihara, 2019; Jeon et al., 2020;

Sang et al., 2020). Notably, RipE1 and RipY not only induced cell death but also triggered ETI responses, such as the activation of defense-related gene expression and restriction of pathogen growth. Moreover, the reverse-genetic approach facilitated the identification of NbPtr1 and RRS-Y that recognize RipE1 and RipY, respectively, in *N. benthamiana*.

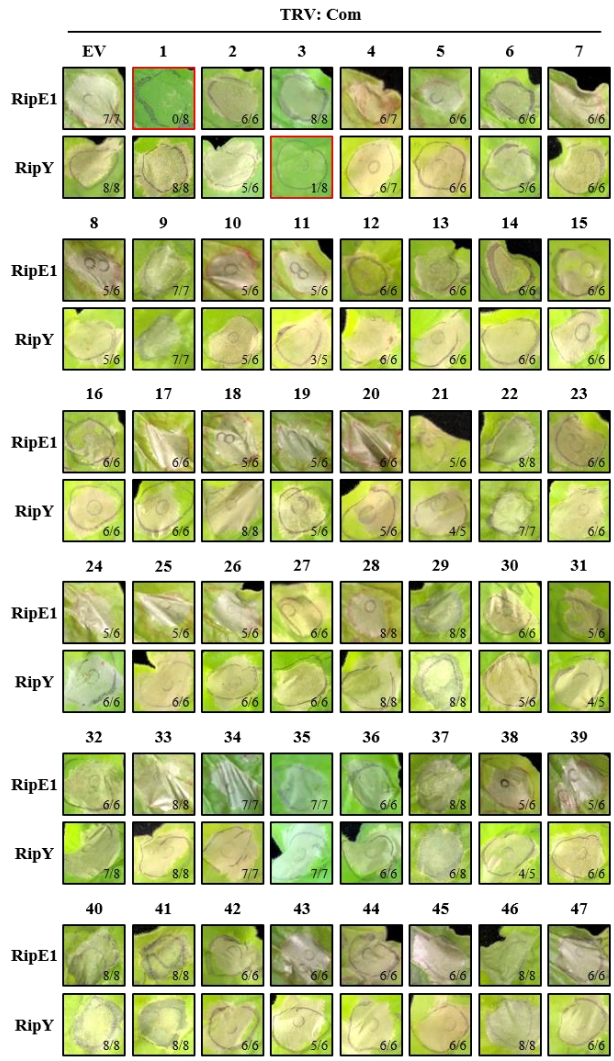

Figure 1-5. RipE1 and RipY-triggered cell death was compromised in *NbNLR*-silenced *N. benthamiana*.

Agrobacterium strains carrying RipE1 or RipY were infiltrated (OD_{600}=0.5) in TRV:EV or TRV:Com1 to Com47 plants. Pictures were taken at 4 dpi. The pictures labeled in red indicate the suppression of cell death induced by RipE1 and RipY in TRV:Com1 and TRV:Com3 plants, respectively. Numbers indicate patches with cell death out of total infiltrated patches.

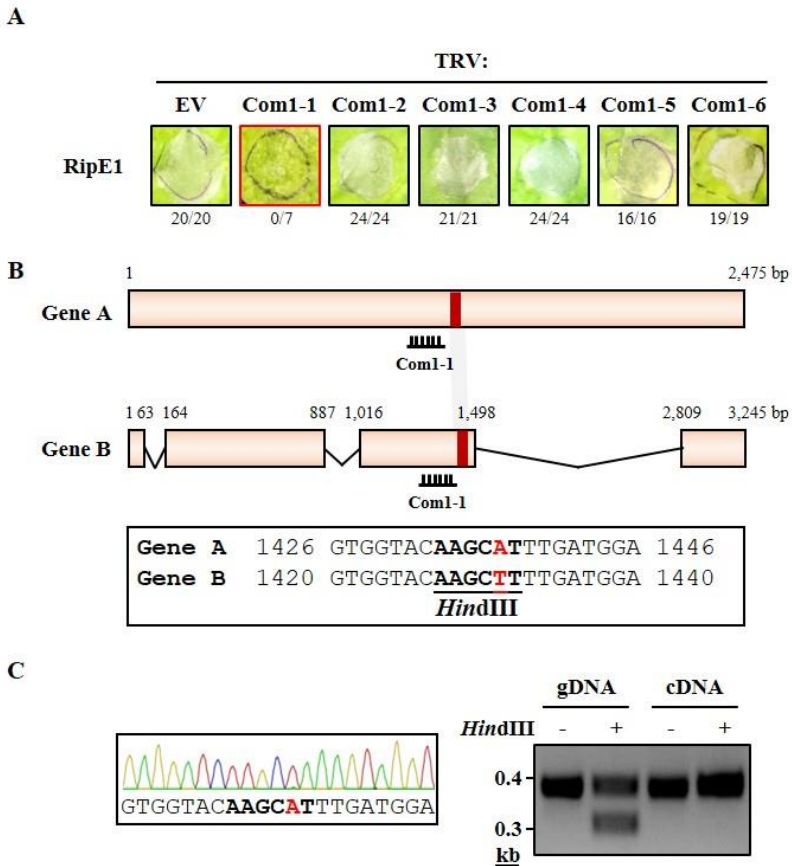

Figure 1-6. Gene A is a candidate NLR required for the RipE1 recognition in *N. benthamiana*.

(A) RipE1-induced cell death was compromised in TRV:Com1-1 plant. *Agrobacterium* strain carrying RipE1 was infiltrated (OD_{600}=0.5) in TRV:EV or TRV:Com1-1 to Com1-6 plants. Pictures were taken at 4 dpi. The picture labeled in red indicates the suppression of cell death induced by RipE1 in TRV:Com1-1 plant. Numbers indicate patches with cell death out of total infiltrated patches. (B) Schematic structures of two NLR genes (Gene A and Gene B) targeted by the Com1-1 fragment. Exons are represented as pink boxes (bp: base pair). Black lines indicate the position of Com1-1 fragment. The vertical red lines indicate the region of a SNP (A/T) on *Hin*dIII recognition sequence. (C) Sequencing analysis and CAPS assay. A

SNP from cDNA of *N. benthamiana* was confirmed using Sanger's sequencing analysis (left panel). The amplified fragments from gDNA and cDNA of *N. benthamiana* were digested with *Hin*dIII restriction enzyme (right panel) (kb, kilobase pair).

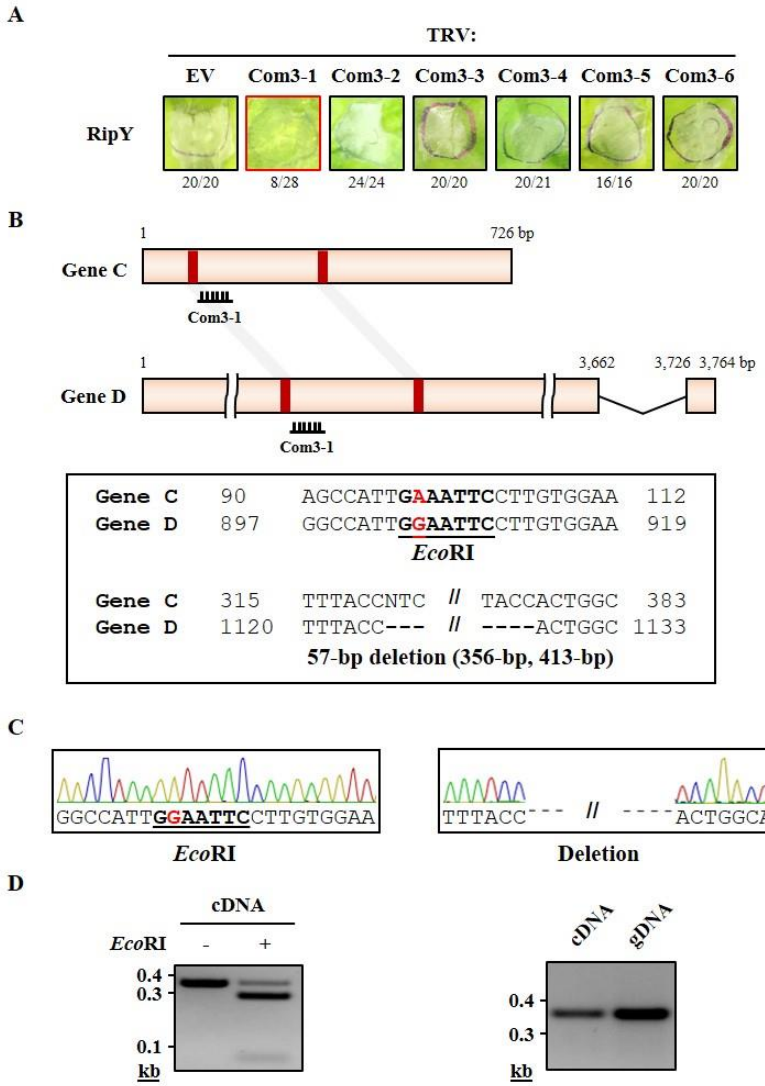

Figure 1-7. Gene D is a candidate NLR required for the RipY recognition in *N. benthamiana*.

(A) RipY-induced cell death was compromised in TRV:Com3-1 plant. *Agrobacterium* strain carrying RipY was infiltrated (OD_{600}=0.5) in TRV:EV and TRV:Com3-1 to Com3-6 plants. Pictures were taken at 4 dpi. The picture labeled in red indicate the suppression of cell death induced by RipY in TRV:Com3-1 plant. Numbers indicate patches with cell death out of total infiltrated patches. (B)

Schematic structures of two NLR genes targeted by the Com3-1 fragment (Gene C and Gene D) and locations of polymorphic regions. Exons are represented as pink boxes (bp: base pair). Black lines indicate the position of Com3-1 fragment. The vertical red lines indicate the regions of a SNP (A/G) on *Eco*RI recognition sequence and 57-bp deletion. (C) Sequencing analysis. A SNP and 57-bp deletion from cDNA of *N. benthamiana* were confirmed using Sanger's sequencing analysis (left and right panel, respectively). (D) CAPS and InDel assays. The DNA fragment amplified from cDNA of *N. benthamiana* was digested with *Eco*RI restriction enzyme (left panel). The size of amplicons from cDNA and gDNA of *N. benthamiana* was analyzed by agarose gel electrophoresis (right panel) (kb, kilobase pair).

DISCUSSION

Chapter 1 demonstrated that *Rps* effectors RipE1 and RipY are recognized by two NLRs, leading to the cell death and restrict pathogen growth in *N. benthamiana*. A series of functional screenings provided the following lines of evidence: (i) multiple *Rps* T3Es induced SGT1-dependent cell death in *N. benthamiana* (Figure 1-2); (ii) the recognition of RipE1 and RipY activates immune responses, which were not dependent on EDS1 nor helper NLRs (Figure 1-3 and 1-4); (iii) a NbNLR-VIGS library allowed to rapidly screen the one-to-one relationship between *Rps* effectors and putative NLRs in *N. benthamiana* (Figure 1-5). The discovery of new effector-NLR pairs will broaden the pool of genetic resistance resources and the understanding of the molecular mechanisms of NLR activation in plants.

Ralstonia species inject various effectors into host cells, and some effectors expose the pathogens to be recognized by the plant immune system (Landry et al., 2020). So far, two NLRs were cloned in Solanaceae plants although many effectors activate immune responses. The TNL Roq1 from *N. benthamiana* and CNL Ptr1 from tomato relative recognize RipB and RipBN, respectively (Schultink et al., 2017; Nakano and Mukaihara, 2019; Mazo-Molina et al., 2020). This study revealed that multiple *Rps* T3Es induce cell death that depends on SGT1 in *N. benthamiana* (Figure 1-2). Therefore, in addition to Roq1 and Ptr1, other unknown resistance proteins may detect different *Rps* T3Es and associate with the cell death induction in *N. benthamiana*. However, caution must be taken in the interpretation of results.

Silencing *NbSGT1* could impair *Agrobacterium*-mediated transient expression and subsequently affect the accumulation of heterologous proteins (Yu et al., 2019). Thus, immunoblot analysis for *Rps* T3Es should be conducted in *NbSGT1*-silenced plants.

The expression of RipA1, RipI, and RipAN still induced the cell death in *NbSGT*-silenced plants. The cell death induced by these effectors might be differentially regulated by other components of NLR chaperone complex (HSP90 and/or RAR1) (Shirasu., 2009). In addition, *Rps* effectors can play roles in pathogenesis as a necrosis-inducing effector. For example, one of T3Es RipBH promotes potato tuber cell death caused by *R. solanacearum* UW551 strain for pathogenesis (Zheng et al., 2023). Thus, the cell death induced by some *Rps* effectors in *NbSGT*-VIGS plants may function as virulence factors to promote disease.

Rps GMI1000 strain is unable to cause bacterial wilt disease in *N. benthamiana* because of the presence of RipP1 and RipAA (Poueymiro et al., 2009). Although RipE1, another avirulent effector from same GMI1000 strain, also triggers immunity in *N. benthamiana*, other *Rps* T3Es – notable RipAC and RipAY have evolved to inhibit RipE1-triggered immunity (Sang et al., 2018; Yu et al., 2020). Therefore, the cell death induced by multiple *Rps* T3Es may be counteracted by other effectors present in *Rps* strains to suppress immune responses in *N. benthamiana*. Pathogens can also evade plant immune system by deleting or impairing the genes of avirulence factors in their genome. Contrary to GMI1000 strain, *Rps* Y45 strain causes bacterial wilt disease in *N. benthamiana* and has small number of T3Es (32 T3Es while GMI1000 has ~70 T3Es) (Li et al., 2011; Sabbagh et al., 2019). This strains lacks or

has pseudogene copy of known avirulent effectors (RipB, RipE1, RipP1, RipAA, RipBN) (Carney and Denny, 1990; Poueymiro et al., 2009; Mazo-Molina et al., 2019; Nakano and Mukaihara, 2019; Jeon et al., 2020; Sang et al., 2020). Interestingly, Y45 strain also lacks RipD, RipH1, RipV1, and RipY, which were shown in this study, to induce immune-associated cell death in *N. benthamiana*. This suggests that the loss of avirulent or cell death-inducing effectors in Y45 may be an adaptation to avoid recognition by *N. benthamiana* immune system.

Advance of sequencing techniques and bioinformatics provides genome-wide NLR analysis in *N. benthamiana* (Bombarely et al., 2012; Seong et al., 2020). Taking advantage of easy application of genetic tools in *N. benthamiana* (Derevnina et al., 2019), new methodologies are recently developed to allow rapid identification of a matching NLR required for recognition of pathogen effector that induce cell death. For example, a hairpin-RNAi library was developed to screen 345 putative NLR genes and could be applied to identify a matching NLR required for recognition of effectors from any plant pathogens that induce cell death in *N. benthamiana* (Brendolise et al., 2017). With improved NLR annotation data, a TRV-based NbNLR-VIGS library was designed (Ahn et al., 2023). Using this reverse-genetic methodology, large-scale screens were conducted and two NLRs NbPtr1 and RRS-Y were rapidly identified in *N. benthamiana* (Figure 1-5, 1-6, and 1-7). Even though NbNLR-VIGS library is efficient, robust, or fast methodology to screen genome-wide NLRs in *N. benthamiana*, several limits should be considered: (i) non-canonical resistance genes may be missed in the screens using this library; (ii) NLRs can have

redundant function; (iii) there may be other components required for effector recognition or initiating signaling pathway. Therefore, the results obtained from this library screens should be carefully interpreted.

Many NLRs act as sensor NLRs by detecting effectors or effector-modified host components and work together helper NLRs to translate the immune signals. Two CNLs PSEUDOMONAS SYRINGAE PV. MACULICOLA 1 (RPM1) and ZAR1 are considered as singletons that both sense effectors and translate the immune signals alone (Ngou et al., 2022). Interestingly, RipE1- and RipY-induced cell death did not require any known helpers NRG1, ADR1, or NRC network in *N. benthamiana* (Figure 1-4). Taken together, these data indicate that NbPtr1 or RRS-Y may act as a sensor NLR through unknown signaling pathways or as a singleton like RPM1 or ZAR1 (Ngou et al., 2022). It would be interesting to investigate whether these two NLRs require other genetic components or form oligomers to induce cell death.

REFERENCES

Ahn, Y.J., Kim, H., Choi, S., Mazo-Molina, C., Prokchorchik, M., Zhang, N., Kim, B., Mang, H., Yoon, H., Segonzac, C., et al. (2023). Ptr1 and ZAR1 immune receptors confer overlapping and distinct bacterial pathogen effector specificities. *New Phytol.* **239**: 1935–1953.

Azevedo, C., Sadanandom, A., Kitagawa, K., Freialdenhoven, A., Shirasu, K., and Schulze-Lefert, P. (2002). The RAR1 interactor SGT1, an essential component of *R* gene-triggered disease resistance. *Science* **295**:2073–2076.

Bombarely, A., Rosli, H.G., Vrebalov, J., Moffett, P., Mueller, L.A., and Martin, G.B. (2012). A draft genome sequence of *Nicotiana benthamiana* to enhance molecular plant-microbe biology research. *Mol. Plant Microbe Interact.* **25**:1523–1530.

Brendolise, C., Montefiori, M., Dinis, R., Peeters, N., Storey, R.D., and Rikkerink, E.H. (2017). A novel hairpin library-based approach to identify NBS–LRR genes required for effector-triggered hypersensitive response in *Nicotiana benthamiana*. *Plant Methods* **13**:32.

Carney, B.F., and Denny, T.P. (1990). A cloned avirulence gene from *Pseudomonas solanacearum* determines incompatibility on *Nicotiana tabacum* at the host species level. *J. Bacteriol.* **172**:4836–4843.

Choi, S., Jayaraman, J., Segonzac, C., Park, H.-J., Park, H., Han, S.-W., and Sohn, K.H. (2017). *Pseudomonas syringae* pv. *actinidiae* type III effectors localized at multiple cellular compartments activate or suppress innate immune responses in *Nicotiana benthamiana*. *Front. Plant Sci.* **8**:2157.

Collier S.M., Hamel L.-P., and Moffett P. (2011). Cell death mediated by the N-terminal domains of a unique and highly conserved class of NB-LRR protein. *Mol. Plant Microbe Interact.* **24**:918–931.

Derevnina, L., Kamoun, S., and Wu, C. (2019). Dude, where is my mutant?

Nicotiana benthamiana meets forward genetics. *New Phytol.* **221**:607–610.

Deslandes, L., Pileur, F., Liaubet, L., Camut, S., Can, C., Williams, K., Holub, E., Beynon, J., Arlat, M., and Marco, Y. (1998). Genetic characterization of *RRS1*, a recessive locus in *Arabidopsis thaliana* that confers resistance to the bacterial soilborne pathogen *Ralstonia solanacearum*. *Mol. Plant Microbe Interact.* **11**:659–667.

Deslandes, L., Olivier, J., Theulières, F., Hirsch, J., Feng, D.X., Bittner-Eddy, P., Beynon, J., and Marco, Y. (2002). Resistance to *Ralstonia solanacearum* in *Arabidopsis thaliana* is conferred by the recessive *RRS1-R* gene, a member of a novel family of resistance genes. *Proc. Natl. Acad. Sci. U.S.A.* **99**:2404–2409.

Dongus, J.A., and Parker, J.E. (2021). EDS1 signalling: At the nexus of intracellular and surface receptor immunity. *Curr. Opin. Plant Biol.* **62**:102039.

Engler, C., Kandzia, R., and Marillonnet, S. (2008). A one pot, one step, precision cloning method with high throughput capability. *PLoS One* **3**:e3647.

Gopalan, S., Wei, W., and He, S.Y. (1996). *hrp* gene-dependent induction of *hin1*: a plant gene activated rapidly by both harpins and the *avrPto* gene-mediated signal. *Plant J.* **10**:591–600.

Hayward, A.C. (1991). Biology and epidemiology of bacterial wilt caused by *Pseudomonas solanacearum*. *Annu. Rev. Phytopathol.* **29**:65–87.

Jayaraman, J., Choi, S., Prokchorchik, M., Choi, D.S., Spiandore, A., Rikkerink, E.H., Templeton, M.D., Segonzac, C., and Sohn, K.H. (2017). A bacterial acetyltransferase triggers immunity in *Arabidopsis thaliana* independent of hypersensitive response. *Sci. Rep.* **7**:3557.

Jeon, H., Kim, W., Kim, B., Lee, S., Jayaraman, J., Jung, G., Choi, S., Sohn, K.H., and Segonzac, C. (2020). *Ralstonia solanacearum* type III effectors with predicted nuclear localization signal localize to various cell compartments and modulate immune responses in *Nicotiana* spp. *Plant Pathol. J.* **36**:43–53.

Jones, A.M., Coimbra, S., Fath, A., Sottomayor, M., and Thomas, H. (2001). Programmed cell death assays for plants. *Methods Cell Biol.* **66**:437–451.

Kim, B., Choi, J., and Segonzac, C. (2022). Tackling multiple bacterial diseases of Solanaceae with a handful of immune receptors. *Hortic. Environ. Biotechnol.* **63**:149–160.

Landry, D., González-Fuente, M., Deslandes, L., and Peeters, N. (2020). The large, diverse, and robust arsenal of *Ralstonia solanacearum* type III effectors and their in planta functions. *Mol. Plant Pathol.* **21**:1377–1388.

Lee, H.-Y., Mang, H., Choi, E., Seo, Y.-E., Kim, M.-S., Oh, S., Kim, S.-B., and Choi, D. (2021). Genome-wide functional analysis of hot pepper immune receptors reveals an autonomous NLR clade in seed plants. *New Phytol.* **229**:532–547.

Li, Z., Wu, S., Bai, X., Liu, Y., Lu, J., Liu, Y., Xiao, B., Lu, X., and Fan, L. (2011). Genome sequence of the tobacco bacterial wilt pathogen *Ralstonia solanacearum*. *J. Bacteriol.* **193**:6088–6089.

Liu, Y., Schiff, M., Marathe, R., and Dinesh-Kumar, S.P. (2002). Tobacco *Rar1*, *EDS1* and *NPR1/NIM1* like genes are required for *N*-mediated resistance to tobacco mosaic virus. *Plant J.* **30**:415–429.

Livak, K.J., and Schmittgen, T.D. (2001). Analysis of relative gene expression data using real-time quantitative PCR and the 2(-Delta Delta C(T)) method. *Methods* **25**:402–408.

Macho, A.P., Guidot, A., Barberis, P., Beuzón, C.R., and Genin, S. (2010). A competitive index assay identifies several *Ralstonia solanacearum* type III effector mutant strains with reduced fitness in host plants. *Mol. Plant Microbe Interact.* **23**:1197–1205.

Mansfield, J., Genin, S., Magori, S., Citovsky, V., Sriariyanum, M., Ronald, P., Dow, M., Verdier, V., Beer, S.V., Machado, M.A., et al. (2012). Top 10 plant pathogenic bacteria in molecular plant pathology. *Mol. Plant Pathol.* **13**:614–629.

Mazo-Molina, C., Mainiero, S., Hind, S.R., Kraus, C.M., Vachev, M., Maviane-

Macia, F., Lindeberg, M., Saha, S., Strickler, S.R., Feder, A., et al. (2019). The *Ptr1* locus of *Solanum lycopersicoides* confers resistance to race 1 strains of *Pseudomonas syringae* pv. *tomato* and to *Ralstonia pseudosolanacearum* by recognizing the type III effectors AvrRpt2 and RipBN. *Mol. Plant Microbe Interact.* **32**:949–960.

Mazo-Molina, C., Mainiero, S., Haefner, B.J., Bednarek, R., Zhang, J., Feder, A., Shi, K., Strickler, S.R., and Martin, G.B. (2020). Ptr1 evolved convergently with RPS2 and Mr5 to mediate recognition of AvrRpt2 in diverse solanaceous species. *Plant J.* **103**:1433–1445.

Nakano, M., and Mukaihara, T. (2019). The type III effector RipB from *Ralstonia solanacearum* RS1000 acts as a major avirulence factor in *Nicotiana benthamiana* and other *Nicotiana* species. *Mol. Plant Pathol.* **20**:1237–1251.

Narusaka, M., Shirasu, K., Noutoshi, Y., Kubo, Y., Shiraishi, T., Iwabuchi, M., and Narusaka, Y. (2009). RRS1 and RPS4 provide a dual *Resistance*-gene system against fungal and bacterial pathogens. *Plant J.* **60**:218–226.

Ngou, B.P.M., Jones, J.D.G., and Ding, P. (2022). Plant immune networks. *Trends Plant Sci.* **27**:255–273.

Parker, J.E., Holub, E.B., Frost, L.N., Falk, A., Gunn, N.D., and Daniels, M.J. (1996). Characterization of *eds1*, a mutation in Arabidopsis suppressing resistance to *Peronospora parasitica* specified by several different *RPP* genes. *Plant Cell* **8**:2033–2046.

Peart, J.R., Mestre, P., Lu, R., Malcuit, I., and Baulcombe, D.C. (2005). NRG1, a CC-NB-LRR protein, together with N, a TIR-NB-LRR protein, mediates resistance against tobacco mosaic virus. *Curr. Biol.* **15**:968–973.

Peeters, N., Carrère, S., Anisimova, M., Plener, L., Cazalé, A.-C., and Genin, S. (2013b). Repertoire, unified nomenclature and evolution of the type III effector gene set in the *Ralstonia solanacearum* species complex. *BMC Genom.* **14**:859.

Pontier, D., Godiard, L., Marco, Y., and Roby, D. (1994). *hsr203J*, a tobacco gene whose activation is rapid, highly localized and specific for incompatible

plant/pathogen interactions. *Plant J.* **5**:507–521.

Poueymiro, M., Cunnac, S., Barberis, P., Deslandes, L., Peeters, N., Cazale-Noel, A.-C., Boucher, C., and Genin, S. (2009). Two type III secretion system effectors from *Ralstonia solanacearum* GMI1000 determine host-range specificity on tobacco. *Mol. Plant Microbe Interact.* **22**:538–550.

Prior, P., Ailloud, F., Dalsing, B.L., Remenant, B., Sanchez, B., and Allen, C. (2016). Genomic and proteomic evidence supporting the division of the plant pathogen *Ralstonia solanacearum* into three species. *BMC Genom.***17**:90.

Prokchorchik, M., Pandey, A., Moon, H., Kim, W., Jeon, H., Jung, G., Jayaraman, J., Poole, S., Segonzac, C., Sohn, K.H., et al. (2020). Host adaptation and microbial competition drive *Ralstonia solanacearum* phylotype I evolution in the Republic of Korea. *Microb. Genom.* **6**:mgen000461

Qi, T., Seong, K., Thomazella, D.P.T., Kim, J.R., Pham, J., Seo, E., Cho, M.-J., Schultink, A., and Staskawicz, B.J. (2018). NRG1 functions downstream of EDS1 to regulate TIR-NLR-mediated plant immunity in *Nicotiana benthamiana*. *Proc. Natl. Acad. Sci. U.S.A.* **115**:E10979–E10987.

Sabbagh, C.R.R., Carrere, S., Lonjon, F., Vailleau, F., Macho, A.P., Genin, S., and Peeters, N. (2019). Pangenomic type III effector database of the plant pathogenic *Ralstonia* spp. *PeerJ* **7**:e7346.

Sang, Y., Wang, Y., Ni, H., Cazalé, A.-C., She, Y.-M., Peeters, N., and Macho, A.P. (2018). The *Ralstonia solanacearum* type III effector RipAY targets plant redox regulators to suppress immune responses. *Mol. Plant Pathol.* **19**:129–142.

Sang, Y., Yu, W., Zhuang, H., Wei, Y., Derevnina, L., Yu, G., Luo, J., and Macho, A.P. (2020). Intra-strain elicitation and suppression of plant immunity by *Ralstonia solanacearum* type-III effectors in *Nicotiana benthamiana*. *Plant Commun.* **1**:100025.

Schultink, A., Qi, T., Lee, A., Steinbrenner, A.D., and Staskawicz, B.J. (2017).

Roq1 mediates recognition of the *Xanthomonas* and *Pseudomonas* effector proteins XopQ and HopQ1. *Plant J.* **92**:787–795.

Seong, K., Seo, E., Witek, K., Li, M., and Staskawicz, B.J. (2020). Evolution of NLR resistance genes with noncanonical N-terminal domains in wild tomato species. *New Phytol.* **227**:1530–1543.

Shirasu, K. (2009). The HSP90-SGT1 chaperone complex for NLR immune sensors. *Annu. Rev. Plant Biol.* **60**:139–164.

Sohn, K.H., Lei, R., Nemri, A., and Jones, J.D.G. (2007). The downy mildew effector proteins ATR1 and ATR13 promote disease susceptibility in *Arabidopsis thaliana*. *Plant Cell* **19**:4077–4090.

Tran, P.-T., Choi, H., Choi, D., and Kim, K.-H. (2016). Virus-induced gene silencing reveals signal transduction components required for the Pvr9-mediated hypersensitive response in *Nicotiana benthamiana*. *Virology* **495**:167–172.

Thomas, N.C., Hendrich, C.G., Gill, U.S., Allen, C., Hutton, S.F., and Schultink, A. (2020). The immune receptor Roq1 confers resistance to the bacterial pathogens *Xanthomonas*, *Pseudomonas syringae*, and *Ralstonia* in tomato. *Front. Plant Sci.* **11**:463.

Wei, C.-F., Kvitko, B.H., Shimizu, R., Crabill, E., Alfano, J.R., Lin, N.-C., Martin, G.B., Huang, H.-C., and Collmer, A. (2007). A *Pseudomonas syringae* pv. *tomato* DC3000 mutant lacking the type III effector HopQ1-1 is able to cause disease in the model plant *Nicotiana benthamiana*. *Plant J.* **51**:32–46.

Wei, H.-L., Chakravarthy, S., Mathieu, J., Helmann, T.C., Stodghill, P., Swingle, B., Martin, G. B., and Collmer, A. (2015). *Pseudomonas syringae* pv. *tomato* DC3000 type III secretion effector polymutants reveal an interplay between HopAD1 and AvrPtoB. *Cell Host Microbe* **17**:752–762.

Wu, C.-H., Abd-El-Haliem, A., Bozkurt, T.O., Belhaj, K., Terauchi, R., Vossen, J.H., and Kamoun, S. (2017). NLR network mediates immunity to diverse plant pathogens. *Proc. Natl. Acad. Sci. U.S.A.* **114**:8113–8118.

Yu, G., Xian, L., Sang, Y., and Macho, A.P. (2019). Cautionary notes on the use of *Agrobacterium*-mediated transient gene expression upon *SGT1* silencing in *Nicotiana benthamiana*. *New Phytol.* **222**:14–17.

Yu, G., Xian, L., Xue, H., Yu, W., Rufian, J.S., Sang, Y., Morcillo, R.J.L., Wang, Y., and Macho, A.P. (2020). A bacterial effector protein prevents MAPK-mediated phosphorylation of SGT1 to suppress plant immunity. *PLoS Pathog.* **16**:e1008933.

Zheng, X., Huang, M., Tan, X., Wang, B., Li, Y., Xue, H., Cheng, D., Qiu, H., Li, W., Song, B., et al. (2023). A toxic ankyrin cysteine protease effector RipBH of brown rot triggered autophagy-associated cell death. *BioRxiv* https://doi.org/10.1101/2023.03.08.531657.

CHAPTER 2

NbPtr1 mediates the recognition of the *Ralstonia pseudosolanacearum* effector RipE1 at plasma membrane in *Nicotiana benthamiana*

I acknowledge that some parts in this chapter either quote or alter from "The *Ralstonia pseudosolanacearum* effector RipE1 is recognized at the plasma membrane by *NbPtr1*, *Nicotiana benthamiana* homolog of *Pseudomonas tomato race 1*" published online in Molecular Plant Pathology (DOI: http://doi.org/10.1111/mpp.13363).

ABSTRACT

NbPtr1, the *Nicotiana benthamiana* homolog of *Solanum lycopersicoides PSEUDOMONAS TOMATO RACE 1* (Ptr1), activates immune responses upon RipE1 recognition and confers resistance to bacterial pathogen carrying RipE1. Here, the experiments highlight the role of NbPtr1 and RipE1 localization on the plasma membrane for RipE1 recognition in *N. benthamiana*. Reverse genetic screens and genetic complementation assays were used to demonstrate that NbPtr1 genetically mediates RipE1 recognition in *N. benthamiana*. Specific silencing of *NbPtr1* completely abolished RipE1-induced hypersensitive response and immunity to *Ralstonia pseudosolanacearum* (*Rps*). In Nb-*ptr1* knock-out plants, expression of the native *NbPtr1* coding sequence was sufficient to restore RipE1 recognition. In addition to the putative catalytic triad cysteine-histidine-aspartate, RipE1 association with the host cell plasma membrane was found necessary for NbPtr1-dependent recognition. Moreover, RipE1 has a predicted proteolytic activity, and biochemical analysis showed that RipE1 expression correlated with the degradation of RPM1-INTERACTING PROTEIN (RIN4), the proposed guardee of Ptr1. These findings provide an additional evidence for the indirect mode of activation of NbPtr1, and supports NbPtr1 relevance for resistance to bacterial wilt disease in Solanaceae.

INTRODUCTION

Ralstonia species causing bacterial wilt disease are considered as one of the most devastating plant bacterial pathogens worldwide. These bacteria form a heterogeneous species complex termed *Ralstonia solanacearum* species complex (RSSC) due to their extensive diversity. Individual RSSC isolates deploy an unusually large number of T3Es that collectively contribute to pathogenicity and virulence (Landry et al., 2020). Although the comparisons of effector repertoire across RSSC isolates revealed a large variation, around 30 effector families are broadly present and considered as "core effectors" (Peeters et al., 2013; Sabbagh et al., 2019). Identification and characterization of nucleotide-binding leucine-rich repeats receptors (NLRs) that recognize these core effectors are major topics of interest in the field of plant–microbe interaction.

RipE1 is one of the core effectors in *R. pseudosolanacearum* (*Rps*), *R. solanacearum* and *R. syzygii* strains isolated from diverse plant species (Mukaihara et al., 2010; Sabbagh et al., 2019). RipE1 sequence bears homology with *Pseudomonas syringae* and *Xanthomonas* spp. effectors belonging to AvrPphE/HopX family, and harbors the conserved cysteine-histidine-aspartate catalytic triad and domain A (Nimchuk et al., 2007; Gimenez-Ibanez et al., 2014; Sang et al., 2020). Similar to other members of the AvrPphE/HopX family, RipE1 expression also induces a robust cell death, indicative of its recognition by the plant immune system (Mansfield et al., 1994; Nimchuk et al., 2007; Jeon et al., 2020; Sang

et al., 2020). Consistently, RipE1 expression leads to the induction of defense-associated gene expression, accumulation of salicylic acid and reduced susceptibility to *Rps* in *N. benthamiana* and *Arabidopsis thaliana* (Sang et al., 2020). A putative catalytic cysteine (C172) is required for RipE1-triggered immunity (Sang et al., 2020).

In chapter 1, a reverse-genetic approach led to the identification of two NLRs required for the recognition of two effectors of *Rps* in *N. benthamiana*. One NLR that mediates RipE1 recognition was named *NbPtr1*, for it is the *N. benthamiana* homolog of *Solanum lycopersicoides* CNL PSEUDOMONAS TOMATO RACE 1 (Ptr1). Ptr1 recognizes the *P. syringae* effector AvrRpt2 and its homolog in *Rps* effector RipBN (Mazo-Molina et al., 2020). While Ptr1 activation mechanism is not yet fully understood, evidence suggests that Ptr1 monitors the state of the plasma membrane-associated RPM1-INTERACTING PROTEIN 4 (RIN4), which is cleaved in presence of the cysteine-protease effectors AvrRpt2 or RipBN (Axtell and Staskawicz, 2003; Mackey et al., 2003; Takemoto and Jones, 2005; Mazo-Molina et al., 2019; Mazo-Molina et al., 2020). In line with this hypothesis, NbPtr1 was recently shown to contribute to the recognition of multiple effectors from other bacteria (*P. syringae* HopZ5, AvrRpm1, AvrB and *X. euvesicatoria* AvrBsT). These effectors are sequence-unrelated to AvrRpt2 but known to modify RIN4 (Chung et al., 2011; Liu et al., 2011; Choi et al., 2021; Ahn et al., 2023).

Here, NbPtr1 was genetically required for the RipE1 recognition using alternative silencing fragments that specifically target *NbPtr1* and a series of genetic

complementation assays in the *NbPtr1*-silenced or knock-out lines. Moreover, NbPtr1 activation led to the immune responses against *Rps* carrying RipE1. RipE1 recognition was dependent on its association with the host cell plasma membrane. Finally, RIN4 degradation in presence of RipE1 supports an indirect mode of action of NbPtr1.

MATERIALS AND METHODS

Plant growth conditions

Nicotiana benthamiana plants were grown in a growth chamber under long-day conditions with 16 h: 8 h, light: dark at 24-26℃ for 4-5 weeks before bacterial infiltration. The stable Nb-*ptr1* knockout plants with a 61-bp deletion induced in the *NbPtr1* coding sequence using a CRISPR were provided by Prof. Gregory Martin's laboratory (Cornell University, USA) (Ahn et al., 2023).

Bacterial strains

Bacterial strains used in this study were *Escherichia coli* DH5α and *A. tumefaciens* AGL1. *E. coli* DH5α and *A. tumefaciens* strains were grown on Low-salt Luria-Bertani medium at 37°C and 28°C, respectively. All bacteria were grown on solid medium for 2 days (1 day for *E. coli*) with appropriate antibiotics. Single colonies were inoculated on liquid medium overnight in a shaker at 200 rpm. Bacterial suspensions were harvested by centrifugation for subsequent experiments.

Plasmid vectors and constructs

Golden Gate compatible gene modules (~1 kb) were amplified by standard PCR with flanking *Bsa*I restriction sites (Engler et al., 2008). RipE1-C172A and RipE1-C172A/H203A/D222A (CHD), and RipE1-C11A were generated using site-directed mutagenesis. The truncated variant RipE1-ΔN86 lacking the first N-terminal 86

amino acids was amplified from the RipE1-wild type (WT) module. The primer sequences are listed in Table 2-1. The NbPtr1 constructs (native NbPtr1 and synthetic NbPtr1 (NbPtr1^{syn})) were provided by Prof. Kee Hoon Sohn's laboratory (Seoul National University, Korea). For *Agrobacterium*-mediated expression, the modules were assembled into the binary vector pICH86988 in fusion with C-terminal epitopes 3xFLAG, 6xHA, or YFP under the control of the 35S cauliflower mosaic virus promoter. Binary vectors were mobilized into *A. tumefaciens* AGL1 using electroporation.

Hypersensitive response cell death assay and quantification

Agrobacterium cells grown in liquid culture were centrifuged at 8,000 rpm and resuspended in infiltration buffer (10 mM $MgCl_2$, 10 mM MES-KOH pH5.6). Cell suspensions were adjusted to proper OD_{600} values and then infiltrated into the leaves of 4 or 5-week old *N. benthamiana* using a needless syringe. The occurrence of cell death was observed and photographed in visible or LED light with red-orange 617 nm and cool white 6500 K at 3 or 4 days post infiltration (dpi). The extent of cell death was estimated by the quantum yield of chlorophyll fluorescence (F_v/F_m, QY) using a closed FluorCam (Photon Systems Instruments, Czech Republic). The default F_v/F_m protocol from FluorCam 7.0 software was used to determine minimum fluorescence (F_0), maximum fluorescence (F_m) and maximum quantum yield of photosystem II (F_v/F_m). The F_v/F_m value of approximately 0.7 is indicative of healthy leaves (Jones et al., 2001; Lee et al., 2021). Each experiment was conducted

independently at least three times, and the combined values were analyzed with ANOVA and appropriate multiple comparison tests using the GraphPad Prism9 software.

Gene expression

Leaf discs of *N. benthamiana* were collected and immediately frozen. Total RNA was isolated using Trizol reagent (Invitrogen, USA) and reverse transcription was performed using Maxima First Strands cDNA Synthesis kit (Thermo Scientific, USA) with 2 μg RNA. Quantitative PCR was conducted on the cDNA using GoTaq qPCR Master Mix (Promega, USA) in the CFX96 Thermal Cycler (Bio-rad, USA). The relative expression was determined using the comparative 2(-Delta Delta C(t)) method and *NbEF1α* as reference (Livak and Schmittgen, 2001). Primers used in quantitative PCR are listed in Table 2-1. All the experiments were repeated at least three times independently and merged values were analyzed with ANOVA and appropriate multiple comparison tests using the GraphPad Prism9 software.

Bacterial growth assay

Rps growth assay was performed by Wenjia Yu in the licensed laboratory of Dr Alberto Macho (Shanghai Center for Plant Stress Biology, China) (Yu and Macho, 2021). Briefly, 4-5 weeks old *N. benthamiana* plants were infiltrated with the indicated Agrobacteria suspension 24 h prior to *Rps* Y45 infection. Leaf discs (4 mm diameter) were harvested at 2 dpi, homogenized and serially diluted in sterile

distilled water before plating on solid phi medium with appropriate antibiotics. Bacterial colonies were enumerated after 2 days incubation at 28℃.

Virus-induced gene silencing

The tobacco rattle virus (TRV)-based vectors (TRV1 and pTRV2) were used for gene-silencing in *N. benthamiana* (Liu et al., 2002). A 1 : 1 ratio mixture of *A. tumefaciens* carrying TRV1 and TRV2 at OD_{600} of 0.5 was infiltrated into cotyledons of two-week-old *N. benthamiana* seedlings. The plants were grown for 4 to 5 weeks before *A. tumefaciens* carrying constructs were infiltrated for transient expression of the gene of interest. For VIGS of *NbPtr1*, short specific fragments (~200-bp) targeting the coding region were designed using Sol Genomics Network VIGS tool (vigs.solgenomics.net), amplified using PCR, and ligated into TRV2 between *Eco*RI and *Bam*HI sites (Table 2-1).

Immunoblot analysis

N. benthamiana leaves were infiltrated with *Agrobacterium* strains carrying desired constructs. Before tissue collapse, leaf tissues were collected and snap-frozen in liquid nitrogen. The frozen tissues were then ground into fine powder in liquid nitrogen. The powder was resuspended in an equal volume of GTEN buffer (10 % glycerol, 50 mM Tris-HCl pH 7.5, 2 mM EDTA, 150 mM NaCl) supplemented with 5 mM DTT, cOmplete protease inhibitor cocktail (1 tablet/40 ml extraction buffer) (Roche, Germany), 0.2% NP-40, and 1% PVPP, and then thawed in ice. The samples

were centrifuged at 1,500*g* at 4°C for 10 min, and the supernatant was filtered through MiraCloth (Millipore, USA). The samples were denatured in 3xSDS protein loading buffer at 96°C for 10 min, separated on SDS-polyacrylamide gel electrophoresis (SDS-PAGE), and blotted on PVDF membranes. The membranes were probed with horseradish peroxidase-conjugated antibodies specific for primary anti-FLAG (Sigma Aldrich, USA), anti-HA (Santa-Cruz, USA), anti-GFP (Santa-Cruz, USA), anti-myc (Cell Signaling Technology, USA), or anti-mCherry (Agrisera, Sweden). The combination of SuperSignal™ West Pico and SuperSignal™ West Femto (Thermo Scientific, USA) was used to visualize epitope-tagged proteins. Chemiluminescence was detected using Azure 400 (Azure Biosystem, USA). The predicted molecular weight of proteins is indicated in Table 2-2.

Confocal microscopy

Agroinfiltration of Nb-*ptr1* mutant leaves with *A. tumefaciens* AGL1 strains carrying C-terminal YFP-tagged RipE1, RipE1-C172A, RipE1-ΔN86, and RipE1-C11A and mCherry-tagged AtFLS2 was performed. The fluorescence signals of YFP and mCherry were observed using a Leica SP8X confocal microscope (Leica Microsystems, Germany) at 2 dpi. The fluorescence of YFP and mCherry was excited at 514 nm and 561 nm, respectively, with a white light laser and captured using channels in the emission range of 520 - 550 nm and 590 - 610 nm, respectively. The LAS X software was used to process the images.

Table 2-1. Primers used in this study

Name	Sequences (5' to 3')	Purpose	References
NbPtr1.a_F	GAATTCATGGCAGAATTTTTCTTGTTCAAC	Silencing fragment cloning	In this study
NbPtr1.a_R	GGATCCCTTCTTCTTAAGGCTTTCCTGAA	Silencing fragment cloning	In this study
NbPtr1.b_F	GAATTCTTTTGAGGAGTTGCCAACTTCGA	Silencing fragment cloning	In this study
NbPtr1.b_R	GGATCCAAAAATTGAAGAGAAGGGAAAGAT	Silencing fragment cloning	In this study
NbEF1α_F	AGAAGGAAGCTGCTGAGATGA	qRT-PCR	In this study
NbEF1α_R	CTTGGGGGTGGTAGCATCC	qRT-PCR	In this study
NbPtr1_F	ATGAAAACAGACGAAAATGAATGG	qRT-PCR	In this study
NbPtr1_R	CTGCCACTGACTGTGCAAGATC	qRT-PCR	In this study
RipE1_GMI1000_C172A_F	GGGGCGGGGAACGCGGGCGAACACGC	Site-directed mutagenesis	In this study
RipE1_GMI1000_C172A_R	GCGTGTTCGCCCGCGTTCCCCGCCCC	Site-directed mutagenesis	In this study
RipE1_GMI1000_C203A_F	ATATCGACGACTTCGACGCCTTCTGGGCAATCGTGC	Site-directed mutagenesis	In this study
RipE1_GMI1000_H203A_R	GCACGATTGCCCAGAAGGCGTCGAAGTCGTCGATAT	Site-directed mutagenesis	In this study
RipE1_GMI1000_D222A_F	CGACGTCTACATCGCCGCATGGGGCAAGG	Site-directed mutagenesis	In this study
RipE1_GMI1000_D222A_R	CCTTGCCCCATGCGGCGATGTAGACGTCG	Site-directed mutagenesis	In this study
RipE1_GMI1000_NΔ86_mod_F	GGTCTCAAATGGCCCGGGATGTCGAC	Golden gate cloning	In this study
RipE1_GMI1000_NΔ86_mod_R	GGTCTCACGAAGCTTTCCGTGGCTGGAGG	Golden gate cloning	In this study
RipE1_GMI1000_C11A_mod_F	CTTCCATTTTACGGGCTTTTCGACCAGCAGTTAGC	Site-directed mutagenesis	In this study
RipE1_GMI1000_C11A_mod_R	GCTAACTGCTGGTCGAAAAGCCCGTAAAATGGAAG	Site-directed mutagenesis	In this study

Table 2-2. Expected molecular weights of protein products

Name	Biochemical tag	Predicted size (kDa)
GFP	-	27
RipE1_GMI1000	C-terminal 3xFLAG	49.6
RipE1_GMI1000_C172A	C-terminal 3xFLAG	49.6
RipE1_GMI1000_NΔ86	C-terminal 3xFLAG	40.5
RipE1_GMI1000_C11A	C-terminal 3xFLAG	49.6
RipE1_GMI1000	C-terminal GFP/YFP	73.5
RipE1_GMI1000_C172A	C-terminal YFP	73.5
RipE1_GMI1000_NΔ86	C-terminal YFP	64.4
RipE1_GMI1000_C11A	C-terminal YFP	73.5
NbPtr1	C-terminal 6xHA	101.9
Snthetic NbPtr1	C-terminal 6xHA	101.9
AtRIN4	N-terminal 4xmyc	28.12
NbRIN4-1	N-terminal 4xmyc	33.95
NbRIN4-2	N-terminal 4xmyc	30.5
NbRIN4-3	N-terminal 4xmyc	38.98
AtFLS2	C-terminal mCherry	155.7

RESULTS

RipE1-induced cell death was compromised in *NbPtr1*-silenced plants.

To confirm *NbPtr1* involvement in RipE1-induced cell death, two distinct VIGS fragments were designed to specifically target *NbPtr1* gene (Figure 2-1A). While RipE1 expression led to a robust macroscopic cell death in TRV:EV plants, it failed to induce cell death in both TRV:NbPtr1.a and TRV:NbPtr1.b plants (Figure 2-1B). The intensity of cell death was measured using the chlorophyll QY values in leaf tissue expressing RipE1 or the unrecognized RipE1-C172A mutant. In accordance, the leaf tissue expressing RipE1 showed a higher QY in TRV:NbPtr1.a and TRV:NbPtr1.b plants than in the TRV:EV control plants (Figure 2-1C). The absence of cell death was not due to lack of protein accumulation, as confirmed by immunoblot analysis (Figure 2-1D). The efficiency of *NbPtr1* silencing was also verified by qRT-PCR in repeated experiments (Figures 2-1E).

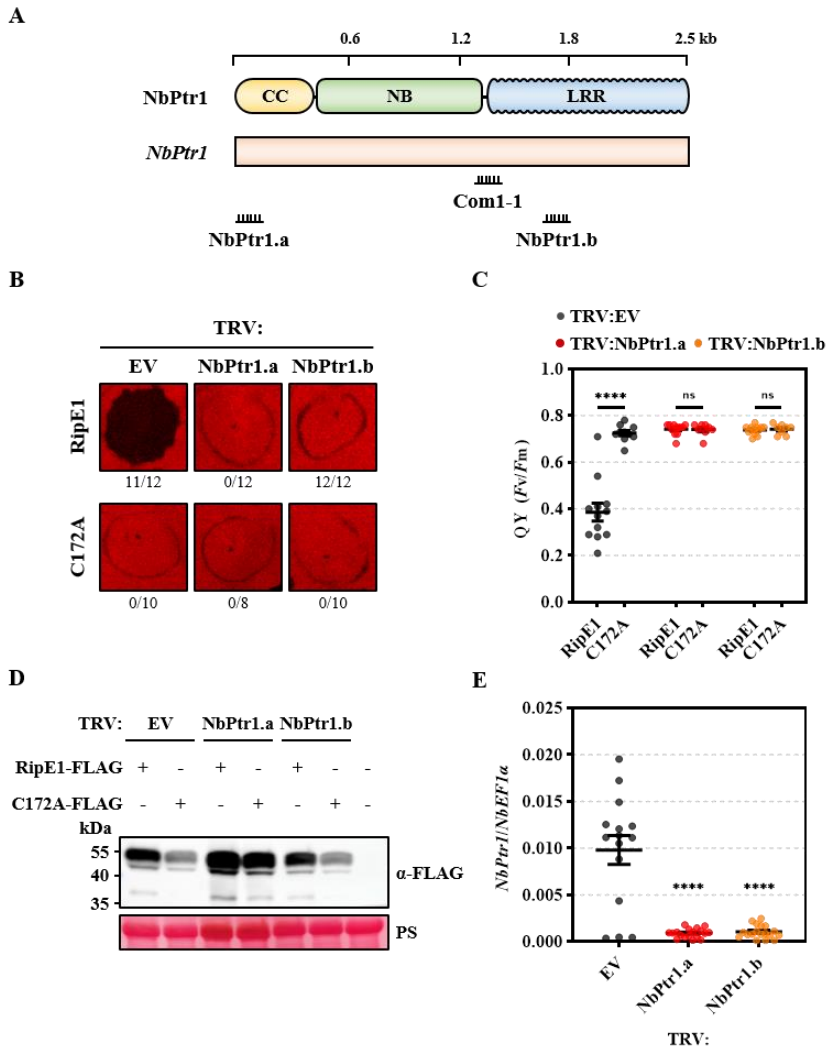

Figure 2-1. RipE1-induced cell death was compromised in *NbPtr1*-silenced plants.

(A) Schematic structure of the *NbPtr1* gene and protein. Exons are represented as a red box (bp: base pair). The CC, NB, and LRR domains are indicated as yellow, green, and blue, respectively. Black lines indicate the position of the library Com1-1 fragment and the alternative silencing fragments (TRV:NbPtr1.a and TRV:NbPtr1.b). (B) RipE1-induced cell death was suppressed in *NbPtr1*-silenced plants. *Agrobacterium* strains carrying RipE1 or RipE1-C172A constructs were

infiltrated (OD_{600} = 0.5) in TRV:EV, TRV:NbPtr1.a, or TRV:NbPtr1.b plants. Photographs were taken 4 days post-infiltration (dpi) under LED light (false color scale). Numbers indicate patches with cell death out of total infiltrated patches. (C) Quantum yield of the photosystem II (QY, *F*v/*F*m) was measured in the infiltrated patches shown in (C). Individual values from independent experiments are indicated as dots. Data were analyzed with two-way ANOVA followed by Sidak's multiple comparison test. Asterisks indicate significant difference between RipE1 constructs in TRV:EV, TRV:NbPtr1.a and TRV:NbPtr1.b plants (****, P<0.0001; ns, not significant). Bars represent mean ± SEM (n=8-12). (D) RipE1 and RipE1-C172A C-terminally fused to 3xFLAG tag accumulate in *NbPtr1*-silenced plants. Immunodetection was performed with anti-FLAG antibody on total protein extracted at 36 h post-infiltration (hpi). Ponceau red staining (PS) attests equal loading of the samples. (E) *NbPtr1* expression was measured by qRT-PCR in TRV:EV, TRV:NbPtr1.a, and TRV:NbPtr1.b plants and normalized to *NbEF1α* expression. Individual values from independent experiments are indicated as dots. Data were analyzed with one-way ANOVA followed by Dunnett's multiple comparison test. Asterisks indicate significant difference with TRV:EV plants (****, P<0.0001). Bars represent mean ± SEM (n=15).

RipE1-induced cell death was complemented by synthetic NbPtr1 in *NbPtr1*-silenced plants.

To further examine the role of NbPtr1 in RipE1 recognition, a genetic complementation assay was performed in *NbPtr1*-silenced plants using a synthetic NbPtr1 construct (NbPtr1^{syn}). NbPtr1^{syn} contains alternative synonymous codons at the beginning of the first exon to avoid silencing triggered by the NbPtr1.a fragment (Wu et al., 2017) (Figure 2-2A). RipE1 or RipE1-C172A mutant were co-expressed with either native NbPtr1 or the silencing-resistant NbPtr1^{syn} in TRV:EV and TRV:NbPtr1.a plants. The co-expression of NbPtr1^{syn} with RipE1 could restore robust cell death in TRV:NbPtr1.a plants, while that of native NbPtr1 with RipE1 did not induce cell death due to the *NbPtr1* silencing by VIGS (Figure 2-2B). In addition, RipE1-C172A did not induce cell death regardless of native NbPtr1 or NbPtr1^{syn} expression in both TRV:EV and TRV:NbPtr1.a plants. The occurrence and absence of cell death were correlated well with low and high QY values, respectively (Figure 2-2C). Immunoblot analysis confirmed the stability of NbPtr1^{syn} and the absence of native NbPtr1 protein accumulation in the TRV:NbPtr1.a plants (Figure 2-2D). The efficiency of *NbPtr1* silencing was also confirmed by qRT-PCR in repeated experiments (Figure 2-2E).

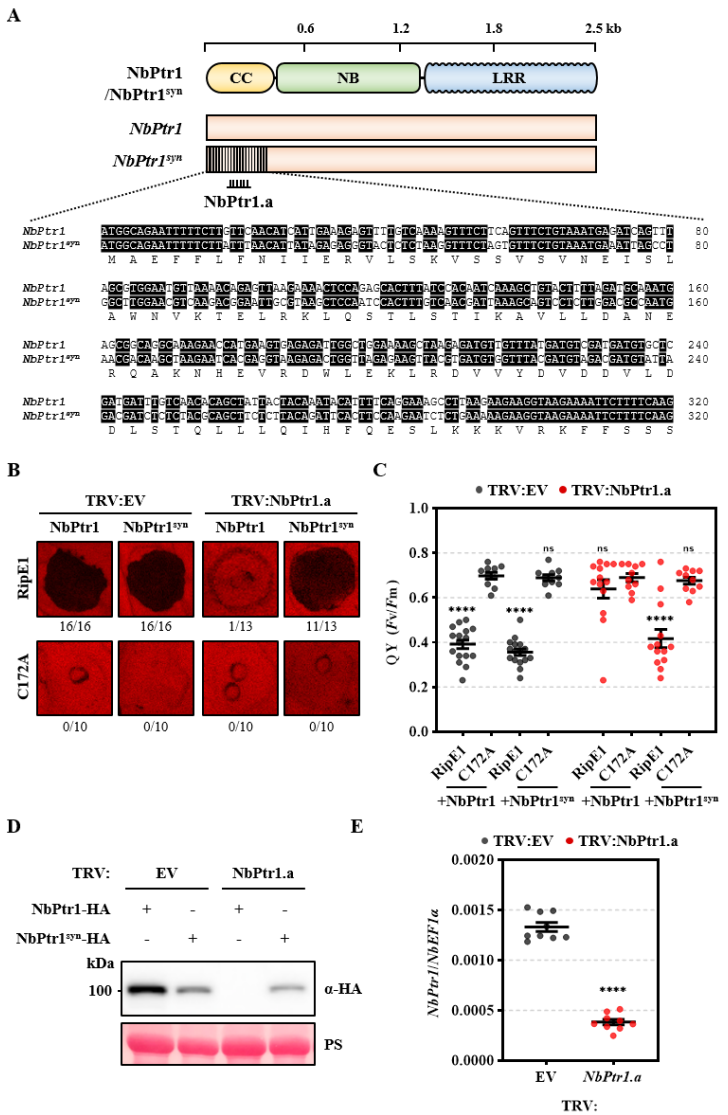

Figure 2-2. RipE1-induced cell death was complemented by synthetic NbPtr1 in *NbPtr1*-silenced plants.

(A) Alignment of *NbPtr1* and *NbPtr1*^{syn} nucleotide sequences (bp: base pair). Consensus sequences between *NbPtr1* and *NbPtr1*^{syn} are highlighted in black. Numbers on the right indicate the nucleotide position in *NbPtr1* and *NbPtr1*^{syn} sequence. (B) Silencing-proof *NbPtr1* (NbPtr1^{syn}) expression restored RipE1-induced cell death in *NbPtr1*-silenced plants. NbPtr1 or NbPtr1^{syn} (OD_{600} = 0.05)

were co-expressed with RipE1 or RipE1-C172A (OD_{600} = 0.4) in TRV:EV or TRV:NbPtr1.a plants. Photographs were taken at 4 dpi under LED light. Numbers indicate patches with cell death out of total infiltrated patches. (C) Quantum yield of the photosystem II (QY, *F*v/*F*m) was measured in the infiltrated patches shown in (c). Data were analyzed with two-way ANOVA followed by Sidak's multiple comparison test. Asterisks indicate significant difference with RipE1 C172A+NbPtr1 (****, P<0.0001; ns, not significant). (D) $NbPtr1^{syn}$ accumulates in TRV:NbPtr1.a plants. Immunodetection was performed with anti-HA antibody on total proteins extracted at 36 hpi. Ponceau red staining (PS) attests equal loading of the samples. (E) *NbPtr1* expression was measured by qRT-PCR in TRV:EV, TRV:NbPtr1.a, and TRV:NbPtr1.b plants and normalized to *NbEF1α* expression. Individual values from independent experiments are indicated as dots. Data were analyzed with one-way ANOVA followed by Dunnett's multiple comparison test. Asterisks indicate significant difference with TRV:EV plants (****, P<0.0001). Bars represent mean ± SEM (n=15).

RipE1-induced cell death was complemented by NbPtr1 in Nb-*ptr1* knock-out plants.

Similar assays were conducted in stable Nb-*ptr1* knockout plants that were generated through a CRISPR-induced deletion of 61-bp in the *NbPtr1* coding sequence (Ahn et al., 2023). The cell death induced by RipE1 was completely abolished in Nb-*ptr1* plants, but it could be restored by expressing the native NbPtr1, demonstrating that NbPtr1 is genetically necessary and sufficient to induce cell death in presence of RipE1 in *N. benthamiana* (Figure 2-3A). The low QY values were measured in the leaf tissue co-expressing RipE1 with native NbPtr1, which was consistent with the recovered cell death (Figure 2-3B). Furthermore, the protein expression of RipE1, RipE1-C172A, and NbPtr1 in Nb-*ptr1* plants was confirmed by immunoblot analysis (Figure 2-3C).

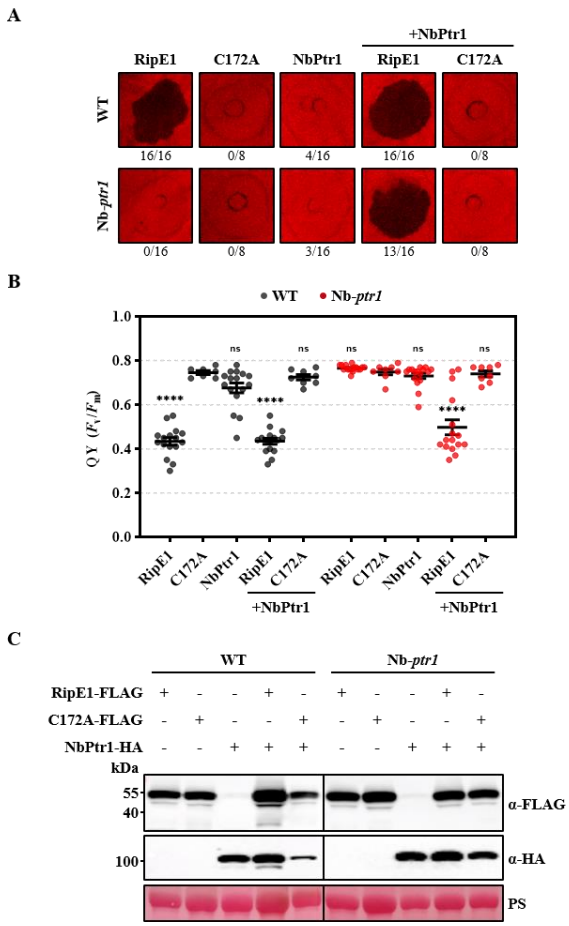

Figure 2-3. RipE1-induced cell death was complemented by NbPtr1 in Nb-*ptr1* knock-out plants.

(A) Native NbPtr1 was sufficient to restore RipE1-induced cell death in Nb-*ptr1* plants. *Agrobacterium* strains carrying RipE1, RipE1-C172A (OD_{600} = 0.4) or NbPtr1 (OD_{600} = 0.05) constructs were infiltrated in WT or Nb-*ptr1* plants. Photographs were taken at 4 dpi under LED light. Numbers indicate patches with cell death out of total infiltrated patches. (B) Quantum yield of the photosystem II (QY, *F*v/*F*m) was measured in the infiltrated patches shown in (A). Individual values from independent experiments are indicated as dots. Data were analyzed with two-way ANOVA followed by Sidak's multiple comparison test. Asterisks indicate

significant difference with WT plants (****, P<0.0001; ns, not significant). Bars represent mean ± SEM (n=8-16). (C) RipE1 and NbPtr1 accumulate in WT and Nb-*ptr1* plants. Immunodetection was performed with anti-FLAG or anti-HA antibodies on total protein extracted at 36 h post-infiltration (hpi). Ponceau red staining (PS) attests equal loading of the samples.

RipE1 recognition by NbPtr1 restricts the growth of *R. pseudosolanacearum.*

Next, the role of *NbPtr1* in RipE1-triggered immunity to *R. pseudosolanacearum* was investigated in collaboration with Dr Alberto Macho laboratory (Shanghai Center for Plant Stress Biology, China). The virulent *Rps* Y45 strain that lacks several effectors recognized by the *N. benthamiana* immune system, including RipB, RipE1, RipP1, RipAA, and RipBN, was used for this experiment (Carney and Denny, 1990; Poueymiro et al., 2009; Mazo-Molina et al., 2019; Nakano and Mukaihara, 2019a; Jeon et al., 2020; Sang et al., 2020). RipE1-GFP induced the cell death in *N. benthamiana* as RipE1-FLAG was used for the previous experiments (Figure 2-4A). A combined agroinfiltration and *Rps* inoculation assay was used as described in Yu and Macho et al. (2021). *N. benthamiana* plants silenced with TRV:EV or TRV:NbPtr1.a were infected with the Y45 strain one day after infiltration with Agrobacterium strains for the expression of RipE1-GFP or GFP (Figure 2-4B). Consistent with the previous report (Sang et al., 2020), Y45 cells grew ~10 times less in TRV:EV plants expressing RipE1 compared to TRV:EV plants expressing GFP. This growth difference was strikingly abolished in TRV:NbPtr1.a plants, where Y45 grew to a similar level in both GFP- and RipE1-expressing tissues. As the stability of RipE1-GFP protein and *NbPtr1* silencing efficiency in this assay was confirmed (Figure 2-4C and 2-4D), these results suggest that *NbPtr1* mediates the recognition of RipE1 and contributes to RipE1-triggered immunity to *Rps*.

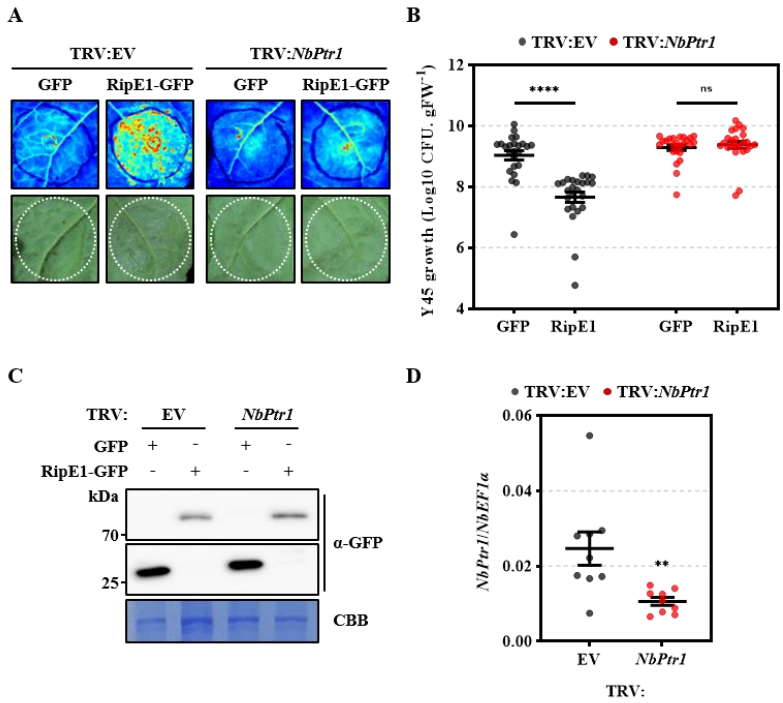

Figure 2-4. RipE1 recognition by NbPtr1 restricts the growth of *R. pseudosolanacearum*.

(A) RipE1-GFP-induced cell death is compromised in *NbPtr1*-silenced plants. *Agrobacterium* strains carrying GFP or RipE1-GFP constructs (OD_{600}=0.2) were infiltrated in wild-type (WT) or *NbPtr1*-silenced plants. Pictures were taken at 2 dpi with a CCD camera (lower panel) or a UV camera (upper panel). (B) RipE1-induced resistance to *R. pseudosolanacearum* was suppressed in *NbPtr1*-silenced plants. *R. pseudosolanacearum* Y45 was infiltrated at 10^5 CFU. ml^{-1} in TRV:EV and TRV:*NbPtr1* plants one day after agroinfiltration of GFP or RipE1-GFP (OD_{600} = 0.2). Bacteria were enumerated at 2 dpi. Individual values from independent experiments are indicated as dots. Data were analyzed with two-way ANOVA followed by Sidak's multiple comparison test. Asterisks indicate significant difference with GFP in TRV:EV and TRV:*NbPtr1* plants (****, P<0.0001; ns, not significant). Bars represent mean ± SEM (n=24). (C) RipE1-GFP accumulates in

TRV:*NbPtr1* plants. Immunodetection was performed with anti-GFP antibody on total protein extracts. Coomassie blue staining (CBB) attests equal loading of the samples. (D) *NbPtr1* expression was measured by qRT-PCR in TRV:EV and TRV:*NbPtr1* plants and normalized to *NbEF1α* expression. Individual values from independent experiments are indicated as dots. Data were analyzed with *t*-test. Asterisks indicate significant difference with TRV:EV plants (**, $P<0.01$). Bars represent mean ± SEM (n=9). These experiments were performed by Dr Wenjia Wu in the laboratory of Alberto Macho, licensed for work with *Ralstonia pseudosolanacearum* at the Shanghai Center for Plant Stress Biology, China.

RipE1 localization at the plasma membrane is essential for recognition by NbPtr1.

As NbPtr1 is required for the recognition of effectors from different families, likely by monitoring the state of the plasma membrane-associated protein RIN4 (Mazo-Molina et al., 2020; Ahn et al., 2023), RipE1 subcellular localization was investigated using laser scanning confocal microscopy. Nakano and colleagues (2019b) reported a nucleocytoplasmic localization for the N-terminally tagged RipE1 (from strain RS1000), while we and others (Jeon et al., 2020; Tsakiri et al., 2023) observed a plasma membrane localization for RipE1 C-terminally tagged with YFP. This difference suggests that RipE1 association with the plasma membrane is mediated through the N-terminal region of the protein. Accordingly, C-terminally YFP-tagged RipE1, RipE1-C172A and RipE1-ΔN86 were transiently expressed in Nb-*ptr1* epidermal cells (Figure 2-5A). RipE1-YFP was clearly associated with the plasma membrane, as the YFP fluorescence overlapped with that of the plasma membrane marker AtFLS2-mCherry. Interestingly, while RipE1-C172A-YFP remained in association with the plasma membrane, the RipE1-ΔN86-YFP presented a nucleocytoplasmic localization. Immunoblot analysis confirmed that C-terminally YFP-tagged RipE1 proteins accumulated in Nb-*ptr1* plants (Figure 2-5B). Moreover, similar to RipE1-C172A, RipE1-ΔN86 could not induce cell death in *N. benthamiana*, despite showing a comparable protein stability (Figure 2-5C, 2-5D and 2-5E). These findings indicate that RipE1 association with the plasma membrane is required for RipE1-induced cell death in addition to the putative catalytic activity.

The N-terminal region of RipE1 was not predicted to participate in the cysteine-protease fold in a predicted structural model (Tsakiri et al., 2022). This region does not contain a myristylation motif that was reported for several plasma membrane-associated T3Es including AvrRpm1 (Nimchuk et al., 2000). Rather, RipE1 contained the only Cysteine residue (Cys11) in this region. In order to examine whether Cys11 is involved in the plasma membrane localization of RipE1 that could potentially be *S*-acetylated *in planta* (Hurst and Hemsley, 2015), RipE1-C11A was generated. However, RipE1-C11A was still associated with the plasma membrane (Figure 2-6A) and could trigger cell death in WT and NbPtr1-expressing Nb-*ptr1* plants (Figure 2-6B and 2-6C). Immunoblot analysis confirmed that C-terminally YFP- or FLAG-tagged RipE1-variant proteins accumulated in Nb-*ptr1* plants (Figure 2-6D). These results indicate that this particular residue was not essential for RipE1 localization and recognition.

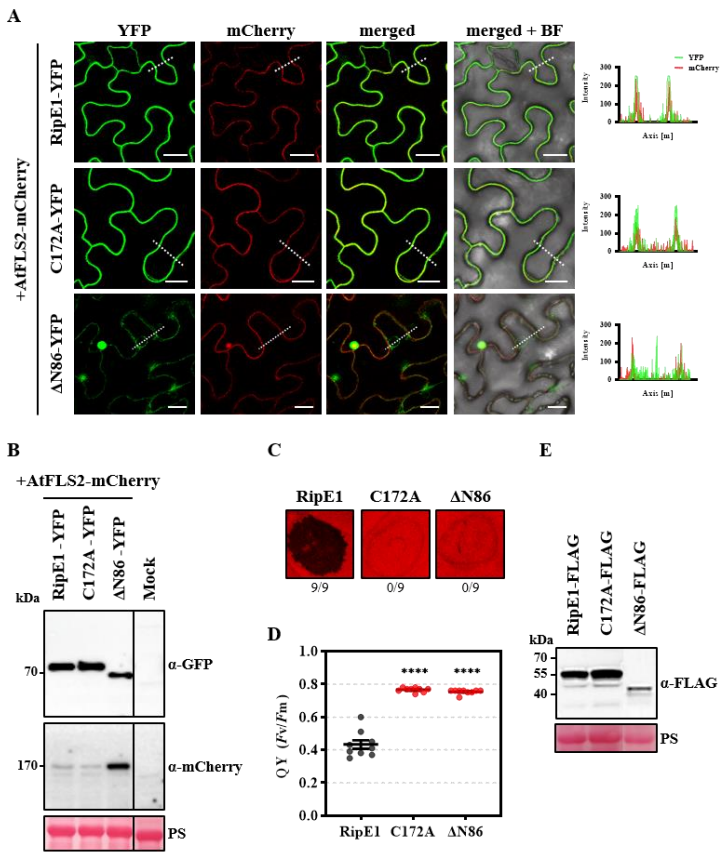

Figure 2-5. RipE1 association with the plasma membrane is essential for recognition by NbPtr1.

(A) RipE1 N-terminus is required for association with the plasma membrane. RipE1, RipE1-C172A, or RipE1-ΔN86 C-terminally fused with YFP (OD_{600} = 0.4) was co-expressed with the plasma membrane marker AtFLS2-mCherry (OD_{600} = 0.1) in Nb-*ptr1* epidermal cells. Confocal micrographs were acquired at 2 dpi (BF, bright field). The fluorescence intensity of YFP and mCherry channels across sections indicated by dotted lines are shown on the right panel. Scale bar indicates 11 μm. (B) Accumulation of RipE1-YFP fusion proteins in Nb-*ptr1* plants. Immunodetection was performed with anti-GFP or anti-mCherry antibodies on total protein extracted

at 36 hpi. Ponceau red staining (PS) attests equal loading of the samples. (C) RipE1 N-terminus is required for recognition by NbPtr1. *Agrobacterium* strains carrying RipE1, RipE1-C172A, or RipE1-ΔN86 were infiltrated (OD_{600} = 0.4) in WT plants. Photographs were taken at 4 dpi under LED light. Numbers indicate patches with cell death out of total infiltrated patches. (D) Quantum yield of the photosystem II (QY, *F*v/*F*m) was measured in the infiltrated patches shown in (C). Individual values from independent experiments are indicated as dots. Data were analyzed with one-way ANOVA followed by Dunnett's multiple comparison test. Asterisks indicate significant difference with RipE1 (****, $P<0.0001$). Bars represent mean ± SEM (n=9). (E) RipE1, RipE1-C172A, and RipE1-ΔN86 accumulate in WT plants. Immunodetection was performed with anti-FLAG antibody on total protein extracted at 36 h post-infiltration. Ponceau red staining (PS) shows equal loading of the samples.

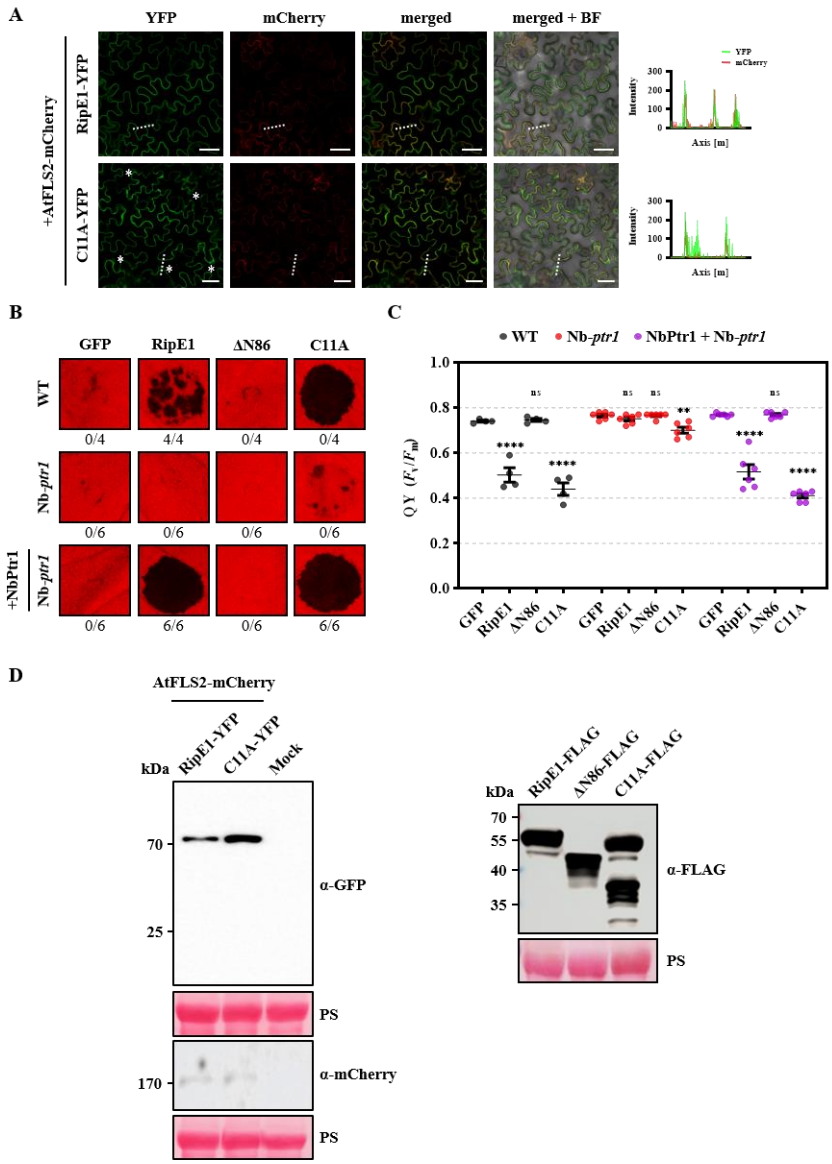

Figure 2-6. RipE1 Cys11 is dispensable for cell death and plasma membrane localization. (A) RipE1-C11A is still associated with the plasma membrane. RipE1 and RipE1-C11A C-terminally fused with YFP (OD_{600} = 0.4) were co-expressed with the plasma membrane marker AtFLS2-mCherry (OD_{600} = 0.1) in Nb-*ptr1* epidermal cells. Confocal micrographs were acquired at 2 dpi (BF, bright field). The fluorescence intensity of YFP and mCherry channels across sections indicated by

dotted lines is shown in the right panel. Asterisks indicate faint fluorescent signals from nucleus. Scale bar indicates 40 μm. (B) RipE1 Cys11 is not required for recognition by NbPtr1. Agrobacteria carrying GFP, RipE1, RipE1-ΔN86, or RipE1-C11A were infiltrated (OD_{600} = 0.5) in WT or Nb-*ptr1* plants without or with NbPtr1 (OD_{600} = 0.05). Photographs were taken at 4 dpi under LED light. Numbers indicate patches with cell death out of total infiltrated patches. (C) Quantum yield of the photosystem II (QY, *F*v/*F*m) was measured in the infiltrated patches shown in (B). Individual values from independent experiments are indicated as dots. Data were analyzed with one-way ANOVA followed by Dunnett's multiple comparison test. Asterisks indicate significant difference with GFP (**, $P<0.01$; ****, $P<0.0001$; ns, not significant). Bars represent mean ± SEM (n=4-6). (D) Protein accumulation of RipE1 variants. The experiments were conducted as described in (A) and (B). Immunodetection was performed with anti-GFP, anti-mCherry, or anti-FLAG antibodies on total protein extracted at 48 h post-infiltration. Ponceau red staining (PS) shows equal loading of the samples.

RipE1 affects the stability of RIN4 proteins in *N. benthamiana.*

Ptr1 autoactivity is suppressed by co-expression of tomato RIN4 (SlRIN4), suggesting that Ptr1 detects AvrRpt2 and RipBN by monitoring SlRIN4, which is cleaved by the catalytic activity of these effectors (Mazo-Molina et al., 2019; Mazo-Molina et al., 2020). RipE1 carries a putative catalytic triad consisting of cysteine (C), histidine (H), aspartate acid (D) suggesting its potential proteolytic function (Nimchuk et al., 2007; Sang et al., 2020). The immune receptor RESISTANCE TO PSEUDOMONAS SYRINGAE 2 (RPS2) spontaneously induces cell death when overexpressed in *N. benthamiana* leaves, and its autoactivity is suppressed by the co-expression of *Arabidopsis* RIN4 (AtRIN4), which is a well-studied negative regulator (Day et al., 2005). AvrRpt2 protease cleaves AtRIN4 protein, re-activating RPS2 (Axtell and Staskawicz, 2003; Mackey et al., 2003; Day et al., 2005).

To investigate the proteolytic role of RipE1 on RIN4 proteins, we tested whether RipE1 could restore RPS2 activation suppressed by AtRIN4. These experiments were conducted in *NbPtr1*-silenced plants to exclude RipE1-immune responses induced by NbPtr1. As expected, expression of RPS2 alone induced cell death in *N. benthamiana*, and the cell death was suppressed when AtRIN4 was co-expressed with RPS2 (Figure 2-7A). Co-expression of RipE1 with RPS2 and RIN4 restored RPS2-mediated cell death in *NbPtr1*-silenced plants, while the catalytic mutant RipE1-CHD (where the three putative catalytic residues are replaced with alanine) did not (Figure 2-7A). This observation was consistent with the QY values (Figure 2-7B). This result indicates that in presence of functional RipE1, RIN4 fragments

required for RPS2 activation could be generated. This prompted us to directly test the stability of RIN4 proteins in the presence of RipE1. For this experiment, RipE1 or RipE1-CHD were co-expressed with AtRIN4 or its homologs in *N. benthamiana* NbRIN4-1, NbRIN4-2 and NbRIN4-3 (Prokchorchik et al., 2020). Co-expression of RipE1 led to reduced abundance of RIN4 proteins from both *Arabidopsis* and *N. benthamiana*, while no change in RIN4 protein stability was observed in presence of RipE1-CHD (Figure 2-7C). These results suggest that RipE1 has a proteolytic activity on RIN4 proteins, and that RIN4 degradation is likely involved in NbPtr1-mediated immunity in *N. benthamiana*.

In chapter 2, genetic complementation assays demonstrated that NbPtr1 is genetically required for RipE1 recognition in *N. benthamiana*. NbPtr1-mediated immunity restricted *Rps* Y45 strain in the presence of RipE1. These results showed that NbPtr1 is able to recognize *Rps* core effector RipE1 as well as RipBN, the homolog of AvrRpt2 from *P. syringae*. RipE1 recognition by NbPtr1 requires RipE1 association with the plasma membrane, while the putative *S*-acylated cysteine residue of RipE1 was not enough to associate with the plasama membrane localization. Furthermore, RipE1 displayed proteolytic activity on plasma membrane-associated RIN4 proteins. This suggests that NbPtr1 recognizes RipE1 at the plasma membrane by monitoring the degradation of RIN4 proteins by RipE1 in *N. benthamiana*.

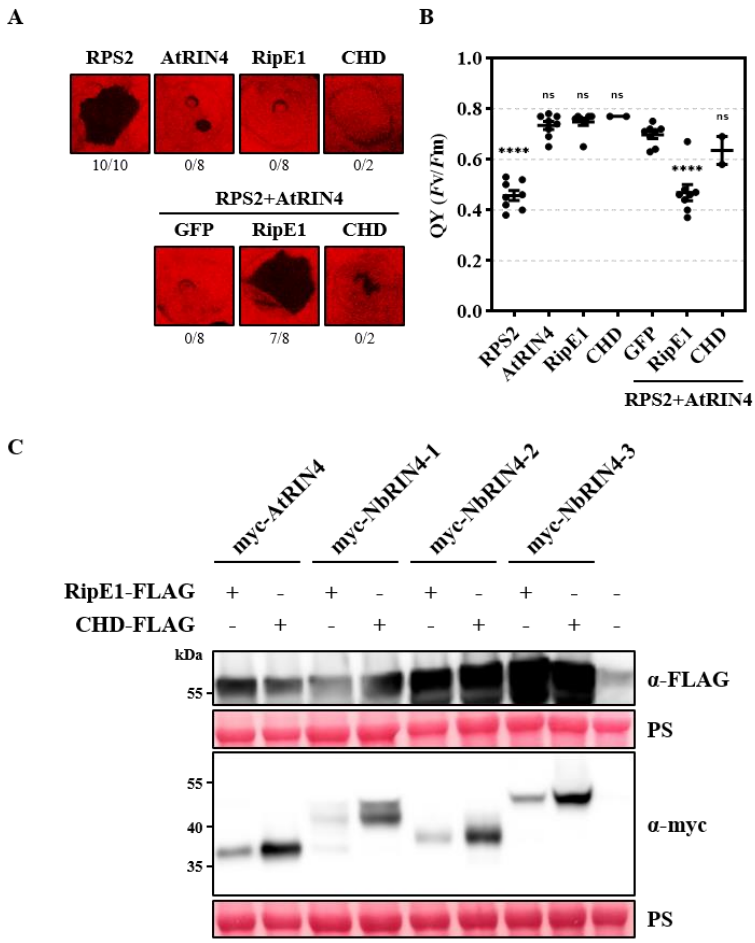

Figure 2-7. RipE1 affects the stability of RIN4 proteins in *N. benthamiana*.

(A) RipE1 breaks RIN4-mediated inhibition of RPS2 autoactivity. RipE1 or RipE1-CHD (OD_{600} = 0.05) was co-expressed with *Arabidopsis* RIN4 (OD_{600} = 0.4) and RPS2 (OD_{600} = 0.1) in *NbPtr1*-silenced plants. Photographs were taken at 2 dpi under LED light. Numbers indicate patches with cell death out of total infiltrated patches. (B) Quantum yield of the photosystem II (QY, *Fv*/*Fm*) was measured in the infiltrated patches shown in (A). Individual values from independent experiments are indicated as dots. Data were analyzed with one-way ANOVA followed by Dunnett's multiple comparison test. Asterisks indicate significant difference with RPS2+RIN4+GFP (****, P<0.0001; ns, not significant). Bars represent mean ±

SEM (n=2-10). (C) RipE1, RipE1-CHD, and RIN4 proteins accumulate in *NbPtr1*-silenced plants. Immunodetection was performed with anti-FLAG or anti-myc antibodies on total protein extracted at 48 h post-infiltration. Ponceau red staining (PS) shows equal loading of the samples.

DISCUSSION

S. lycopersicoides Ptr1 confers resistance to *P. syringae* pv. *tomato* race 1 strains and *R. pseudosolanacearum* CMR15 strain expressing AvrRpt2 and RipBN, respectively (Mazo-Molina et al., 2019; Mazo-Molina et al., 2020). StPr1 from potato and NbPtr1 from *N. benthamiana*, which are orthologs of Ptr1, are also able to recognize these two effectors and induce cell death when they are co-expressed with effectors. Here, it was found that NbPtr1 is a functional CNL that recognizes yet another effector, RipE1 from *Rps* GMI1000 strain. NbPtr1 mediates immune responses leading to the restriction of virulent Y45 strain upon the RipE1 recognition in *N. benthamiana*. While RipBN presence is restricted to CMR15 strain, which is mainly distributed in Africa (phylotype III), RipE1 is a core effector highly conserved across four phylotypes (Peeters et al., 2013; Sabbagh et al., 2019), suggesting that NbPtr1 can confer broader *Ralstonia* recognition specificity. Moreover, a recent study has revealed that NbPtr1 perceives multiple effectors from different bacterial pathogens, including AvrRpt2, AvrRpm1, AvrB, HopZ5, and AvrBsT (Ahn et al., 2023). Together with the present work, these studies highlight the potential of Ptr1 and its homologs as suitable genetic resource for engineering disease resistance against multiple bacterial pathogens in crops (Kim et al., 2022).

On the other hand, bacterial pathogens have adapted to suppress effector-triggered immunity using other T3Es. For example, RipAY within GMI1000 inhibits RipE1-triggered immunity by degrading cellular glutathione in *N. benthamiana*

(Sang et al., 2018; Sang et al., 2020). Another T3E of GMI1000, RipAC, targets the immune regulator SGT1 to prevent the mitogen-activated protein kinase (MAPK)-mediated phosphorylation of SGT1 that is required for ETI triggered by RipE1 (Yu et al., 2020). This reflects the active adaptation of GMI1000 to subvert RipE1-induced immunity by targeting immune functions through other T3E virulence activities.

Despite being recognized by the *N. benthamiana* immune system, GMI1000 has evolved other T3Es that suppress RipE1-triggered immunity rather than losing RipE1. This reflects the importance of RipE1 for *Ralstonia* virulence. Recent studies have shown that RipE1 can target diverse host proteins in *Arabidopsis*. Tsakiri et al. (2023) have showed that RipE1 from GMI1000 localizes at the plasma membrane and cleaves Exo70B1, which is a subunit of the conserved exocyst complex tethering secretory vesicles to the plasma membrane (Synek et al., 2021). The exocyst complex plays a critical role in targeted exocytosis processes, such as transport of cell wall components and plasma membrane-associated proteins like the pattern-recognition receptor FLS2, as well as other components responses to pathogens (Baudin et al., 2017; Žárský, 2022). The exocyst complex is involved in diverse cellular processes, including physiological mechanisms and immune responses, therefore, might be an attractive host target by bacterial T3Es. Interestingly, we observed here that the *Arabidopsis* FLS2 tagged with mCherry could not accumulate well when the plasma membrane-associated RipE1 variants (RipE1-YFP and RipE1-C172A-YFP) were co-expressed compared to when the N-terminal truncated RipE1

(ΔN86-YFP) was co-expressed (Figure 2-5).

A recent study has revealed that RIN4, a well-studied guardee that regulates both PTI and ETI, interacts with Exo70B1, leading to its recruitment at the plasma membrane (Sabol et al., 2017; Toruño et al., 2019). It is noteworthy that RIN4 proteins from *Arabidopsis* and *N. benthamiana* were degraded in the presence of RipE1 (Figure 2-7). Although it is speculated that RipE1 may target both Exo70B1 and RIN4 to manipulate host physiological mechanisms or/and suppress immune responses in host plants, it is unknown whether RipE1 catalytic activity on these proteins activates NbPtr1 in *N. benthamiana*.

Another study showed that RipE1 from RS1000 strain degrades a transcription factor JAZ repressor via its protease activity, thereby activating jasmonic acid (JA) signaling to suppress SA-mediated immune responses in *Arabidopsis* (Nakano and Mukaihara, 2019b). Nakano and Mukaihara, (2019b) also showed that RipE1 localizes to the nucleocytoplasmic region. In contrast, Tsakiri et al. (2023) reported that RipE1 localizes the cell periphery, which aligns with the observation in Figure 2-5. These conflicting outcomes might be due to the utilization of RipE1 constructs tagged with YFP at different locations (C-terminus in Tsakiri et al. (2023); Jeon et al. (2020) and this study, and N-terminus in Nakano and Mukaihara (2019b)).

Consistent to the plasma membrane localization, an *S*-acylated residue was predicted in the very N-terminus of RipE1. However, the RipE1-C11A still localized to the plasma membrane and induced cell death. It remains possible that RipE1 recruitment to the plasma membrane occurs through electrostatic interactions of

basic residues (12 arginine are present in the 1-86 aa region) with negatively charged phospholipids or alternatively that RipE1 binds to plasma membrane associated proteins (Heo et al., 2006; McLaughlin and Murray, 2005). These findings suggest that RipE1 can target multiple host proteins at the plasma membrane with its proteolytic activity to promote *Ralstonia* virulence, but some of these targets might be monitored and guarded by NLRs in host plants.

REFERENCES

Ahn, Y.J., Kim, H., Choi, S., Mazo-Molina, C., Prokchorchik, M., Zhang, N., Kim, B., Mang, H., Yoon, H., Segonzac, C., et al. (2023). Ptr1 and ZAR1 immune receptors confer overlapping and distinct bacterial pathogen effector specificities. *New Phytol.* **239**: 1935–1953.

Axtell, M.J., and Staskawicz, B.J. (2003). Initiation of RPS2-specified disease resistance in *Arabidopsis* is coupled to the AvrRpt2-directed elimination of RIN4. *Cell* **112**:369–377.

Baudin, M., Hassan, J.A., Schreiber, K.J., and Lewis, J.D. (2017). Analysis of the ZAR1 immune complex reveals determinants for immunity and molecular interactions. *Plant Physiol.***174**:2038–2053.

Carney, B.F., and Denny, T.P. (1990). A cloned avirulence gene from *Pseudomonas solanacearum* determines incompatibility on *Nicotiana tabacum* at the host species level. *J. Bacteriol.* **172**:4836–4843.

Choi, S., Prokchorchik, M., Lee, H., Gupta, R., Lee, Y., Chung, E.-H., Cho, B., Kim, M.-S., Kim, S.T., and Sohn, K.H. (2021). Direct acetylation of a conserved threonine of RIN4 by the bacterial effector HopZ5 or AvrBsT activates RPM1-dependent immunity in *Arabidopsis*. *Mol. Plant* **14**:1951–1960.

Chung, E.-H., Cunha, L. da, Wu, A.-J., Gao, Z., Cherkis, K., Afzal, A.J., Mackey, D., and Dangl, J.L. (2011). Specific threonine phosphorylation of a host target by two unrelated type III effectors activates a host innate immune receptor in plants. *Cell Host Microbe* **9**:125–136.

Day, B., Dahlbeck, D., Huang, J., Chisholm, S.T., Li, D., and Staskawicz, B.J. (2005). Molecular basis for the RIN4 negative regulation of RPS2 disease resistance. *Plant Cell* **17**:1292–1305.

Engler, C., Kandzia, R., and Marillonnet, S. (2008). A one pot, one step, precision

cloning method with high throughput capability. *PLoS One* **3**:e3647.

Gimenez-Ibanez, S., Boter, M., Fernández-Barbero, G., Chini, A., Rathjen, J.P., and Solano, R. (2014). The bacterial effector HopX1 targets JAZ transcriptional repressors to activate jasmonate signaling and promote infection in *Arabidopsis*. *PLoS Biol.* **12**:e1001792.

Jeon, H., Kim, W., Kim, B., Lee, S., Jayaraman, J., Jung, G., Choi, S., Sohn, K.H., and Segonzac, C. (2020). *Ralstonia solanacearum* type III effectors with predicted nuclear localization signal localize to various cell compartments and modulate immune responses in *Nicotiana* spp. *Plant Pathol J* **36**:43–53.

Jones, A.M., Coimbra, S., Fath, A., Sottomayor, M., and Thomas, H. (2001). Programmed cell death assays for plants. *Methods Cell Biol.* **66**:437–451.

Kim, B., Choi, J., and Segonzac, C. (2022). Tackling multiple bacterial diseases of Solanaceae with a handful of immune receptors. *Hortic. Environ. Biotechnol.* **63**:149–160.

Landry, D., González-Fuente, M., Deslandes, L., and Peeters, N. (2020). The large, diverse, and robust arsenal of *Ralstonia solanacearum* type III effectors and their in planta functions. *Mol. Plant Pathol.* **21**:1377–1388.

Lee, H.-Y., Mang, H., Choi, E., Seo, Y.-E., Kim, M.-S., Oh, S., Kim, S.-B., and Choi, D. (2021). Genome-wide functional analysis of hot pepper immune receptors reveals an autonomous NLR clade in seed plants. *New Phytol.* **229**:532–547.

Liu, Y., Schiff, M., Marathe, R., and Dinesh-Kumar, S.P. (2002). Tobacco *Rar1*, *EDS1* and *NPR1/NIM1* like genes are required for *N*-mediated resistance to tobacco mosaic virus. *Plant J.* **30**:415–429.

Liu, J., Elmore, J.M., Lin, Z.-J.D., and Coaker, G. (2011). A receptor-like cytoplasmic kinase phosphorylates the host target RIN4, leading to the activation of a plant innate immune receptor. *Cell Host Microbe* **9**:137–146.

Livak, K.J., and Schmittgen, T.D. (2001). Analysis of relative gene expression data using real-time quantitative PCR and the 2(-Delta Delta C(T)) method.

Methods **25**:402–408.

Mackey, D., Belkhadir, Y., Alonso, J.M., Ecker, J.R., and Dangl, J.L. (2003). *Arabidopsis* RIN4 is a target of the type III virulence effector AvrRpt2 and modulates RPS2-mediated resistance. *Cell* **112**:379–389.

Mansfield, J., Jenner, C., Hockenhull, R., Bennett, M.A., and Stewart, R. (1994). Characterization of *avrPphE*, a gene for cultivar-specific avirulence from *Pseudomonas syringae* pv. *phaseolicola* which is physically linked to *hrpY*, a new *hrp* gene identified in the halo-blight bacterium. *Mol. Plant Microbe Interact.* **7**:726–739.

Mazo-Molina, C., Mainiero, S., Hind, S.R., Kraus, C.M., Vachev, M., Maviane-Macia, F., Lindeberg, M., Saha, S., Strickler, S.R., Feder, A., et al. (2019). The *Ptr1* locus of *solanum lycopersicoides* confers resistance to race 1 strains of *Pseudomonas syringae* pv. *tomato* and to *Ralstonia pseudosolanacearum* by recognizing the type III effectors AvrRpt2 and RipBN. *Mol. Plant Microbe Interact.* **32**:949–960.

Mazo-Molina, C., Mainiero, S., Haefner, B.J., Bednarek, R., Zhang, J., Feder, A., Shi, K., Strickler, S.R., and Martin, G.B. (2020). Ptr1 evolved convergently with RPS2 and Mr5 to mediate recognition of AvrRpt2 in diverse solanaceous species. *Plant J.* **103**:1433–1445.

Mukaihara, T., Tamura, N., and Iwabuchi, M. (2010). Genome-wide identification of a large repertoire of *Ralstonia solanacearum* type III effector proteins by a new functional screen. *Mol. Plant Microbe Interact.* **23**:251–262.

Nakano, M., and Mukaihara, T. (2019a). The type III effector RipB from *Ralstonia solanacearum* RS1000 acts as a major avirulence factor in *Nicotiana benthamiana* and other *Nicotiana* species. *Mol. Plant Pathol.* **20**:1237–1251.

Nakano, M., and Mukaihara, T. (2019b). Comprehensive identification of PTI suppressors in type III effector repertoire reveals that *Ralstonia solanacearum* activates jasmonate signaling at two different steps. *Int. J. Mol. Sci.* **20**:E5992.

Nimchuk, Z.L., Fisher, E.J., Desveaux, D., Chang, J.H., and Dangl, J.L. (2007). The HopX (AvrPphE) family of *Pseudomonas syringae* type III effectors require a catalytic triad and a novel N-terminal domain for function. *Mol. Plant Microbe Interact.* **20**:346–357.

Peeters, N., Carrère, S., Anisimova, M., Plener, L., Cazalé, A.-C., and Genin, S. (2013b). Repertoire, unified nomenclature and evolution of the type III effector gene set in the *Ralstonia solanacearum* species complex. *BMC Genom.* **14**:859.

Poueymiro, M., Cunnac, S., Barberis, P., Deslandes, L., Peeters, N., Cazale-Noel, A.-C., Boucher, C., and Genin, S. (2009). Two type III secretion system effectors from *Ralstonia solanacearum* GMI1000 determine host-range specificity on tobacco. *Mol. Plant Microbe Interact.* **22**:538–550.

Prokchorchik, M., Choi, S., Chung, E.-H., Won, K., Dangl, J.L., and Sohn, K.H. (2020). A host target of a bacterial cysteine protease virulence effector plays a key role in convergent evolution of plant innate immune system receptors. *New Phytol.* **225**:1327–1342.

Sabbagh, C.R.R., Carrere, S., Lonjon, F., Vailleau, F., Macho, A.P., Genin, S., and Peeters, N. (2019). Pangenomic type III effector database of the plant pathogenic *Ralstonia* spp. *PeerJ* **7**:e7346.

Sabol, P., Kulich, I., and Žárský, V. (2017). RIN4 recruits the exocyst subunit EXO70B1 to the plasma membrane. *J. Exp. Bot.* **68**:3253–3265.

Sang, Y., Wang, Y., Ni, H., Cazalé, A.-C., She, Y.-M., Peeters, N., and Macho, A.P. (2018). The *Ralstonia solanacearum* type III effector RipAY targets plant redox regulators to suppress immune responses. *Mol. Plant Pathol.* **19**:129–142.

Sang, Y., Yu, W., Zhuang, H., Wei, Y., Derevnina, L., Yu, G., Luo, J., and Macho, A.P. (2020). Intra-strain elicitation and suppression of plant immunity by *Ralstonia solanacearum* type-III effectors in *Nicotiana benthamiana*. *Plant Commun.* **1**:100025.

Synek, L., Pleskot, R., Sekereš, J., Serrano, N., Vukašinović, N., Ortmannová,

J., Klejchová, M., Pejchar, P., Batystová, K., Gutkowska, M., et al. (2021). Plasma membrane phospholipid signature recruits the plant exocyst complex via the EXO70A1 subunit. *Proc. Natl. Acad. Sci. U.S.A.* **118**:e2105287118.

Takemoto, D., and Jones, D.A. (2005). Membrane release and destabilization of *Arabidopsis* RIN4 following cleavage by *Pseudomonas syringae* AvrRpt2. *Mol. Plant Microbe Interact.* **18**:1258–1268.

Toruño, T.Y., Shen, M., Coaker, G., and Mackey, D. (2019). Regulated disorder: posttranslational modifications control the RIN4 plant immune signaling hub. *Mol. Plant Microbe Interact.* **32**:56–64.

Tsakiri, D., Kotsaridis, K., Marinos, S., Michalopoulou, V.A., Kokkinidis, M., and Sarris, P.F. (2023). The core effector RipE1 of *Ralstonia solanacearum* interacts with and cleaves Exo70B1 and is recognized by the Ptr1 immune receptor. *BioRxiv* https://doi.org/ 10.1101/2022.08.31.506019.

Wu, C.-H., Abd-El-Haliem, A., Bozkurt, T.O., Belhaj, K., Terauchi, R., Vossen, J.H., and Kamoun, S. (2017). NLR network mediates immunity to diverse plant pathogens. *Proc. Natl. Acad. Sci. U.S.A.* **114**:8113–8118.

Yu, W., and Macho, A. (2021). A fast and easy method to study *Ralstonia solanacearum* virulence upon transient gene expression or gene silencing in *Nicotiana benthamiana* leaves. *Bio Protoc.* **11**:e4116.

Yu, G., Xian, L., Xue, H., Yu, W., Rufian, J.S., Sang, Y., Morcillo, R.J.L., Wang, Y., and Macho, A.P. (2020). A bacterial effector protein prevents MAPK-mediated phosphorylation of SGT1 to suppress plant immunity. *PLoS Pathog.* **16**:e1008933.

Žárský, V. (2022). Exocyst functions in plants: secretion and autophagy. *FEBS Lett.* **596**:2324–2334.

CHAPTER 3

The plasma membrane-associated RRS-Y mediates the recognition of the *Ralstonia pseudosolanacearum* effector RipY in *Nicotiana benthamiana*

I acknowledge that some parts in this chapter either quote or alter my work reported in "A plasma membrane nucleotide-binding leucine-rich repeat receptor mediates the recognition of the *Ralstonia pseudosolanacearum* effector RipY in *Nicotiana benthamiana*" published online in Plant Communications (DOI: https://doi.org/10.1016/j.xplc.2023.100640).

ABSTRACT

The *N. benthamiana* immune system detects the *Ralstonia pseudosolanacearum* (*Rps*) effector RipY. A multiplexed NbNLR-VIGS library identified RESISTANCE TO RALSTONIA SOLANACEARUM RIPY (RRS-Y), a coiled-coil nucleotide-binding leucine-rich repeat receptor (CNL), which mediates the recognition of RipY in *N. benthamiana*. Genetic complementation assays in *RRS-Y*-silenced plants and stable *rrs-y* knockout mutants demonstrated that *RRS-Y* was sufficient to activate RipY-induced cell death and RipY-induced immunity to *Rps*. Further, structure-function analysis of RRS-Y was performed using a stable *rrs-y* knockout line. Mutational analysis on the phosphate binding loop (P-loop) and methionine-histidine-aspartate motif revealed that the nucleotide-binding (NB) domain is critical for RRS-Y activation. The plasma membrane localization of RRS-Y is necessary for cell death signaling via CC domain carrying the putative palmitoylated cysteine residues that mediate RRS-Y plasma membrane localization. Additionally, RRS-Y was observed to form the self-association in the absence of RipY *in planta*. Moreover, RRS-Y broadly recognized RipY homologs across *Ralstonia* species, and the RipY recognition by RRS-Y was determined by C-terminal region of RipY. Overall, these findings provide an additional effector/receptor pair system that deepens our understanding of CNL activation in plants.

INTRODUCTION

Plants possess intracellular immune receptors to monitor pathogen virulence proteins called effectors (Dodds and Rathjen, 2010; Kourelis and van der Hoorn, 2018). These receptors are the nucleotide-binding leucine rich repeat receptors (NLRs), which are the largest family of resistance (R) proteins. Upon activation, NLRs induce immune responses (also known as effector-triggered immunity, ETI) that include the hypersensitive response (HR), which is a type of programmed cell death. NLRs have modular structure with a C-terminal leucine-rich repeat (LRR) domain, a central nucleotide-binding domain shared by APAF-1, various plant *R* proteins and CED-4 (NB-ARC or nucleotide-binding domain (NBD/NB), helical domain 1 (HD1/ARC1), and winged-helix domain (WHD/ARC2), hereafter NB), and a variable N-terminal domain. The LRR domain is considered to function for effector recognition and intra-molecular regulation of NLRs (Ade et al., 2007; Faustin et al., 2007; Ma et al., 2020; Martin et al., 2020). In general, the NB domain of NLRs acts as a molecular switch for signaling, which can be turned “on” or “off” by ATP or ADP binding, respectively (Wang et al., 2019). Certain motifs within NB domain, such as the phosphate-binding loop (P-loop) and methionine-histidine-aspartate (MHD) motif, are highly conserved and associated with ATP/ADP binding. The P-loop motif, which contains a lysine (K) residue, is required for binding ATP, while the MHD motif is necessary for ADP binding (Tameling et al., 2006; van Ooijen et al., 2008; Wang et al., 2019; Martin et al., 2020). Mutations in these two motifs can result in

the loss of NLR activation and effector-independent cell death induction (autoactivation), respectively (Tameling et al., 2006; van Ooijen et al., 2008; Bernoux et al., 2011; Bernoux et al., 2016; Maruta et al., 2022).

NLRs are broadly classified into three subgroups based on N-terminal domains: TNLs, CNLs, and RNLs, which contain Toll/Interleukin-1 receptor/Resistance (TIR) domain, coiled-coil (CC) domain, and RPW8-like CC (RPW8) domain, respectively (Jones et al., 2016). The TIR, CC, or RPW8 domains are suggested to function as the signaling domains that trigger immune responses when NLRs oligomerize (Wang et al., 2019; Ma et al., 2020; Jacob et al., 2021). For instance, the CNL HOPZ-ACTIVATED RESISTANCE 1 (ZAR1) forms a pentameric resistosome when it detects the modifications of receptor-like cytoplasmic kinases. The activation of ZAR1 triggers changes in intramolecular interaction, and ATP binding within the interface by the NBD and HD1 stabilizes the active ZAR1 protomer (Wang et al., 2019). The interaction between active ZAR1 protomers is mediated by all subdomains, including NBD, HD1, WHD, and LRR, through hydrophobic and/or polar interactions, resulting in the formation of the pentameric ZAR1 resistosome (Wang et al., 2019). The released α-helix of the CC domain forms a funnel-shaped structure at the plasma membrane acting as a calcium channel that triggers immunity (Wang et al., 2019; Bi et al., 2021). NLRs functions to sense pathogens (sensor NLRs) or initiate signaling (helper NLRs or executor NLRs) (Adachi et al., 2019a). While many NLRs interact with helper NLRs to translate immune signals upon detecting pathogens, some NLRs, such as ZAR1 and RESISTANCE TO PSEUDOMONAS

SYRINGAE PV. MACULICOLA 1 (RPM1), can both sense and signal as singletons (Adachi et al., 2019a; Ngou et al., 2022).

Ralstonia species cause bacterial wilt disease in plants, including economically important Solanaceae crops (Hayward, 1991; Mansfield et al., 2012). The *R. solanacearum* species complex (RSSC) was commonly classified into four phylotypes based on the geographic origin of the strains (phylotype I, Asia; phylotype II, Americas; phylotype III, Africa; phylotype IV, Indonesia and Japan). More recently, the RSSC has been reclassified into three species: *R. solanacearum* (phylotype II strains), *R. pseudosolanacearum* (*Rps*, phylotype I and III strains), and *R. syzygii* (phylotype IV strains) (Fegan and Prior, 2005; Prior et al., 2016). The RSSC employs the type III secretion system and injects approximately 70 type III effectors (T3Es) referred to as *Ralstonia*-injected protein (Rip) into the host cell for pathogenicity (Peeters et al., 2013; Sabbagh et al., 2019). While only a limited number of NLRs have been identified as responsible for recognizing T3Es, the genetic complexity of *Rps* makes developing resistant crop varieties a challenging task. Therefore, it is crucial to mine new genetic resistance and to expand our understanding of the plant immune system.

In chapter 1, we showed that multiple T3Es from *R. pseudosolanacearum* induce cell death in *Nicotiana* species when transiently expressed through agroinfiltration. Moreover, the NbNLR-VIGS library screening revealed that RRS-Y recognizes RipY in *N. benthamiana*. In chapter 3, a CNL we named RRS-Y was found to be genetically required for the recognition of RipY and to activate immunity against *R.*

pseudosolanacearum in the presence of RipY. RRS-Y was also characterized as a functional CNL that localizes to the plasma membrane via the signaling CC domain and can form the self-association *in planta*. Intriguingly, RRS-Y was able to recognize different RipY homologs conserved across the RSSC, and the C-terminus of RipY was important for recognition by RRS-Y. These findings could contribute to a better understanding of the molecular mechanism of CNL-dependent immunity in plants.

MATERIALS AND METHODS

Plant growth conditions and bacterial strains

N. benthamiana were grown in a growth chamber under long-day conditions with 16 h: 8 h, light: dark at 24-26°C for 4-5 weeks before bacterial infiltration. Bacterial strains used in this study were *Escherichia coli* DH5α and *A. tumefaciens* AGL1. *E. coli* DH5α and *A. tumefaciens* strains were grown on Low-salt Luria-Bertani medium at 37°C and 28°C, respectively. All bacteria were grown on solid medium for 2 days (1 day for *E. coli*) with appropriate antibiotics. Single colonies were inoculated on liquid medium overnight in a shaker at 200 rpm. Bacterial suspensions were harvested by centrifugation for subsequent experiments.

Plasmid construction and mobilization

Golden Gate compatible gene modules (~1 kb) were amplified by standard PCR with flanking *Bsa*I restriction sites (Engler et al., 2008). For Golden Gate cloning, RipY alleles (CMR15v4_30690, RCFBP_21236, and RPSI07_3157) were synthesized by Twist Bioscience (USA) and cloned into the entry vector pICH41021. The modules of truncated RipY were obtained by amplification from the RipY Pe_1 using primers listed in Table 3-1. The modules for native RRS-Y were amplified from *N. benthamiana* cDNA. The synthetic fragment of *RRS-Y* (*RRS-Y*^{syn}) was designed using codon optimization tool from Integrated DNA technologies (IDT) (https://www.idtdna.com/CodonOpt). The synthetic fragment was synthesized by

Twist Bioscience (USA) then cloned into entry vector pICH41021. Site-directed mutagenesis was used to introduce the mutations to the CC or NB domains of RRS-Y. All primer sequences used in this study are listed in Table 3-1. For *Agrobacterium*-mediated expression, the modules were assembled into the binary vector pICH86988 with C-terminal epitope 3xFLAG, 6xHA, YFP, or mCherry under the control of the 35S cauliflower mosaic virus promoter. Binary vectors were mobilized into *A. tumefaciens* AGL1 using electroporation.

Hypersensitive response cell death assay and quantification

Agrobacteria cells grown in liquid culture were centrifuged at 8,000 rpm and resuspended in infiltration buffer (10 mM $MgCl_2$, 10 mM MES-KOH pH5.6). Cell suspensions were adjusted to OD_{600} of 0.4 ~ 0.5 and infiltrated into leaf tissues of 4 or 5-week old *N. benthamiana* using a needless syringe. Cell death occurrence was observed and photographed in visible or LED light (red-orange 617 nm and cool white 6500 K) at 3 or 4 days post infiltration (dpi). The extent of cell death was estimated by the quantum yield of chlorophyll fluorescence (F_v/F_m, QY) using a closed FluorCam (Photon Systems Instruments, Czech Republic). The default F_v/F_m protocol from FluorCam 7.0 software was used to determine minimum fluorescence (F_0), maximum fluorescence (F_m) and maximum quantum yield of photosystem II (F_v/F_m). The F_v/F_m value was around 0.7 in healthy leaves (Jones et al., 2001; Lee et al., 2021). All the experiments were repeated at least three times independently and merged values were analyzed with ANOVA and appropriate multiple comparison

tests using the GraphPad Prism9 software.

Gene expression

A. tumefaciens carrying effector constructs were infiltrated in leaf tissues of *N. benthamiana* and leaf discs were harvested before tissue collapse (~36 h post-infiltration). Total RNA was extracted using Trizol reagent (Invitrogen, USA) and cDNA was synthesized from 2 µg RNA using Maxima First Strands cDNA Synthesis kit (Thermo Scientific, USA) according to the manufacturer's instructions. cDNA was amplified by quantitative PCR using GoTaq qPCR Master Mix (Promega, USA) in the CFX96 Thermal Cycler (Bio-rad, USA). The relative expression was determined using the comparative 2(-Delta Delta C(t)) method and *NbEF1α* as reference (Livak and Schmittgen, 2001). Primers used in quantitative PCR are listed in Table 3-1. All the experiments were repeated at least three times independently and merged values were analyzed with ANOVA and appropriate multiple comparison tests using the GraphPad Prism9 software.

Bacterial growth assay

R. pseudosolanacearum growth assay was performed by Wenjia Yu in the licensed laboratory of Dr Alberto Macho (Shanghai Center for Plant Stress Biology, China) (Yu and Macho, 2021). Briefly, 4-5 weeks old *N. benthamiana* plants were infiltrated with the indicated Agrobacteria suspension 24 h prior to *Rps* Y45 infection. Leaf discs (4 mm diameter) were harvested at 2 dpi, homogenized and serially diluted in

sterile distilled water before plating on solid phi medium with appropriate antibiotics. Bacterial colonies were enumerated after 2 days incubation at 28°C.

Virus-induced gene silencing

Gene-silencing in *N. benthamiana* was conducted using the TRV-based vectors pTRV1 and pTRV2 (Liu et al., 2002). Two week-old *N. benthamiana* seedlings were infiltrated with a 1 : 1 ratio mixture of *A. tumefaciens* carrying pTRV1 and pTRV2 at OD_{600} of 0.5 into cotyledons. The plants were grown for 4 to 5 weeks before *A. tumefaciens* carrying constructs were infiltrated for transient expression of gene of interest. For VIGS of *RRS-Y*, short specific fragments (~200-bp) targeting the coding region were designed using Sol Genomics Network VIGS tool (vigs.solgenomics.net). Fragments were ligated into pTRV2 between *Eco*RI and *Bam*HI sites.

RNA-guided Cas9-mediated knockout of RRS-Y

Guide RNAs targeting *RRS-Y* were designed and introduced into a single guide RNA (sgRNA) scaffold by PCR (Parry et al., 2016). The primers used for producing gRNAs are listed in Table 3-1. Two sgRNAs were cloned into entry vector pICSL01009 containing *Arabidopsis* U6 promoter (Nekrasov et al., 2013). The entry vectors carrying sgRNA1 and sgRNA2 driven by a U6 promoter, Cas9 driven by the 35S promoter, and the *nptII* (kanamycin resistance) selection marker were assembled into the binary vector pAGM4723 (Weber et al., 2011). The confirmed construct was

transformed into *A. tumefaciens* AGL1 strain. Agroinfiltration was performed at OD_{600} of 0.5 in *N. benthamiana* leaves, and the infiltrated explants were incubated on selective Murashige and Skoog (MS) basal salt mixture medium (Duchefa Biochemie, Netherlands) for tissue culture. The primary transformants (T_0) were regenerated from the explants, and Cas9-induced mutations were confirmed by Sanger sequencing analysis.

Phylogenic analysis

Amino acid sequences of RipY proteins were obtained Ralsto T3E database (https://iant.toulouse.inra.fr/bacteria/annotation/site/prj/T3Ev3/). The global sequence alignment was built with the Blosum62 cost matrix, and the phylogenic tree was constructed by the neighbor-joining method with Jukes-Cantor genetic distance model and the ankyrin (ANK)-repeat containing protein WP_091733534.1 from *Mitsuaria* spp. as the outgroup using Geneious Tree Builder (Biomatters Ltd., New Zealand).

Immunoblot analysis and co-immunoprecipitation assay

N. benthamiana leaves were infiltrated with *Agrobacterium* strains carrying desired constructs. Leaf tissues were collected before tissue collapse (~43 h post-infiltration) and frozen in liquid nitrogen. Frozen tissues were ground to a fine powder in liquid nitrogen. One volume of powder was resuspended in an equal volume of GTEN buffer (10 % glycerol, 50 mM Tris-HCl pH 7.5, 2 mM EDTA, 150 mM NaCl)

supplemented with 5 mM DTT, cOmplete protease inhibitor cocktail (1 tablet/40 ml extraction buffer) (Roche, Germany), 0.2% NP-40, and 1% PVPP, then thawed in ice. The samples were centrifuged at 1,500*g* at 4°C for 10 min, and the supernatant was filtered through MiraCloth (Millipore, USA). The samples were denatured in 3x SDS protein loading buffer at 96°C for 10 min. For co-IP, the extracts were mixed with 30 µl GFP-trap beads (Chromotek, Germany) and incubated on rotary shaker at 4°C for 2 h. Samples were gently centrifuged and washed with IP buffer (GTEN buffer supplemented with 5 mM DTT, cOmplete protease inhibitor cocktail, and 0.2 % NP-40*).* The proteins bound to beads were eluted in 3x SDS protein loading buffer at 96°C for 10 min. The denatured proteins were separated on SDS-polyacrylamide gel electrophoresis (SDS-PAGE) and blotted on PVDF membranes. The membranes were probed with horseradish peroxidase-conjugated antibodies specific for primary anti-FLAG (Sigma Aldrich, USA), anti-HA (Santa-Cruz, USA), anti-GFP (Santa-Cruz, USA), or anti-mCherry (Agrisera, Sweden). Epitope-tagged proteins were visualized by the combination of SuperSignal™ West Pico and SuperSignal™ West Femto (Thermo Scientific, USA). Chemiluminescence was detected using Azure 400 (Azure Biosystem, USA). The predicted molecular weight of proteins is indicated in Table 3-2.

Plasma membrane protein fractionation

Agrobacterium carrying RRS-Y constructs tagged with a C-terminal 6xHA (RRS-Y, RRS-Y$^{C97A/C101A}$, RRS-Y^{D502V}, or RRS-Y$^{C97A/C101A/D502V}$) (OD_{600}=0.4) were co-

infiltrated with P19 (OD_{600}=0.1) in the entire leaves of *N. benthamiana*. Leaf tissues were collected before tissue collapse (~43 h post-infiltration) and immediately frozen in liquid nitrogen. The frozen tissues were ground to a fine powder in liquid nitrogen. Total protein extracts were prepared from half of the frozen tissues obtained from the entire infiltrated leaf using GTEN buffer as described above. The remaining frozen tissues from the entire infiltrated leaf were used to prepare the plasma membrane fraction. The plasma membrane proteins were enriched using the Minute™ Plant Plasma Membrane Protein Isolation Kit (Invent Biotechnologies, USA) in accordance with the manufacturer's instructions.

Confocal microscopy

A. tumefaciens AGL1 strains carrying C-terminally YFP-tagged RipY and its truncated variants, mCherry-tagged RipY, YFP-tagged RRS-Y and its variants were infiltrated in *rrs-y27*. The AtFLS2 tagged with mCherry at the C-terminus was used as a plasma membrane marker (Robatzek et al., 2006) and co-expressed with other constructs. YFP and mCherry signals were detected with Leica SP8X confocal microscope (Leica Microsystems, Germany) at 2 days post infiltration. The fluorescence of YFP and mCherry was excited at 514 nm and 561 nm with a white light laser and captured by the channels in the emission range 520 - 550 nm and 590 - 610 nm, respectively. Images were processed using LAS X software.

Table 3-1. Primers used in this study

Name	Sequences (5' to 3')	Purpose	References
RRS-Y.a_F1	GAATTCAGACCAAAGGAAGAAGTATCTACC	Silencing fragment cloning	In this study
RRS-Y.a_R1	GGATCCTTGTCTACTGCTTCTCTTTGTTGG	Silencing fragment cloning	In this study
RRS-Y.b_F1	GAATTCAAGGAAGGTTGCGTAAAAATGC	Silencing fragment cloning	In this study
RRS-Y.b_R1	GGATCCCATTAGGGAGATAACCACATGTTT	Silencing fragment cloning	In this study
RRS-Y.c_F1	GAATTCAAGCACATATGGAATGTGTATGAC	Silencing fragment cloning	In this study
RRS-Y.c_R1	GGATCCCATTTGCCTAAATTCTTGGGATATA	Silencing fragment cloning	In this study
RRS-Y_F1	ACTCTCTGAGAAGAAAATACTTG	qRT-PCR	In this study
RRS-Y_R1	GTGCTGCTGTCCACTCTATT	qRT-PCR	In this study
NbEF1α_F	AGAAGGAAGCTGCTGAGATGA	qRT-PCR	In this study
NbEF1α_R	CTTGGGGGTGGTAGCATCC	qRT-PCR	In this study
NbHin1_F	GCTTGGTTTTATTGGGAGAT	qRT-PCR	In this study
NbHin1_R	ATGATCTGCCATTAGACCCT	qRT-PCR	In this study
NbHsr203J_F	GGAGGAGCTTAAATTGCCGC	qRT-PCR	In this study
NbHsr203J_R	TTCAGAACCAGTTACAGGGT	qRT-PCR	In this study
RRS-Y_mod1_F	GGTCTCAAATGGCTGTGGTCAGTTTCAT	Golden gate cloning	In this study
RRS-Y_mod1_R	GGTCTCATTCTTCAGCAGCTGGAGTGC	Golden gate cloning	In this study
RRS-Y_mod2_F	GGTCTCAAGAAATCTCAACCAGTAAGT	Golden gate cloning	In this study
RRS-Y_mod2_R	GGTCTCAGATGAACATCTATGATATTTCC	Golden gate cloning	In this study
RRS-Y_mod3_F	GGTCTCACATCAAGAAAGTTTAAGTAGG	Golden gate cloning	In this study
RRS-Y_mod3_R	GGTCTCACGAACTTATGCATGTCCTCTT	Golden gate cloning	In this study
RRS-Y_F2	GCTAGGGGTTATATGTATGGTT	Genotyping of *rrs-y* KO lines	In this study
RRS-Y_R2	GGATCCTTGTCTACTGCTTCTCTTTGTTGG	Genotyping of *rrs-y* KO lines	In this study

RRS-Y_1-152/210_mod_F	GGTCTCAAATGGCTGTGGTCAGTTTCAT	Golden gate cloning	In this study
RRS-Y_1-152_mod_R	GGTCTCACGAAGTCTTTTCCTTCGTTAGAAAGGAGT	Golden gate cloning	In this study
RRS-Y_1-210_mod_R	GGTCTCACGAATATCCCTACAATTTTACAGTCCT	Golden gate cloning	In this study
RRS-Y_K218R_mod1_F	ATGGGTGGCATAGGCAGGACTACTCTTGCCAAG	Site-directed mutagenesis	In this study
RRS-Y_K218R_mod1_R	CTTGGCAAGAGTAGTCCTGCCTATGCCACCCAT	Site-directed mutagenesis	In this study
RRS-Y_D502V_mod2_F	GTTGCGTAAAAATGCATGTCATGGTTCGGGACTTTG	Site-directed mutagenesis	In this study
RRS-Y_D502V_mod2_R	CAAAGTCCCGAACCATGACATGCATTTTTACGCAAC	Site-directed mutagenesis	In this study
RRS-Y_C97A_F	CAATGAAGCTAAAACGCGTTTGAAGGCTTTAAAT	Site-directed mutagenesis	In this study
RRS-Y_C97A_R	GGATGTTTTCCAGATTTTAAAATCTGGAAAACATCCATTTAAAGCCTTCAAA	Site-directed mutagenesis	In this study
RRS-Y_C101A_F	CGCGTTTTAGCTTCATTGCGCGTTTGAAGTGTTTAAATGGAGCTTTTCCAGA	Site-directed mutagenesis	In this study
RRS-Y_C101A_R	TTTTCTCTCAAGGCCTTGAGAGAAAATCTGGAAAAGCTCCATTTAAACACTTCAAACGCG	Site-directed mutagenesis	In this study
RipY_GMI1000_Pe_57_mod1_F	GGTCTCAAATGCCGGTGGCCGGCTCCGA	Golden gate cloning	In this study
RipY_GMI1000_Pe_57_mod1_R	GGTCTCAGCGAGCGGGCCAGCTCGAAAAGG	Golden gate cloning	In this study
RipY_GMI1000_Pe_57_mod2_F	GGTCTCATCGCCGCACATCGATCTGAA	Golden gate cloning	In this study
RipY_GMI1000_Pe_57_mod2_R	GGTCTCAATGGCCTCGACTGTCTCGAATGC	Golden gate cloning	In this study
RipY_GMI1000_Pe_57_mod3_F	GGTCTCACCATGGAGGCGATGGCTGCC	Golden gate cloning	In this study
RipY_GMI1000_Pe_57_mod3_R	GGTCTCACGAACGGCCCGGCATGGACGTC	Golden gate cloning	In this study
RipY_Pe_1_mod3_731_R	GGTCTCACGAACCCCATTTTCAGCAGGTGC	Golden gate cloning	In this study
RipY_Pe_1_mod3_435_R	GGTCTCACGAATCCGATAAGGCGTGTCACC	Golden gate cloning	In this study
RipY_Pe_1_mod1_111_F	GGTCTCAAATGGTCAACGCGAACGGGACC	Golden gate cloning	In this study
RipY_Pe_1_mod2_436_F	GGTCTCAAATGAAGCCAGGCCGATTGTCC	Golden gate cloning	In this study

RRS-Y_sgRNA_F	TGTGGTCTCAATTGCTTCTTGACCAAAGACCAAGTTTTAGAGCTAGAAATAGCAAG	sgRNA cloning for CRISPR-Cas9	In this study
RRS-Y_sgRNA_scaffold_R	TGTGGTCTCAAGCGTAATGCCAACTTTGTAC	sgRNA cloning for CRISPR-Cas9	In this study

Table 3-2. Expected molecular weights of protein products

Name	Biochemical tag	Predicted size (kDa)
GFP	-	27
	N-terminal 3xFLAG	31.31
RipY_Pe_1_1-929	C-terminal 3xFLAG	104.01
	C-terminal YFP/GFP	127.92
	C-terminal mCherry	127.84
RipY_Pe1_1-731	C-terminal YFP	106.42
RipY_Pe1_1-435	C-terminal YFP	73.97
RipY_Pe1_111-929	C-terminal YFP	116.55
RipY_Pe1_436-929	C-terminal YFP	81.26
RipY_Pe_57	C-terminal 3xFLAG	104.01
RipY_GMI1000	C-terminal 3xFLAG	104.02
RipY_CMR15v4_30690	C-terminal 3xFLAG	104.04
RipY_RCFBP_21236	C-terminal 3xFLAG	106.13
RipY_RPSI07_3157	C-terminal 3xFLAG	106.22
RRS-Y	C-terminal 6xHA	145.48
	C-terminal YFP	165.02
Synthetic RRS-Y	C-terminal 6xHA	145.48
RRS-Y_K218R	C-terminal 6xHA	145.51
RRS-Y_D502V	C-terminal 6xHA	145.47
RRS-Y_C97A_C101A	C-terminal 6xHA	145.42
RRSY_C97A_C101A_ D502V	C-terminal 6xHA	145.4
CC_1-152	C-terminal 6xHA	24.86
	C-terminal YFP	44.47
CC_1-210	C-terminal 6xHA	31.88

	C-terminal YFP	51.42
CC_1-152_CC/AA	C-terminal 6xHA	24.79
	C-terminal YFP	44.41
H+ATPase	-	90-95
PEPC	-	110
AtFLS2	C-terminal mCherry	155.7

RESULTS

RRS-Y is genetically required for RipY recognition.

In chapter 1, the CNL RRS-Y was identified as a corresponding NLR required for the recognition of RipY using a NbNLR-VIGS library screening. To confirm *RRS-Y* requirement for RipY-induced cell death, additional VIGS assays were conducted using alternative silencing fragments. Three alternative 150-bp fragments were designed to target different regions of *RRS-Y* and cloned into the TRV-based vector (Figure 3-1A). Consistent with the results obtained with TRV:Com3-1 construct (Figure 1-7A), RipY-induced cell death was completely suppressed in TRV:RRS-Y.a, TRV:RRS-Y.b, and TRV:RRS-Y.c plants, while RipE1-induced cell death was not affected (Figure 3-1B). QY measurements correlated with the cell death occurrence (Figure 3-1C). Silencing efficiency was determined by qRT-PCR analysis for *RRS-Y* transcript level (Figure 3-1D). These results show that *RRS-Y* is specifically required for RipY-induced cell death.

Next, a synthetic version of *RRS-Y* (hereafter, *RRS-Y*^{syn}) (Wu et al., 2017) containing alternative codons was designed to prevent VIGS by the RRS-Y.c fragment (Figure 3-2A). Co-expression of RipY with RRS-Y^{syn}, but not with RRS-Y, induced cell death in TRV:RRS-Y.c plants (Figure 3-2B). QY measurements correlated with the cell death occurrence (Figure 3-2C). Moreover, RRS-Y^{syn} protein accumulated in TRV:RRS-Y.c plants while RRS-Y was not detectable, confirming that RRS-Y^{syn} can evade silencing in TRV:RRS-Y.c plants (Figure 3-2D). These

results demonstrate that *RRS-Y* is genetically required for RipY-induced cell death in *N. benthamiana*.

To examine *RRS-Y* genetic requirement for RipY recognition in a stable null background, CRISPR/Cas9 system was used to mutagenize *RRS-Y* (Nekrasov et al., 2013). After *Agrobacterium*-mediated transformation of *N. benthamiana* leaf explants, two independent mutant plants, *rrs-y23* and *rrs-y27*, were obtained (Figure 3-3A). The Cas9-induced mutations in *RRS-Y* consisted of three distinct types of deletions leading to frameshift (2-bp deletion, *rrs-y23*) or early stop codon (1-bp deletion, *rrs-y27a*; 7-bp deletion, *rrs-y27b*). In contrast to the RipE1-induced cell death, RipY-induced cell death was absent in both *rrs-y23* and *rrs-y27* plants (Figure 3-3A). This indicates that in *rrs-y23* and *rrs-y27* plants, the CRISPR-Cas9-induced mutations in the *RRS-Y* gene specifically abolished RipY recognition. Next, RRS-Y was transiently expressed to test whether it is sufficient to restore RipY-induced cell death in *rrs-y27* mutants. Co-expression of RipY with RRS-Y induced cell death in *rrs*-y27 plants (Figure 3-3B and 3-3C). Although, the accumulation of *NbHIN1* and *NbHsr203J* transcripts was not fully abolished in *rrs-y*27 plants, the accumulation of *NbHIN1* and *NbHsr203J* transcripts was significantly enhanced when RipY was co-expressed with RRS-Y in *rrs-y27* consistent to cell death recovery (Figure 3-3D).

RRS-Y protein was predicted to have typical features of a CNL with a coiled-coil domain at the N-terminus, a NB domain with conserved motifs in the central region, and at least 13 putative leucine-rich repeat motifs at the C-terminus (Figure 3-4). Furthermore, in accordance with the lack of RipY-induced cell death in *N.*

tabacum (Figure 1-1), no putative *RRS-Y* orthologs could be identified in available databases of this species.

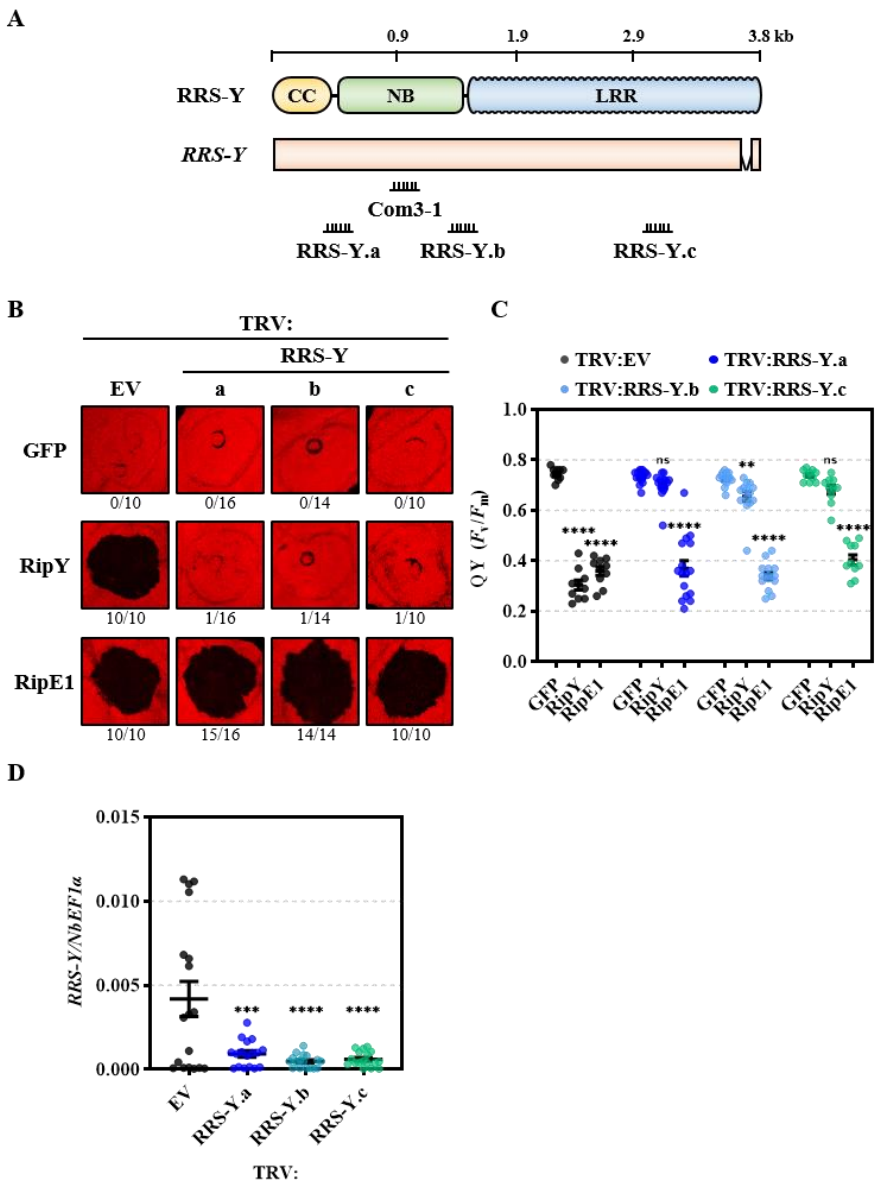

Figure 3-1. RipY-induced cell death was compromised in *RRS-Y*-silenced plants. (A) Schematic structure of the *RRS-Y* gene and protein. Exons are represented as a red box (bp: base pair). The CC, NB, and LRR domains are indicted as yellow, green, and blue, respectively. Black lines indicate the position of the library Com3-1 fragment and the alternative silencing fragments (TRV:RRS-Y.a, TRV:RRS-Y.b,

and TRV:RRS-Y.c). (B) RipY-induced cell death is compromised in *RRS-Y*-silenced plants. *Agrobacterium* strains carrying GFP, RipY, or RipE1 constructs (OD_{600}=0.5) were infiltrated in TRV:EV, TRV:RRS-Y.a, TRV:RRS-Y.b, or TRV:RRS-Y.c plants. Pictures were taken at 4 dpi. Numbers indicate patches with cell death out of total infiltrated patches. (C) Quantum yield (QY, *F*v/*F*m) was measured in the infiltrated patches. Individual values from independent experiments are indicated as dots. Data were analyzed with one-way ANOVA followed by Dunnett's multiple comparison test. Asterisks indicate statistically significant differences with GFP (**, $P<0.01$ ****, $P<0.0001$; ns, not significant). Bars represent mean ± SEM (n=10-16). (D) Relative expression of *RRS-Y* in silenced plants was determined by quantitative RT-PCR and normalized by *NbEF1α*. Individual values from independent experiments are indicated as dots. Data were analyzed by one-way ANOVA followed by Dunnett's multiple comparison test. Asterisks indicate statistically significant differences with TRV:EV (***, $P<0.001$; ****, $P<0.0001$). Bars represent mean ± SEM (n=18).

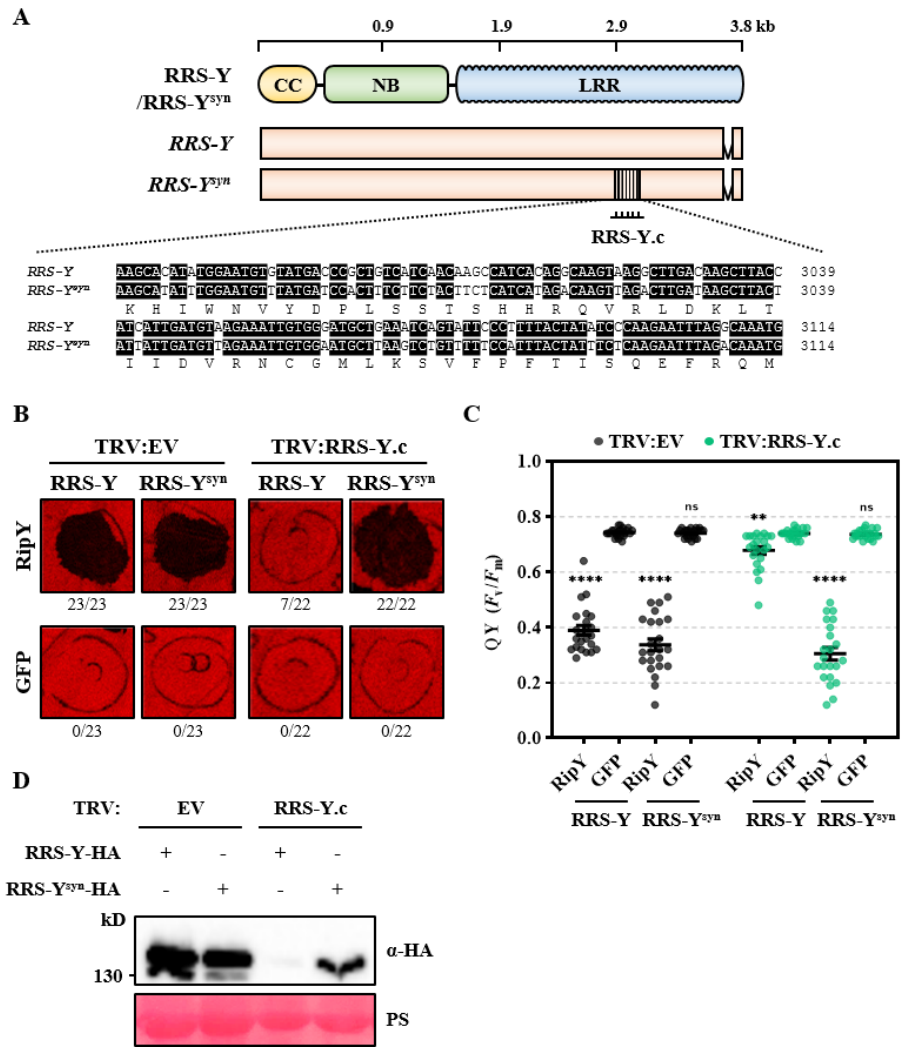

Figure 3-2. RipY-induced cell death was complemented by synthetic RRS-Y in *RRS-Y*-silenced plants.

(A) Alignment of *RRS-Y* and *RRS-Y^{syn}* nucleotide sequences (bp: base pair). Consensus sequences between *RRS-Y* and *RRS-Y^{syn}* are highlighted in black. Numbers on the right indicate the nucleotide position in *RRS-Y* and *RRS-Y^{syn}* sequence. (B) Synthetic RRS-Y (RRS-Y^{syn}) complements RipY-induced cell death in *RRS-Y*-silenced *N. benthamiana*. RRS-Y and RRS-Y^{syn} were co-expressed with GFP or RipY (OD_{600}=0.5) in TRV:EV or TRV:RRS-Y.c plants. Pictures were taken

4 dpi. Numbers indicate patches with cell death out of total infiltrated patches. (C) Quantum yield (QY, *F*v/*F*m) was measured in the infiltrated patches. Individual values from independent experiments are indicated as dots. Data were analyzed with two-way ANOVA followed by Sidak's multiple comparison test. Asterisks indicate statistically significant differences with GFP+RRS-Y (**, $P<0.01$; ****, $P<0.0001$; ns, not significant). Bars represent mean ± SEM (n=22-23). (D) Accumulation of RRS-Y^{syn}. *Agrobacterium* strains carrying RRS-Y or RRS-Y^{syn} constructs (OD_{600}=0.5) were infiltrated in TRV:EV or TRV:RRS-Y.c plants. Total protein extracts were immunoblotted with anti-HA antibody. Ponceau red staining (PS) attests equal loading of the samples.

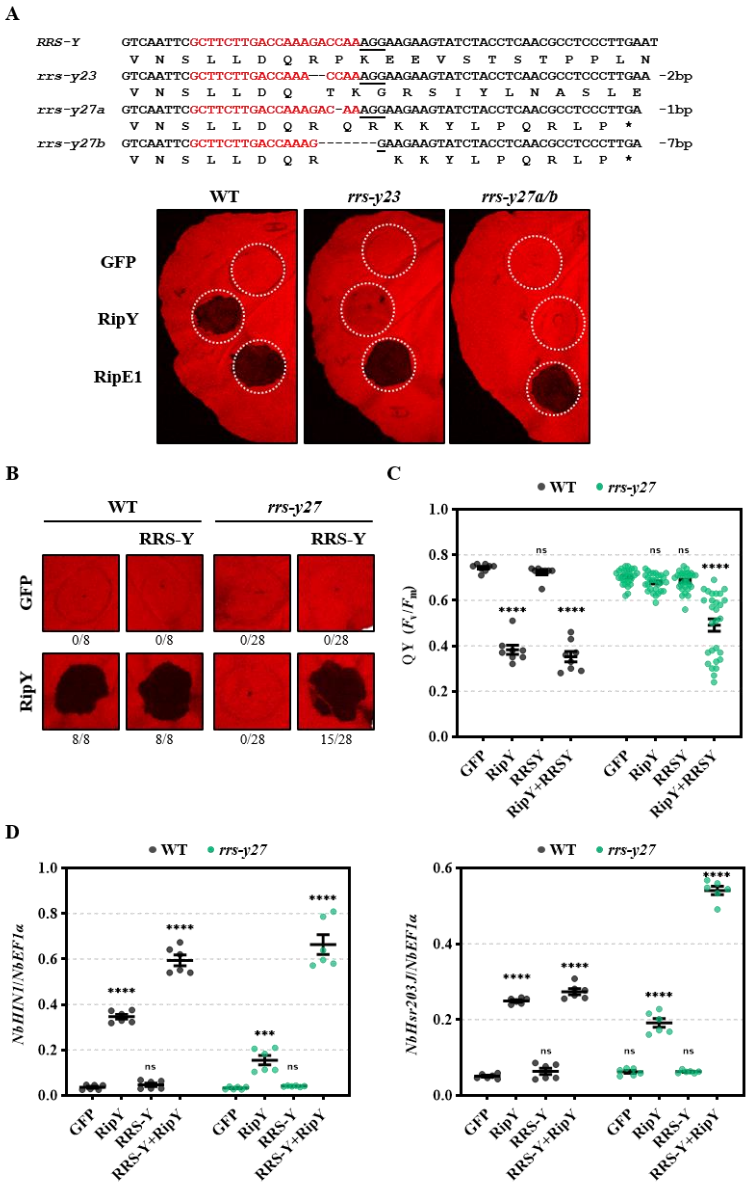

Figure 3-3. RipY-induced cell death was complemented by native RRS-Y in *rrs-y* stable knockout plants.

(A) *RRS-Y* mutant lines obtained by CRISPR/Cas9 in *N. benthamiana*. Sequence alignment with three distinct indels in *RRS-Y* gene of independent T0 transformants (*rrs-y23*, *rrs-y27a*, and *rrs-y27b*). Sequences targeted by sgRNA and PAM motif are

shown in red and underlined, respectively. *Agrobacterium* strains carrying GFP, RipY, or RipE1 constructs (OD_{600}=0.5) were infiltrated in wild-type (WT) or *rrs-y* mutant lines. Pictures were taken at 4 dpi. (B) *RRS-Y* expression is sufficient to restore RipY-induced cell death in *rrs-y27* mutant. *Agrobacterium* strains carrying GFP, RipY, or RRS-Y constructs (OD_{600}=0.5) were infiltrated in WT or *rrs-y27* plants. Pictures were taken at 4 dpi. Numbers indicate patches with cell death out of total infiltrated patches. (C) Quantum yield (QY, *F*v/*F*m) was measured in the infiltrated patches. Individual values from independent experiments are indicated as dots. Data were analyzed with two-way ANOVA followed by Sidak's multiple comparison test. Asterisks indicate statistically significant differences with GFP (****, P<0.0001; ns, not significant). Bars represent mean ± SEM (n=8-28). (D) *RRS-Y* is sufficient for RipY-induced *NbHIN1* and *NbHsr203J* transcript accumulation. *Agrobacterium* strains carrying GFP, RipY, or RRS-Y constructs (OD_{600}=0.5) were infiltrated in wild-type (WT) or *rrs-y27* plants. Gene expression was determined by quantitative RT-PCR and normalized by *NbEF1α*. Individual values from independent experiments are indicated as dots. Data were analyzed by two-way ANOVA followed by Sidak's multiple comparison test. Asterisks indicate statistically significant differences with GFP (***, P<0.001; ****, P<0.0001; ns, not significant). Bars represent mean ± SEM (n=6).

Figure 3-4. RRS-Y harbors typical features of a CNL.

(A) Schematic structure of RRS-Y carrying conserved motifs of CNL. Yellow, green, and blue indicate the coiled-coil (CC), nucleotide-binding (NB), and leucine-rich repeats (LRR) domain, respectively. The conserved motifs are shown on the right of each domain. (B) RRS-Y protein sequence. The protein sequence corresponding to domain and motif is indicated as same color described in (A). The highly conserved motif sequences of CNL are underlined. The key residues in NB domain for NLR activity are shown in red. Numbers on the right indicate the amino acid position in RRS-Y sequence.

RRS-Y mediates RipY-induced immunity to *R. pseudosolanacearum.*

To determine whether RipY recognition by RRS-Y can activate immunity against *Rps*, a combined agroinfiltration and *Rps* inoculation assay was conducted in the laboratory of Dr. Alberto Macho (Shanghai Center for Plant Stress Biology, China). The *Rps* Y45 strain (Y45) was chosen because this strain can cause disease in *N. benthamiana* and is lacking RipY as well as several other recognized T3Es (Li et al., 2011). Firstly, RipY-GFP fusion could trigger cell death in *N. benthamiana*, as the RipY-FLAG that was used in all the previous assay. As expected, the cell death induced by RipY-GFP was abolished in the *rrs-y27* plants (Figure 3-5A). Next, RipY-GFP or GFP were expressed by agroinfiltration before inoculation of Y45, and Y45 growth was measured at 2 days post inoculation (Figure 3-5B). In WT plants, Y45 growth was restricted in tissues expressing RipY, growing around 10-fold less than in tissues expressing GFP. On the other hand, Y45 growth was comparable in RipY- and GFP-expressing tissues of the *rrs-y* mutant, suggesting that RRS-Y activates immune responses upon RipY recognition. Immunoblotting confirmed that the loss of cell death and differential bacterial growth were not due to lack of RipY protein accumulation (Figure 3-5C). These results demonstrate that *RRS-Y* mediates not only cell death induction but also resistance to pathogenic *Rps* in *N. benthamiana*.

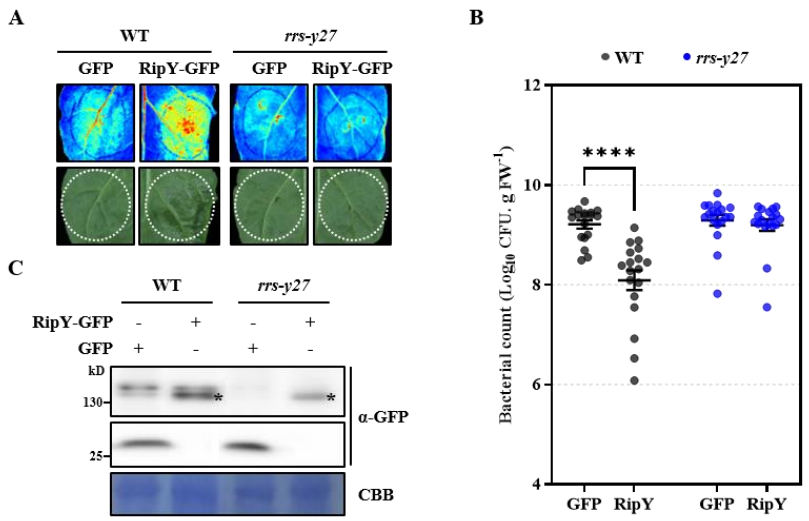

Figure 3-5. RRS-Y mediates RipY-induced immunity to *Ralstonia pseudosolanacearum*.

(A) RipY-GFP-induced cell death is compromised in *rrs-y27* plants. *Agrobacterium* strains carrying GFP or RipY-GFP constructs (OD_{600}=0.2) were infiltrated in wild-type (WT) or *rrs-y27* plants. Pictures were taken at 2 dpi with a CCD camera (lower panel) or a UV camera (upper panel). (B) RipY-induced restriction of pathogen growth is impaired in *rrs-y27* plants. *R. pseudosolanacearum* strain Y45 was infiltrated at 10^5 CFU. ml^{-1} in WT or *rrs-y27* plants 2 days after agroinfiltration of GFP or RipY-GFP (OD_{600}=0.2). Bacterial enumeration 2 days after inoculation in three independent experiments is presented (bar: mean with SEM). Asterisks indicate significant differences compared with GFP control (**** P<0.0001). (C) Protein accumulation of RipY-GFP. Agroinfiltration was conducted as described in (A). Total proteins were extracted at 2 dpi and subjected to immunoblot analysis with anti-GFP antibody. Asterisks indicate the expected protein size. Coomassie blue staining (CBB) indicates equal loading of the samples. These experiments were performed by Dr Wenjia Wu in the laboratory of Alberto Macho, licensed for work with *Ralstonia pseudosolanacearum* at the Shanghai Center for Plant Stress Biology, China.

RRS-Y is a functional CNL that associates with the plasma membrane.

As RRS-Y was a newly identified CNL in this study, the functionality of RRS-Y was tested. The NB domain of NLRs is responsible for the transition to the activated state, with the P-loop motif being the key ATP-binding region. Mutations within P-loop motif often lead to loss-of-function (Walker et al., 1982; Takken et al., 2006). Moreover, mutations in the highly conserved MHD motif of NLRs cause auto-activation (Tameling et al., 2006). To generate NB domain mutants of RRS-Y, the lysine (K) residue within P-loop and the aspartate (D) residue within MHD motif were substituted with arginine (R) and valine (V), respectively, and generated RRS-Y^{K218R} and RRS-Y^{D502V} (Figure 3-6A). RRS-Y^{K218R} expression failed to induce cell death when co-expressed with RipY in the *rrs-y*27 mutant while RRS-Y^{WT} expression induced cell death. Conversely, RRS-Y^{D502V} expression induced cell death regardless of the presence of RipY (Figure 3-6A). QY measurements correlated with the cell death occurrence (Figure 3-6B). Immunodetection of RRS-Y^{WT}-HA, RRS-Y^{K218R}-HA, RRS-Y^{D502V}-HA, and RipY-FLAG showed that all the proteins accumulated in the *rrs-y27* mutant, confirming that the absence of cell death was not due to lack of protein accumulation (Figure 3-6C). These results indicate that RRS-Y NB domain is functional and required for the immune signaling in presence of RipY.

In order to investigate whether RipY is recognized by RRS-Y in the same cellular compartment *in planta*, the subcellular localization of RRS-Y and RipY was examined using confocal microscopy after agroinfiltration in *N. benthamiana* leaf

epidermis. Interestingly, both RRS-Y-YFP and RipY-YFP fusion proteins accumulated at the cell periphery (Figure 3-6D). As no cytoplasmic strands could be observed, we further demonstrated that both proteins localized to the plasma membrane by co-expressing RRS-Y-YFP or RipY-YFP with the plasma membrane-localized receptor AtFLS2 (Robatzek et al., 2006) fused to mCherry (Figure 3-6D). Although RRS-Y-YFP fluorescence was rather faint, it also overlapped with RipY-mCherry fluorescence when the two proteins were co-expressed in the same cells (Figure 3-6D), indicating that the T3E and the immune receptor localize to the same subcellular compartment. Immunodetection confirmed the accumulation of proteins from the constructs used for subcellular localization in the *rrs-y27* mutant plants (Figure 3-6E).

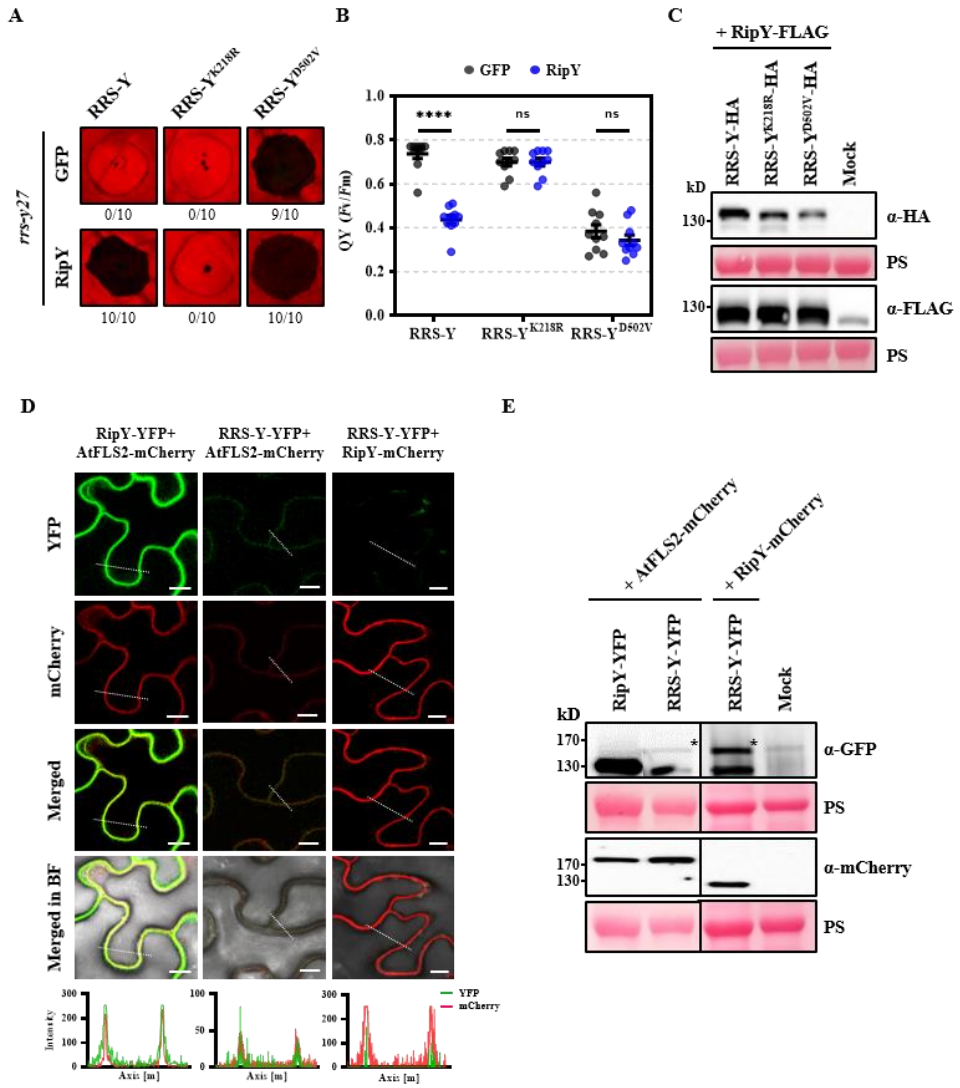

Figure 3-6. RRS-Y is a functional CNL that associates with the plasma membrane.

(A) The NB domain is critical for RRS-Y activation. *Agrobacterium* strains carrying GFP, RipY, RRS-Y^{WT} (RRS-Y), RRS-Y^{K218R}, or RRS-Y^{D502V} constructs (OD_{600}=0.5) were infiltrated in *rrs-y27* plants. Pictures were taken at 4 dpi. Numbers indicate patches with cell death out of total infiltrated patches. (B) Quantum yield (QY, *F*v/*F*m) was measured in the infiltrated patches. Individual values from independent

experiments are indicated as dots. Data were analyzed with two-way ANOVA followed by Sidak's multiple comparison test. Asterisks indicate statistically significant differences (****, $P<0.0001$; ns, not significant). Bars represent mean ± SEM (n=10). (C) Accumulation of RRS-Y and its variants in presence of RipY in *rrs-y27* plants. *Agrobacterium* strains carrying RipY, RRS-Y^{WT} (RRS-Y), RRS-Y^{K218R}, or RRS-Y^{D502V} constructs (OD_{600}=0.5) were infiltrated in *rrs-y27* plants. Total protein extracts were immunoblotted with anti-HA or anti-FLAG antibodies. Ponceau red staining (PS) attests equal loading of the samples. (D) Both RipY and RRS-Y localize to plasma membrane in the epidermal cells. AtFLS2-mCherry was used as a plasma membrane marker. *Agrobacterium* strains carrying RipY-YFP/mCherry or RRS-Y-YFP constructs (OD_{600}=0.4) and *Agrobacterium* strain carrying AtFLS2-mCherry construct (OD_{600}=0.2) were infiltrated in *rrs-y27* plants. Images were acquired by confocal microscopy at 2 dpi (bright field, BF). YFP and mCherry fluorescence intensity across the sections indicated by dotted lines are shown under the images. Scale bars indicate 11 μm. (E) Accumulation of RipY-YFP/mCherry, RRS-Y-YFP, and AtFLS2-mCherry. The experiment was conducted as described on (D). Total protein extracts were immunoblotted with anti-GFP or anti-mCherry antibodies. Ponceau red staining (PS) attests equal loading of the samples.

CC domain of RRS-Y localizes at the plasma membrane and is sufficient to signal cell death.

Several studies have highlighted the role of the CC domain of CNLs for association with the plasma membrane (Qi et al., 2012; Wang et al., 2019; Wang et al., 2020). As the functional boundaries between CC and NB domain can be difficult to assign (Bentham et al., 2018), two constructs were designed to investigate the function of RRS-Y CC domain: $CC_{1\text{-}152}$ that corresponds to the ZAR1 CC domain able to trigger cell death (Baudin et al., 2017) and $CC_{1\text{-}210}$ that covers the RRS-Y N-terminal region down to the beginning of the predicted NB domain (Figure 3-4). Additionally, two cysteines (C97 and C101) that were predicted as palmitoylation sites (GPS-Lipid http://lipid.biocuckoo.org; (Xie et al., 2016)) were replaced by alanine (A) in the RRS-Y CC domain. Both $CC_{1\text{-}152}$-YFP and $CC_{1\text{-}210}$-YFP fusion proteins localized at the plasma membrane, as shown by the overlap with AtFLS2-mCherry signal (Figure 3-7A). However, $CC_{1\text{-}152}^{C97A/C101A}$-YFP signal was observed in intracellular structures, indicating an incomplete recruitment at the plasma membrane. All three CC constructs accumulated to a similar level in total protein extracts (Figure 3-7B).

Overexpression of the CC domain of several group 10 CNLs can induce effector-independent cell death (Wróblewski et al., 2018; Lee et al., 2021). As RRS-Y belongs to this CNL group 10 (Seong et al., 2020), the CC domain of RRS-Y was tested for cell death induction. In WT plants, $CC_{1\text{-}152}$ expression induced cell death reproducibly to similar extend as the autoactive RRS-Y^{D502V} (Figure 3-7C). Conversely, $CC_{1\text{-}210}$ and $CC_{1\text{-}152}^{C97A/C101A}$ constructs could not signal. QY

measurement correlated with the occurrence of cell death (Figure 3-7D), and the stability of the proteins was confirmed by immunodetection (Figure 3-7E). These results support the importance of RRS-Y CC domain for signaling, and suggest that RRS-Y association with the plasma membrane is essential for its function.

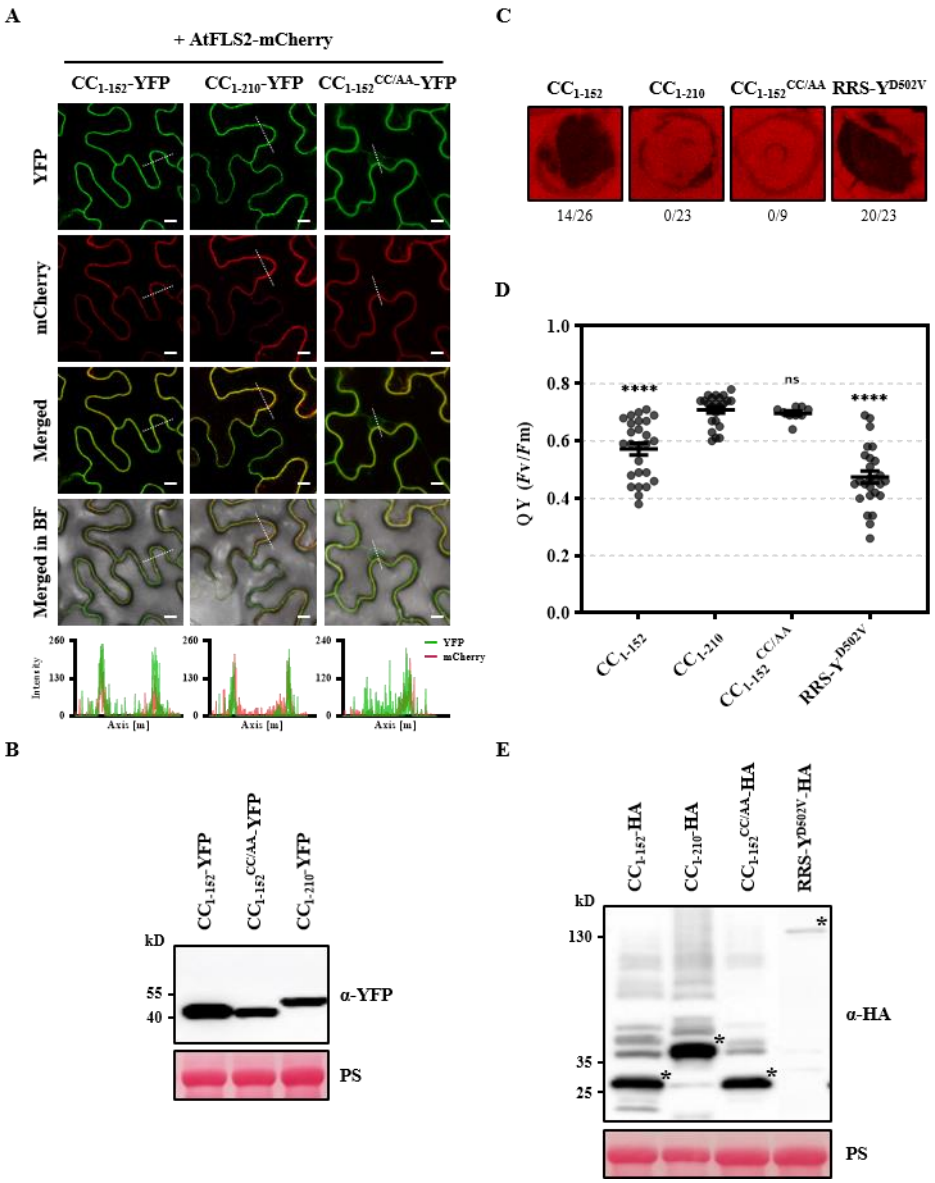

Figure 3-7. CC domain of RRS-Y localizes at the plasma membrane and is sufficient to signal cell death.

(A) RRS-Y CC domain associates with the plasma membrane in epidermal cells. *Agrobacterium* strains carrying $CC_{1\text{-}152}$-YFP, $CC_{1\text{-}210}$-YFP, or $CC_{1\text{-}152}^{C97A/C101A}$-YFP ($CC_{1\text{-}152}^{CC/AA}$) constructs ($OD_{600}$=0.4) and *Agrobacterium* strain carrying AtFLS2-

mCherry construct (OD_{600}=0.2) were infiltrated in *rrs-y27* plants. Images were acquired by confocal microscopy at 2 dpi. YFP and mCherry fluorescence intensity across the sections indicated by dotted lines are shown under the images. Scale bars indicate 11 μm. (B) Accumulation of C-terminal YFP-tagged RRS-Y CC variants. *Agrobacterium* strains carrying RRS-Y CC variant constructs (OD_{600}=0.5) were infiltrated in *rrs-y27* plants. Total protein extracts were immunoblotted with anti-GFP antibody. Ponceau red staining (PS) attests equal loading of the samples. (C) Two cysteine residues are required for cell death signaling of RRS-Y CC domain. *Agrobacterium* strains carrying $CC_{1\text{-}152}$-YFP, $CC_{1\text{-}210}$-YFP, $CC_{1\text{-}152}^{CC/AA}$-YFP, or RRS-$Y^{D502V}$ constructs (OD_{600}=0.5) were infiltrated in WT plants. Pictures were taken at 4-6 dpi. Numbers indicate patches with cell death out of total infiltrated patches. (D) Quantum yield (QY, *F*v/*F*m) was measured in the infiltrated patches. Individual values from independent experiments are indicated as dots. Data were analyzed with one-way ANOVA followed by Dunnett's multiple comparisons test. Asterisks indicate statistically significant differences with $CC_{1\text{-}210}$ (****, P<0.0001; ns, not significant). Bars represent mean ± SEM (n=9-26). (E) Accumulation of C-terminal HA-tagged RRS-Y CC variants and autoactive RRS-Y^{D502V}. *Agrobacterium* strains carrying RRS-Y CC variants or autoactive RRS-Y^{D502V} constructs (OD_{600}=0.5) were infiltrated in WT plants. Total protein extracts were immunoblotted with anti-HA antibody. Asterisks indicate the expected protein size. Ponceau red staining (PS) attests equal loading of the samples.

CC domain of RRS-Y mediates association with the plasma membrane and is critical for RRS-Y signaling.

To confirm that plasma membrane localization is necessary for RRS-Y signaling, the mutations C97A and C101A were introduced in the full length RRS-Y (RRS-$Y^{C97A/C101A}$) and RRS-Y^{D502V} (RRS-$Y^{C97A/C101A/D502V}$) constructs, and plasma membrane protein fractionation was performed (Figure 3-8A). Consistent with the localization of RRS-Y-YFP, RRS-Y and RRS-Y^{D502V} were detected in the plasma membrane-enriched protein extract. However, despite a similar accumulation in total proteins, RRS-$Y^{C97A/C101A}$ and RRS-$Y^{C97A/C101A/D502V}$ proteins were not detectable in the plasma membrane fraction (Figure 3-8A). Moreover, the co-expression of RRS-$Y^{C97A/C101A}$ or RRS-$Y^{C97A/C101A/D502V}$ with RipY did not induce cell death while that of RRS-Y with RipY induced cell death (Figure 3-8B). RRS-Y^{D502V} expression showed autoactivity independent on RipY presence, which could explain the low accumulation of RRS-Y^{D502V} in the plasma membrane fraction as shown in Figure 3-8A. QY measurement correlated with the occurrence of cell death (Figure 3-8C). Altogether, these results indicate that RRS-Y signaling requires the association with the plasma membrane through the CC domain.

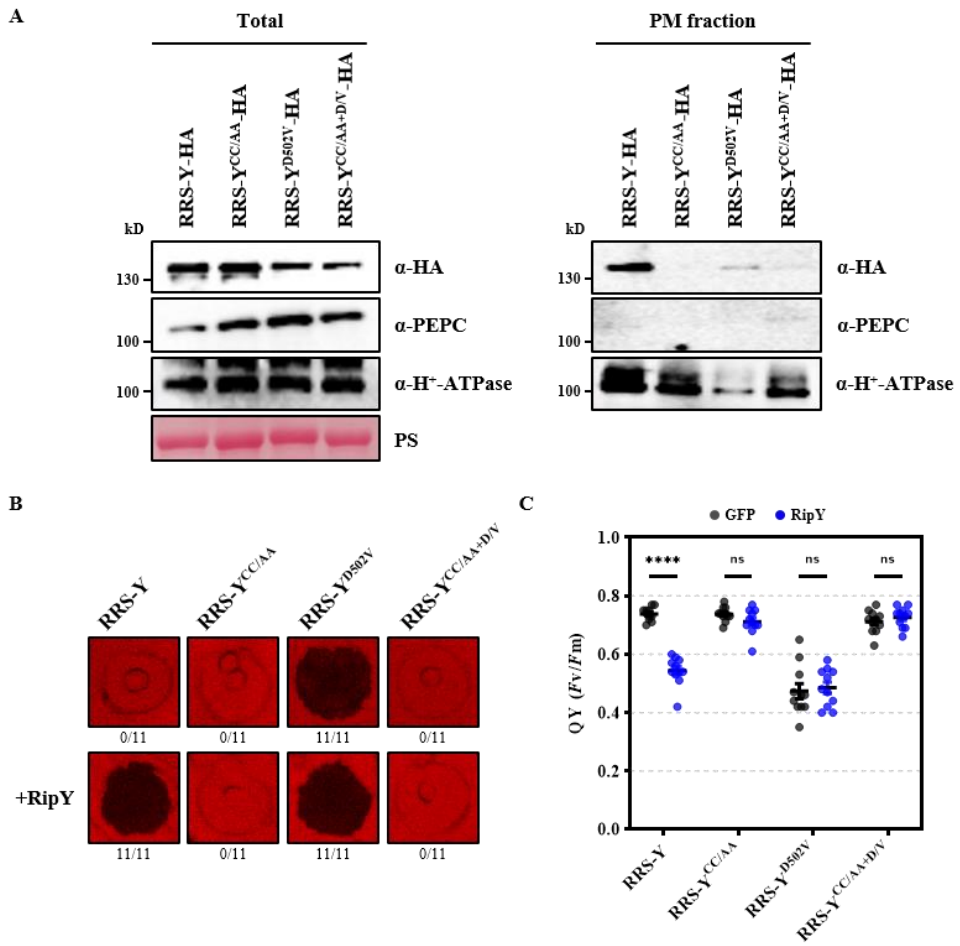

Figure 3-8. CC domain of RRS-Y mediates association with the plasma membrane and is critical for RRS-Y signaling.

(A) Mutation in two cysteine residues affects the plasma membrane localization of RRS-Y. *Agrobacterium* strains carrying RRS-Y-HA, RRS-$Y^{C97A/C101A}$-HA (RRS-$Y^{CC/AA}$), RRS-Y^{D502V}-HA, or RRS-$Y^{C97A/C101A/D502V}$-HA (RRS-$Y^{CC/AA+D/V}$) constructs (OD_{600}=0.4) were co-infiltrated with P19 (OD_{600}=0.1) in *rrs-y27* plants. Immunoblotting analysis was conducted on total proteins and plasma membrane (PM) fractions of *rrs-y27* plants with the indicated antibodies. PEPC and H+-ATPase were used as cytosol and PM protein markers, respectively. Ponceau red staining (PS) attests equal loading of the samples. (B) Mutation in two cysteine residues affects RipY recognition of RRS-Y. *Agrobacterium* strains carrying RRS-Y-HA, RRS-

$Y^{CC/AA}$-HA, RRS-Y^{D502V}-HA, or RRS-$Y^{CC/AA+D/V}$-HA constructs were co-infiltrated with RipY at OD_{600} of 0.4 in *rrs-y27* plants. Pictures were taken at 4 dpi. Numbers indicate patches with cell death out of total infiltrated patches. (C) Quantum yield (QY, *F*v/*F*m) was measured in the infiltrated patches. Individual values from independent experiments are indicated as dots. Data were analyzed with two-way ANOVA followed by Sidak's multiple comparison test. Asterisks indicate statistically significant differences (****, $P<0.0001$; ns, not significant). Bars represent mean ± SEM (n=11).

Self-association of RRS-Y is independent of the presence of RipY.

Previous studies have shown that some NLRs, including RPM1, MLA1, Sr50, and RPS5, undergo self-association prior to effector-triggered activation (Ade et al., 2007; Maekawa et al., 2011; Cesari et al., 2016; El Kasmi et al., 2017). Conversely, the CNL ZAR1 oligomerizes into a pentamer upon the effector recognition acting as a cation channel in the plasma membrane (Wang et al., 2019; Hu et al., 2020; Bi et al., 2021). To investigate whether RRS-Y has the ability to self-associate, and whether the effector elicits its self-association, RRS-Y constructs tagged with different C-terminal epitopes (RRS-Y-HA and RRS-Y-YFP) were generated. Co-expression of both RRS-Y constructs with or without RipY construct in the *rrs-y27* mutant was followed by co-immunoprecipitation using GFP-trap beads to pull-down RRS-Y-YFP from total protein extracts. RRS-Y-HA was detected in extract enriched with the RRS-Y-YFP, regardless of the presence of RipY (Figure 3-9). These results suggest that RRS-Y can self-associate in an effector-independent manner, consistent with other CNLs, such as RPM1 and MLA1 (Maekawa et al., 2011; El Kasmi et al., 2017). The precise role of self-associated RRS-Y remains to be determined.

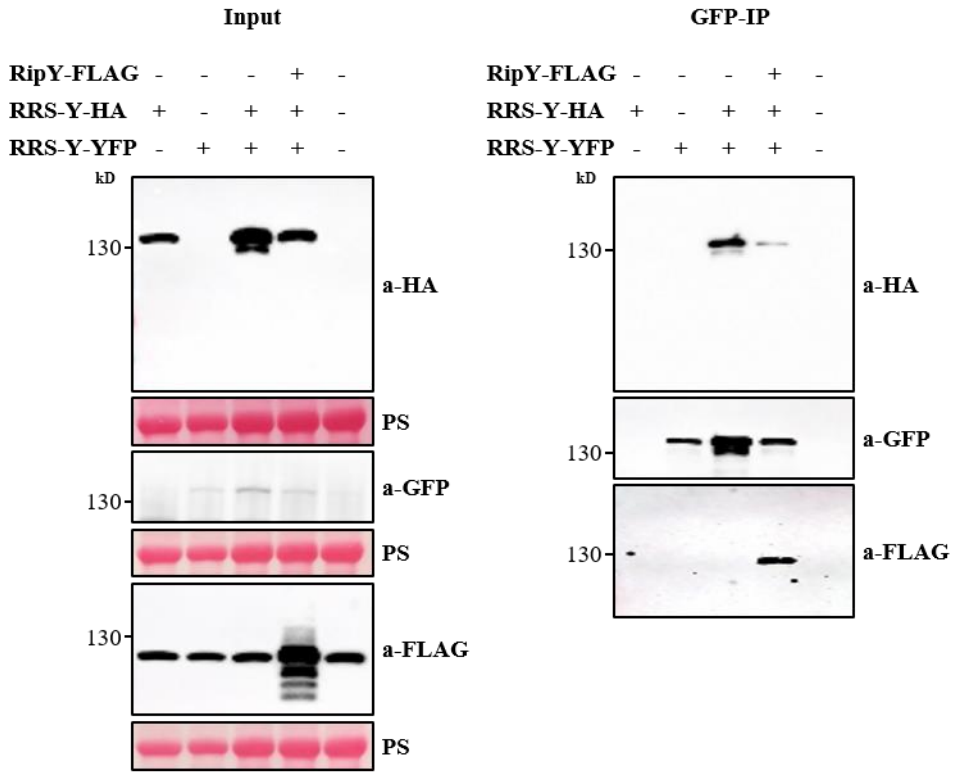

Figure 3-9. RRS-Y can form the self-association independent on RipY presence in *N. benthamiana.*

Agrobacterium strains carrying RRS-Y-HA, RRS-Y-YFP, or RipY-FLAG constructs (OD_{600}=0.2) were co-infiltrated in *rrs-y27* plants. Total protein extracts (input) were incubated on GFP-trap beads (GFP-IP) followed by immunoblotting with the indicated antibodies. Ponceau red staining (PS) attests the equal loading of the input samples.

RRS-Y perceives RipY natural variants across *Ralstonia* spp.

RipY is a relatively large T3E with no predicted enzymatic activity but contains a central region with multiple ankyrin (ANK) repeats (Peeters et al., 2013). RipY alleles are broadly present among strains of *Rps* (phylotype I and III), *R. solanacearum* (phylotype IIA and IIB), and *R. syzygii* (phylotype IV) (Prior et al., 2016). A phylogenetic tree was generated with the RipY protein sequences available in the RalstoT3E database (Peeters et al., 2013), and the Korean *R. pseudosolanacearum* phylotype I strains that contain polymorphic RipY alleles (Prokchorchik et al., 2020) (Figure 3-10). RipY sequence is highly conserved among strains within the *Rps* species, with over 99% amino acid (aa) identity between 30 Korean isolates (Prokchorchik et al., 2020). Similarly, RipY sequence is less polymorphic to other phylotype I strains (reference strain GMI1000, 99.57% aa identity; CMR15v4, 89.24% aa identity). Increased sequence polymorphism (~ 72% aa identity) was observed in strains classified in phylotype II / *R. solanacearum* or phylotype IV / *R. syzygii* (Figure 3-11).

To examine whether RRS-Y recognizes polymorphic RipY alleles from four phylotypes, RipY sequences were cloned from *Ralstonia* strains Pe57, GMI1000 and CMR15v4 (phylotype I, *Rps*), RCFBP (phylotype II, *R. solanacearum*), and RPSI07 (phylotype IV, *R. syzygii*) (Figure 3-12). These representative RipY alleles induced varied but significant degree of cell death when expressed in wild-type *N. benthamiana* (Figure 3-12A), with the exception of RipY_RCFBP, which accumulated poorly (Figure 3-13). The five selected RipY alleles did not induce cell

death in *rrs-y27* plants. However, co-expression of RRS-Y with all the RipY variants, including RipY_RCFBP, restored cell death in *rrs-y27* (Figure 3-12A). QY measurement correlated with the occurrence of cell death (Figure 3-12B). These results indicate a broad specificity for the recognition of RipY by RRS-Y in *N. benthamiana*.

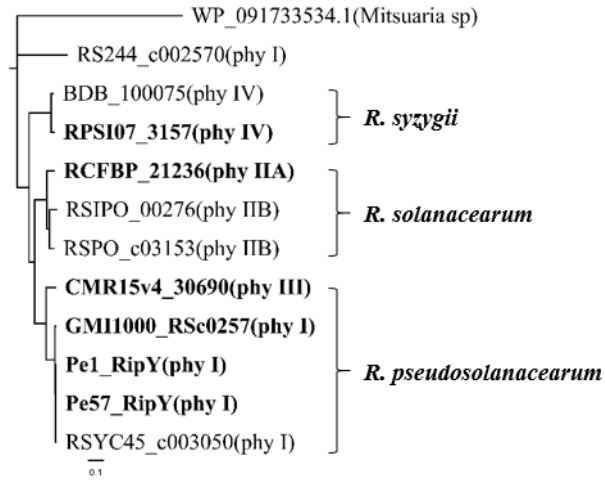

Figure 3-10. RipY phylogenetic tree

Phylogenetic tree of RipY protein sequences from *Ralstonia* spp. RipY protein sequences were obtained from Ralsto T3E database (https://iant.toulouse.inra.fr/bacteria/annotation/site/prj/T3Ev3/). The tree was built using neighbor-joining method and the *Mitsuaria* spp. ankyrin-repeat domain-containing protein as the outgroup. RipY sequences indicated in bold were cloned for transient expression in *N. benthamiana*.

A

Strain	Amino acid identity (%)
Pe57	99.78
GMI1000_RSc0257	99.57
CMR15v4_30690	89.24
RCFBP_21236	76.16
RPSI07_3157	71.76

B

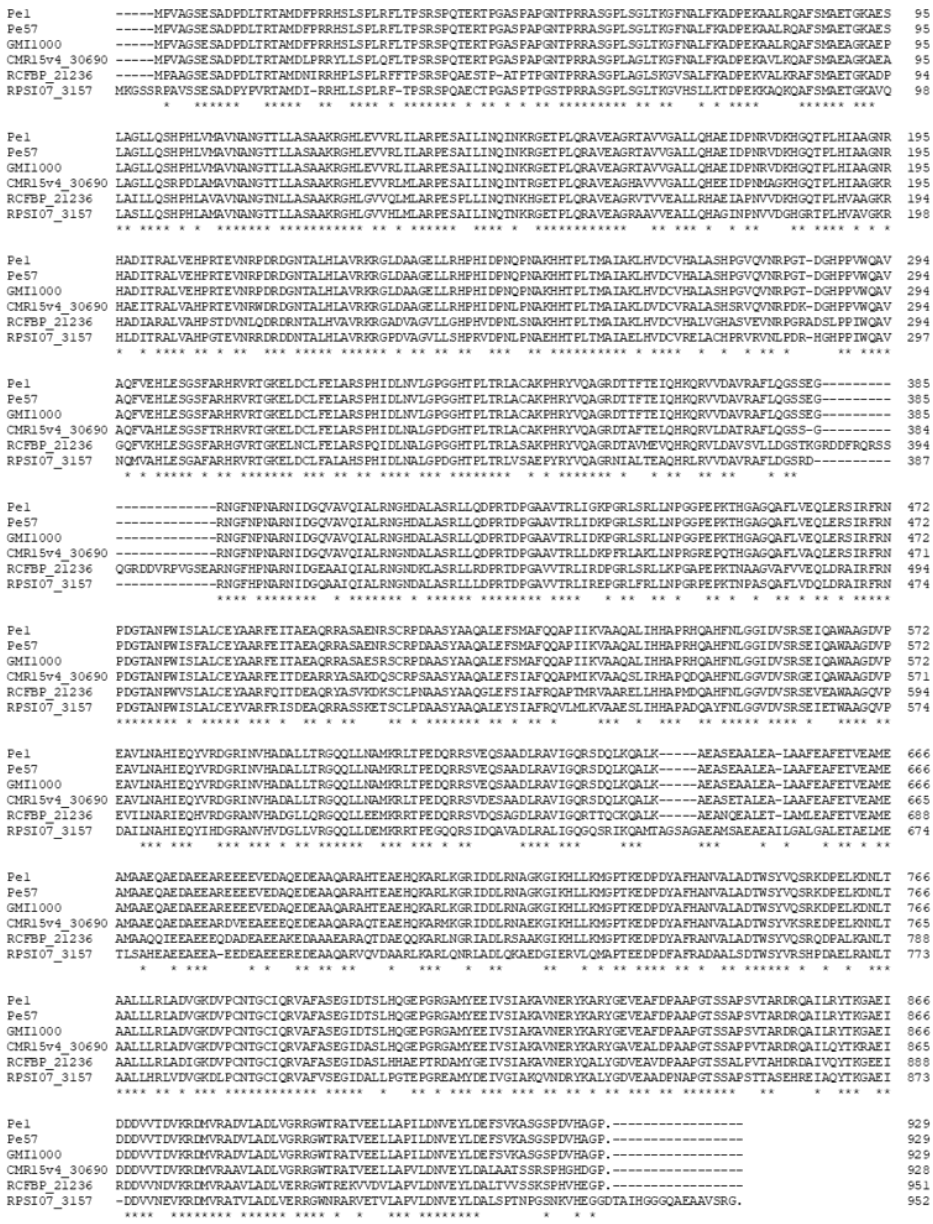

Figure 3-11. RipY natural variation in *Ralstonia* species

(A) Comparison of amino acid sequences of RipY homologs from Korean (Pe1, Pe57) and representative strains of *Ralstonia* species (GMI1000 and CMR15v4 for *R. pseudosolanacearum*; RCFBP_21236 for *R. solanacearum*; RPSI07_3157 for *R. syzygii*). (B) MUSCLE alignment of RipY protein sequences. Asterisks indicate consensus sequences between RipY proteins (dots: stop codon). Numbers on the right indicate the amino acid position in RipY sequences.

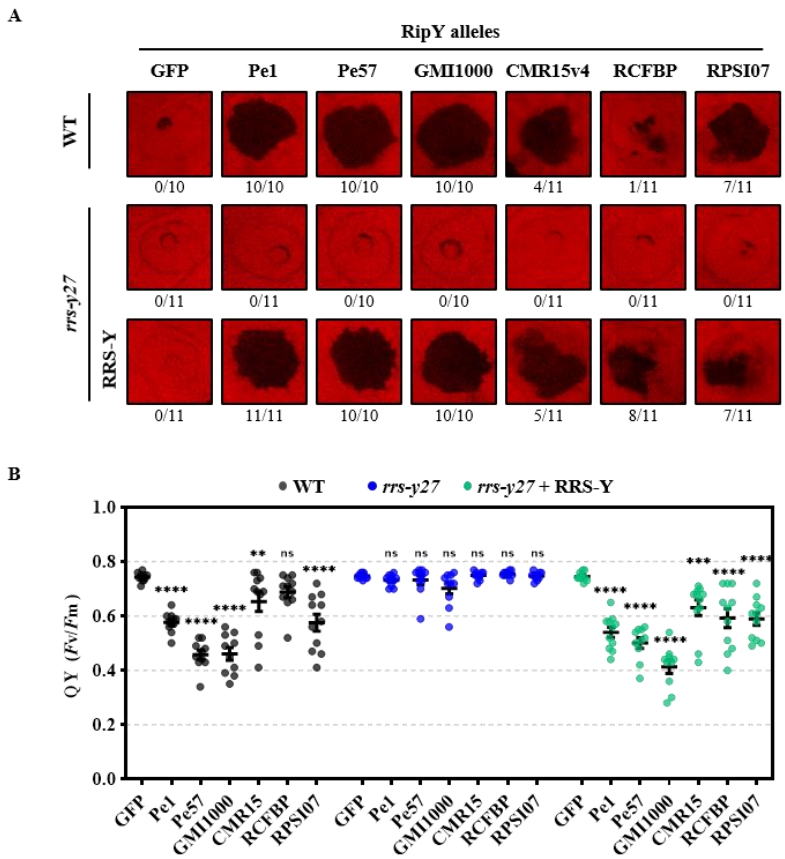

Figure 3-12. RRS-Y perceives RipY natural variants across *Ralstonia* spp.

(A) RipY orthologs induce RRS-Y-dependent cell death. *Agrobacterium* strains carrying GFP, RipY alleles, or RRS-Y (OD_{600}=0.5) were infiltrated in WT or *rrsy27* plants. Pictures were taken at 4 dpi. Numbers indicate patches with cell death out of total infiltrated patches. (B) Quantum yield (QY, *F*v/*F*m) was measured in the infiltrated patches. Individual values from independent experiments are indicated as dots. Data were analyzed with two-way ANOVA followed by Dunnett's multiple comparison test. Asterisks indicate statistically significant differences with GFP (**, *P*<0.01; ***, *P*<0.001; ****, *P*<0.0001; ns, not significant). Bars represent mean ± SEM (n=10-11).

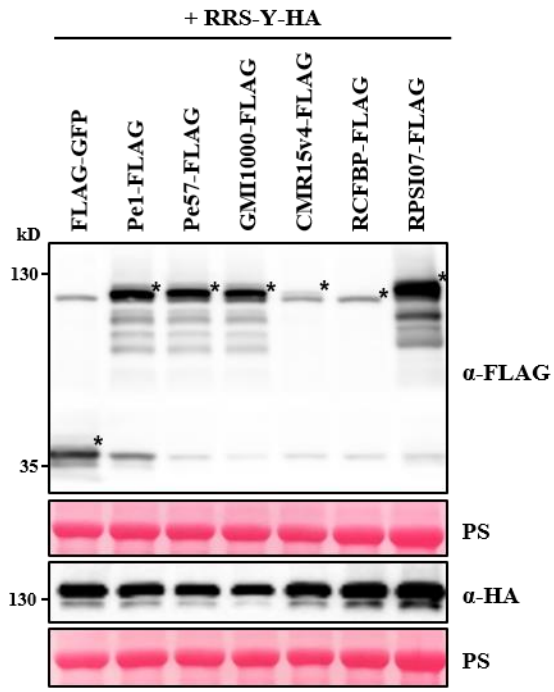

Figure 3-13. Accumulation of RipY homologs in *rrs-y27* plants

Protein accumulation of RipY from Pe1, Pe57, GMI1000, CMR15v4, RCFBP, and RPSI07 in *rrs-y27* plants. *Agrobacterium* strains carrying GFP, RRS-Y, or RipY constructs (OD_{600}=0.5) were infiltrated in *rrsy27* plants. Total protein extracts were immunoblotted with anti-FLAG or anti-HA antibodies. Asterisks indicate the expected protein size. Ponceau red staining (PS) attests equal loading of the samples.

C-terminus of RipY is critical for RRS-Y recognition.

The structure of RipY was predicted using bioinformatics tools AlphaFold2. RipY consists of three domains: an N-terminal putative type III secretion signal (unfolded, 1-76 aa), a region containing at least 10 ankyrin (ANK) repeats (77-556 aa) and an characterized two α-helical bundle region (557-929 aa) distinct from ANK repeat region. The ANK repeat domain plays a role in structural platform motifs mediating the protein-protein interactions, and no enzymatic activity was predicted in RipY protein. It suggests that RRS-Y recognizes RipY through physical interaction.

In order to identify the minimum domain required for the recognition by RRS-Y, four RipY protein truncations lacking the C-terminal region ($RipY_{1-731}$), the C-terminal half ($RipY^{1-435}$), the N-terminal unstructured region ($RipY_{111-929}$), or the N-terminal half ($RipY_{436-929}$), were generated based on the predicted RipY protein structure (Figure 3-14A). While both N-terminal truncations retained the ability to trigger cell death in WT plants and in the *rrs-y27* mutant when co-expressed with RRS-Y, the C-terminal truncations did not (Figure 3-14B and 3-14C). Interestingly, RipY C-terminally truncated variants were still associated with the plasma membrane, conversely to the N-terminal truncations which presented a nucleo-cytoplasmic localization (Figure 3-15). These data indicate that RipY N-terminus (1-111 aa) is required for RipY recruitment at the plasma membrane, and that the C-terminus is essential for RipY recognition by RRS-Y.

Co-immunoprecipitation was conducted to test the possible interaction between RSS-Y and RipY, as both proteins localized in the same cellular compartment (Figure

3-6D). RRS-Y-HA was detected in protein extract enriched for RipY-YFP but not in extract enriched with the GFP control (Figure 3-16). RRS-Y-HA was also present in extract enriched with the different N-terminal and C-terminal RipY truncations, suggesting that RRS-Y and RipY can associate, likely through several ANK-repeats in the central domain of RipY. Together these results suggest that although RRS-Y and RipY may reside in the same protein complex at the plasma membrane, additional factors associated with RipY C-terminus are required for RRS-Y activation.

In chapter 3, RRS-Y was characterized as a functional NLR that recognizes RipY and mediates immunity to *Rps* in *N. benthamiana*. RRS-Y and RipY were both found in the plasma membrane *in planta*. The CC domain of RRS-Y was necessary for mediating the association with plasma membrane, which was critical for immune signaling. Interestingly, RRS-Y was able to recognize RipY alleles from different *Ralstonia* species, and the C-terminus of RipY are crucial for RRS-Y recognition. Hence, the RRS-Y/RipY system provides a novel model for investigating CNL activation in plants.

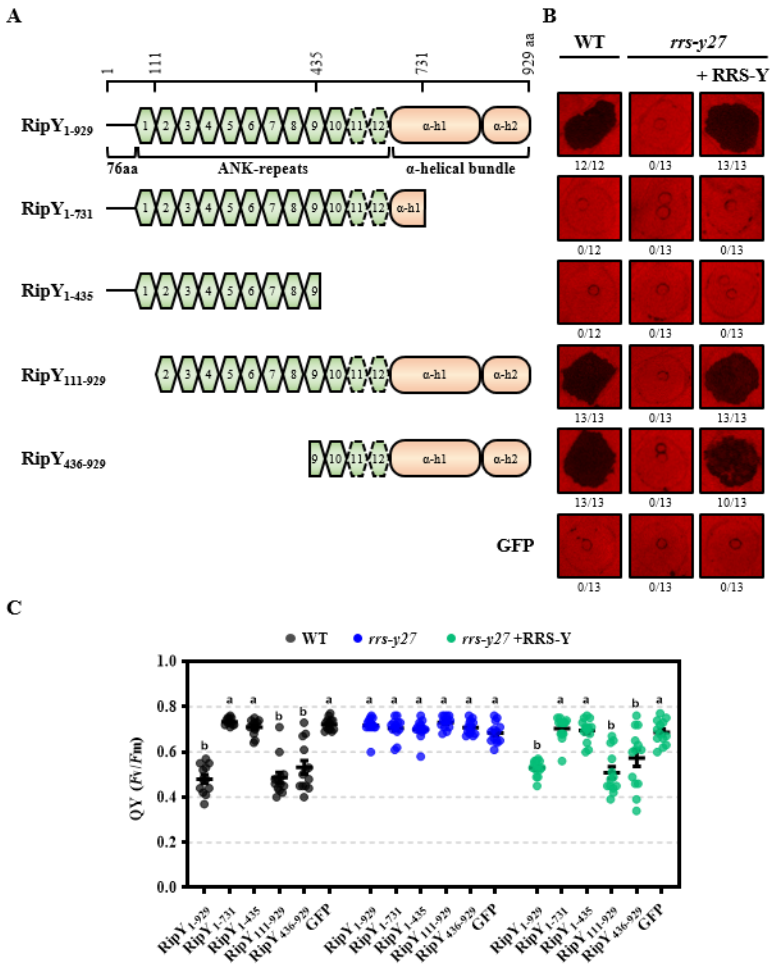

Figure 3-14. C-terminus of RipY is critical for RRS-Y recognition.

(A) Schematic structures of RipY effector and its truncated variants based on the protein structure prediction using AlphaFold2. Predicted ankyrin (ANK) repeats and α-helical bundle are represented as green and yellow, respectively (aa: amino acid). The presence of degenerated ANK11 and ANK12 is indicated by the dashed line. The N-terminal unfolded region (76 aa) was indicated by vertical line. (B) C-terminal truncations of RipY abolish its ability to induce cell death. *Agrobacterium* strains carrying GFP, RipY, truncated RipY mutants, or RRS-Y constructs (OD_{600}=0.5) were infiltrated in WT or *rrsy27* plants. Pictures were taken at 4-6 dpi. Numbers indicate

patches with cell death out of total infiltrated patches. (C) Quantum yield (QY, *F*v/*F*m) was measured in the infiltrated patches. Individual values from independent experiments are indicated as dots. Data were analyzed with two-way ANOVA followed by Dunnett's multiple comparison test. Different letters of each construct indicate significant differences with GFP ($P<0.0001$). Bars represent mean ± SEM (n=12-13).

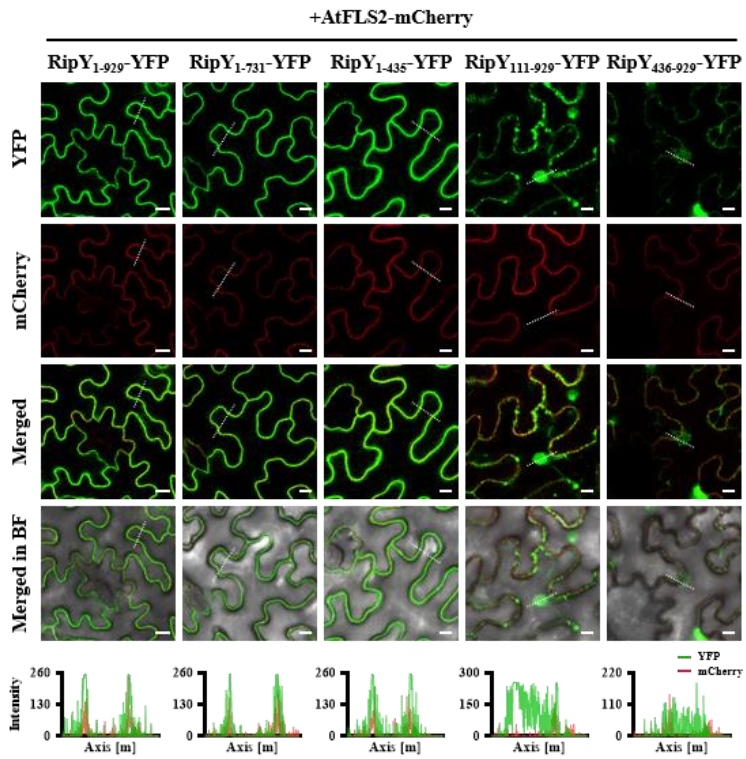

Figure 3-15. N-terminus of RipY associates with the plasma membrane in epidermal cells.

Agrobacterium strains carrying RipY$_{1\text{-}929}$-YFP, RipY$_{1\text{-}731}$-YFP, RipY$_{1\text{-}435}$-YFP, RipY$_{111\text{-}929}$-YFP, or RipY$_{436\text{-}929}$-YFP (OD_{600}=0.4) and *Agrobacterium* strain carrying AtFLS2-mCherry construct (OD_{600}=0.2) were infiltrated in *rrs-y27* plants. Images were acquired by confocal microscopy at 2 dpi. YFP and mCherry fluorescence intensity across the sections indicated by dotted lines are shown under the images. Scale bars indicate 11 μm.

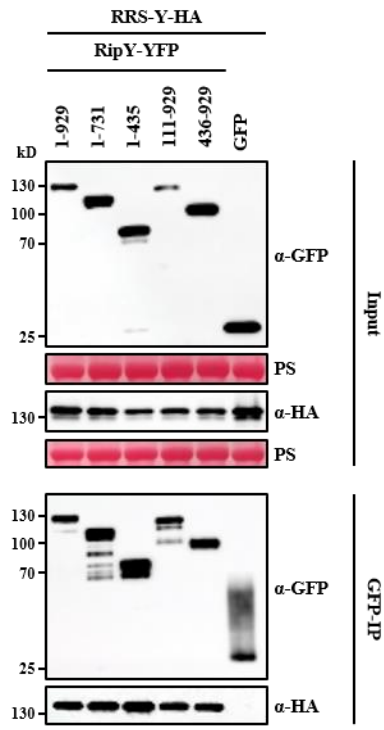

Figure 3-16. Truncated RipY interacts with RRS-Y *in planta.*

Agrobacterium strains carrying GFP, RipY-YFP, truncated RipY variants, or RRS-Y-HA constructs (OD_{600}=0.4) were co-infiltrated in *rrsy27* plants. Total protein extracts (input) were incubated on GFP-trap beads (GFP-IP) followed by immunoblotting with the indicated antibodies. Ponceau red staining (PS) attests the equal loading of the input samples.

DISCUSSION

RRS-Y is required for the restriction of *R. pseudosolanacearum* growth in presence of RipY, which suggests its potential to confer resistance to bacterial wilt in *N. benthamiana* and to serve as a new source of resistance in other Solanaceae species. In tomato, the expression of *Roq1* or *Ptr1* confers resistance against *Rps* strains carrying the corresponding effectors RipB and RipBN, respectively (Thomas et al., 2020; Mazo-Molina et al., 2020). However, resistance to *Rps* remains challenging to assess in natural conditions. *Rps* concomitantly delivers multiple effectors that either trigger or prevent recognition. For example, two *Rps* effectors, RipAY and RipAC, are reported as suppressors of the immune responses triggered by RipE1 in *N. benthamiana* (Sang et al., 2018; Yu et al., 2020). These type of effectors can mask the activation of ETI at multiple levels that is induced by RipE1 recognition by immune system. In addition, some *Rps* strains can evade the detection of immune system by losing the effectors recognized by immune receptors. For example, *Rps* Y45 strain lacks or has pseudogene of most HR-inducing effectors, including RipP1, RipAA, RipE1, and RipY, and can cause bacterial wilt disease in *N. benthamiana* (Poueymiro et al., 2009; Li et al., 2011; Jeon et al., 2020; Sang et al., 2020). It is possible that the loss of these effectors in *Rps* Y45 may be an adaptation circumventing the *N. benthamiana* immune system. Therefore, the use of the RRS-Y resistance gene alone in crops will place a significant selection pressure on *Ralstonia*, highlighting the importance of deploying multiple NLR genes to achieve

a more durable resistance against *Ralstonia*.

Ralstonia strains carrying RipY could be identified across the RSSC, suggesting the benefit this effector could bring during plant infection. In accordance with this broad conservation, RipY has been shown to promote pathogenicity during competition assays in eggplants (Macho et al., 2010). Here, despite significant sequence variation, different RipY homologs were recognized by RRS-Y and triggered *N. benthamiana* immune responses. Considering the broad specificity of RRS-Y and its presence in the same subcellular compartment as RipY, it was hypothesized that RRS-Y activation relies on the direct binding of RipY. Indeed, the two proteins in the same complex were detected by co-immunoprecipitation (Figure 3-16). As no enzymatic activity could be predicted from RipY sequence, it seems unlikely that RRS-Y monitors the status of a guardee host factor. However, the N-terminal truncated RipY proteins ($RipY_{111-929}$-YFP and $RipY_{436-929}$-YFP) were found in different cellular compartments than the plasma membrane-associated RRS-Y, and could still induced cell death, suggesting that additional factor(s) may be involved in RipY-RRS-Y interaction (Figure 3-14). Therefore, the possibility is not excluded that the detected complex contains additional host components required for RRS-Y and RipY interaction.

Several pieces of evidence suggest that RRS-Y may function as singleton in *N. benthamiana*. First, there are no other NLR genes in the genomic location of *RRS-Y* that could potentially pair with *RRS-Y* (https://solgenomics.net/organism/Nicotiana_benthamiana/genome)**.** Second, *RRS-*

Y falls outside the clade of Solanaceae NLRs that requires NRC helpers for their function (Wu et al., 2017; Seong et al., 2020). Indeed, the cell death induced by RipY did not require any helper NLRs, including NRC2/3/4, in *N. benthamiana* (Figure 1-4). Third, RRS-Y belongs to group 10 of Solanaceae NLRs, some NLRs of which are described as autonomous and ancient NLRs (ANLs; Lee et al., 2021). ANLs could be executor NLRs as their CC domains alone are sufficient to induce immune response-related cell death when transiently expressed in *N. benthamiana* (Wróblewski et al., 2018; Adachi et al., 2019b; Lee et al., 2021). Similarly, the CC_{1-152} domain of RRS-Y was able to trigger cell death when transiently expressed *in N. benthamiana*, suggesting that RRS-Y not only detects the RipY effector but also transmits immune signals via its CC domain. Interestingly, RRS-Y localized to the plasma membrane, and its CC domain was responsible for its plasma membrane localization. RRS-Y plasma membrane localization was essential to induce cell death upon RipY recognition in *N. benthamiana*. In contrast, the loss of RRS-Y plasma membrane localization prevented the ability to induce cell death. These characteristics are similar to the typical singleton *Arabidopsis* CNL ZAR1. Smilar to ZAR1, RRS-Y signals the cell death without the requirement of any known genetic components. Additionally, the association of RRS-Y with the plasma membrane through its CC domain is crucial for its cell death activity. Although a deeper characterization of RRS-Y functional domains is necessary to decipher its mode of action, altogether these results suggest that RRS-Y may function as a singleton NLR at plasma membrane similar to ZAR1 or alternatively activate immune responses

through a yet unknown signaling pathway.

Furthermore, the coexpression of RRS-Y proteins fused with different C-terminal epitopes revealed self-association, which was not dependent on the presence of RipY. Similarly, Arabidopsis CNLs ZAR1 and RPM1 have been shown to self-associate. ZAR1 forms self-association in the presence of effector, while RPM1 self-associates in both resting and active status (Ade et al., 2007; El-Kasmi et a., 2017; Wang et al., 2019). The self-association activity of these CNLs relies on the functional P-loop of NB-ARC domain (El-Kasmi et a., 2017; Wang et al., 2019). These results suggest that RRS-Y forms the self-association dependent on functional P-loop like other CNLs. However, it remains to be tested through further experiment.

The N-terminal α1 of ZAR1 CC domain is essential for the cell death activity and the plasma membrane localization of ZAR1. However, it does not affect the self-association and oligomeric complex during ZAR1 activation (Wang et al., 2019). Considering the shared biochemical features with ZAR1 mentioned earlier, it will be interesting to determine whether the *S*-acylated cysteine residues on RRS-Y CC domain responsible for the plasma membrane localization affect the self-association of RRS-Y.

It was observed that the accumulation of *NbHIN1* and *NbHsr203J* transcripts was not fully abolished, and that the expression of defense-related genes was still activated when RipY was transiently expressed in *rrs-y*27 plants (Figure 3-3D). This suggests that RipY may be additionally detected in a RRS-Y independent manner, or that the overexpression of RipY leads to some level of cell toxicity.

RipY is predicted as an ankyrin (ANK) repeats containing effector (Peeters et al., 2013). ANK repeats are motifs commonly found in proteins that participate in protein-protein interactions in nature (Bork, 1993; Mosavi et al., 2004). This reflects that ANK-containing effectors may have a high binding affinity to host proteins and contribute to virulence in host plants. Recent study reported that ANK-containing effector RipBH from UW551 strain, which causes brown rot on potato, functions in virulence by triggering the autophagy-associated cell death to promote tuber rotting (Zheng et al., 2023). RipBH is likely a cysteine protease with self-cleavage activity, but its host target protein remains unknown (Zheng et al., 2023).

In addition, some of ANK containing proteins in animal pathogens play important roles in pathogenesis by mimicking or interfering with the host function. For instance, *Legionella pneumophila* delivers AnkX effector into host cells via a type IV secretion system. AnkX localizes to cytoplasm where it interferes with microtubule-dependent vesicular transport (Cazalet et al., 2004; Pan et al., 2008). The molecular mechanism by which RipY manipulates host cellular processes remains to be uncovered, and these studies will be facilitated in the *rrs-y* null background.

In chapter 3, RRS-Y is a plasma membrane CNL, which recognizes RipY and mediates immunity to *Rps* in *N. benthamiana*. The CC domain of RRS-Y is required for mediating the association with plasma membrane, which is critical for immune signaling. In addition, RRS-Y self-associates in the absence of RipY, suggesting that RRS-Y activation could form the oligomeric resistosome like ZAR1. However, there

is still a lack of evidence for the self-association leading to the formation of high-molecular-weight complexes upon RRS-Y activation. Furthermore, RRS-Y shows broad recognition specificity of natural RipY variants across RSSC. The C-terminal region of RipY is required but not sufficient for RRS-Y recognition. It will be interesting to explore the remaining questions. Does the C-terminus of RipY have any enzymatic activity for pathogenesis in *N. benthamiana*? Does the C-terminal region determine the recognition specificity of RipY natural variants? Or Do the additional factor(s) associate with the interacting RipY and RRS-Y?

REFERENCES

Adachi, H., Derevnina, L., and Kamoun, S. (2019a). NLR singletons, pairs, and networks: evolution, assembly, and regulation of the intracellular immunoreceptor circuitry of plants. *Curr. Opin. Plant Biol.* **50**:121–131.

Adachi, H., Contreras, M.P., Harant, A., Wu, C., Derevnina, L., Sakai, T., Duggan, C., Moratto, E., Bozkurt, T.O., Maqbool, A., et al. (2019b). An N-terminal motif in NLR immune receptors is functionally conserved across distantly related plant species. *eLife* **8**:e49956.

Ade, J., DeYoung, B.J., Golstein, C., and Innes, R.W. (2007). Indirect activation of a plant nucleotide binding site-leucine-rich repeat protein by a bacterial protease. *Proc. Natl. Acad. Sci. U.S.A.* **104**:2531–2536.

Baudin, M., Hassan, J.A., Schreiber, K.J., and Lewis, J.D. (2017). Analysis of the ZAR1 immune complex reveals determinants for immunity and molecular interactions. *Plant Physiol.* **174**:2038–2053.

Bentham, A.R., Zdrzałek, R., De la Concepcion, J.C., and Banfield, M.J. (2018). Uncoiling CNLs: structure/function approaches to understanding CC domain function in plant NLRs. *Plant Cell Physiol.* **59**:2398–2408.

Bernoux, M., Ve, T., Williams, S., Warren, C., Hatters, D., Valkov, E., Zhang, X., Ellis, J.G., Kobe, B., and Dodds, P.N. (2011). Structural and functional analysis of a plant resistance protein TIR domain reveals interfaces for self-association, signaling, and autoregulation. *Cell Host Microbe* **9**:200–211.

Bernoux, M., Burdett, H., Williams, S.J., Zhang, X., Chen, C., Newell, K., Lawrence, G.J., Kobe, B., Ellis, J.G., Anderson, P.A., et al. (2016). Comparative analysis of the flax immune receptors L6 and L7 suggests an equilibrium-based switch activation model. *Plant Cell* **28**:146–159.

Bi, G., Su, M., Li, N., Liang, Y., Dang, S., Xu, J., Hu, M., Wang, J., Zou, M., Deng, Y., et al. (2021). The ZAR1 resistosome is a calcium-permeable

channel triggering plant immune signaling. *Cell* **184**:3528-3541.

Bork, P. (1993). Hundreds of ankyrin-like repeats in functionally diverse proteins: mobile modules that cross phyla horizontally? *Proteins* **17**:363–374.

Cazalet, C., Rusniok, C., Brüggemann, H., Zidane, N., Magnier, A., Ma, L., Tichit, M., Jarraud, S., Bouchier, C., Vandenesch, F., et al. (2004). Evidence in the *Legionella pneumophila* genome for exploitation of host cell functions and high genome plasticity. *Nat. Genet.* **36**:1165–1173.

Cesari, S., Moore, J., Chen, C., Webb, D., Periyannan, S., Mago, R., Bernoux, M., Lagudah, E. S., and Dodds, P.N. (2016). Cytosolic activation of cell death and stem rust resistance by cereal MLA-family CC-NLR proteins. *Proc. Natl. Acad. Sci. U.S.A.* **113**:10204–10209.

Dodds, P.N., and Rathjen, J.P. (2010). Plant immunity: towards an integrated view of plant–pathogen interactions. *Nat. Rev. Genet.* **11**:539–548.

El Kasmi, F., Chung, E.-H., Anderson, R.G., Li, J., Wan, L., Eitas, T.K., Gao, Z., and Dangl, J.L. (2017). Signaling from the plasma-membrane localized plant immune receptor RPM1 requires self-association of the full-length protein. *Proc. Natl. Acad. Sci. U.S.A.* **114**.

Faustin, B., Lartigue, L., Bruey, J.-M., Luciano, F., Sergienko, E., Bailly-Maitre, B., Volkmann, N., Hanein, D., Rouiller, I., and Reed, J.C. (2007). Reconstituted NALP1 inflammasome reveals two-step mechanism of caspase-1 activation. *Mol. Cell* **25**:713–724.

Fegan, M., and Prior, P. (2005). How complex is the *Ralstonia solanacearum* species complex. *Bacterial wilt disease and the Ralstonia solanacearum species complex* **1**:449–461.

Hayward, A.C. (1991). Biology and epidemiology of bacterial wilt caused by *Pseudomonas solanacearum*. *Annu. Rev. Phytopathol.* **29**:65–87.

Hu, M., Qi, J., Bi, G., and Zhou, J.-M. (2020). Bacterial effectors induce oligomerization of immune receptor ZAR1 *in vivo*. *Mol. Plant* **13**:793–801.

Jacob, P., Kim, N.H., Wu, F., El Kasmi, F., Chi, Y., Walton, W.G., Furzer, O.J., Lietzan, A.D., Sunil, S., Kempthorn, K., et al. (2021). Plant "helper"

immune receptors are Ca^{2+} -permeable nonselective cation channels. *Science* **373**:420–425.

Jeon, H., Kim, W., Kim, B., Lee, S., Jayaraman, J., Jung, G., Choi, S., Sohn, K.H., and Segonzac, C. (2020). *Ralstonia solanacearum* type III effectors with predicted nuclear localization signal localize to various cell compartments and modulate immune responses in *Nicotiana* spp. *Plant Pathol. J.* **36**:43–53.

Jones, A.M., Coimbra, S., Fath, A., Sottomayor, M., and Thomas, H. (2001). Programmed cell death assays for plants. *Methods Cell Biol.* **66**:437–451.

Jones, J.D.G., Vance, R.E., and Dangl, J.L. (2016). Intracellular innate immune surveillance devices in plants and animals. *Science* **354**:aaf6395.

Kourelis, J., and van der Hoorn, R.A.L. (2018). Defended to the nines: 25 years of resistance gene cloning identifies nine mechanisms for R protein function. *Plant Cell* **30**:285–299.

Lee, H.-Y., Mang, H., Choi, E., Seo, Y.-E., Kim, M.-S., Oh, S., Kim, S.-B., and Choi, D. (2021). Genome-wide functional analysis of hot pepper immune receptors reveals an autonomous NLR clade in seed plants. *New Phytol.* **229**:532–547.

Li, Z., Wu, S., Bai, X., Liu, Y., Lu, J., Liu, Y., Xiao, B., Lu, X., and Fan, L. (2011). Genome sequence of the tobacco bacterial wilt pathogen *Ralstonia solanacearum*. *J. Bacteriol.* **193**:6088–6089.

Livak, K.J., and Schmittgen, T.D. (2001). Analysis of relative gene expression data using real-time quantitative PCR and the 2(-Delta Delta C(T)) Method. *Methods* **25**:402–408.

Ma, S., Lapin, D., Liu, L., Sun, Y., Song, W., Zhang, X., Logemann, E., Yu, D., Wang, J., Jirschitzka, J., et al. (2020). Direct pathogen-induced assembly of an NLR immune receptor complex to form a holoenzyme. *Science* **370**:eabe3069.

Macho, A.P., Guidot, A., Barberis, P., Beuzón, C.R., and Genin, S. (2010). A competitive index assay identifies several *Ralstonia solanacearum* type III

effector mutant strains with reduced fitness in host plants. *Mol. Plant Microbe Interact.* **23**:1197–1205.

Maekawa, T., Cheng, W., Spiridon, L.N., Töller, A., Lukasik, E., Saijo, Y., Liu, P., Shen, Q.-H., Micluta, M.A., Somssich, I.E., et al. (2011). Coiled-coil domain-dependent homodimerization of intracellular barley immune receptors defines a minimal functional module for triggering cell death. *Cell Host Microbe* **9**:187–199.

Mansfield, J., Genin, S., Magori, S., Citovsky, V., Sriariyanum, M., Ronald, P., Dow, M., Verdier, V., Beer, S.V., Machado, M.A., et al. (2012). Top 10 plant pathogenic bacteria in molecular plant pathology. *Mol. Plant Pathol.* **13**:614–629.

Martin, R., Qi, T., Zhang, H., Liu, F., King, M., Toth, C., Nogales, E., and Staskawicz, B.J. (2020). Structure of the activated ROQ1 resistosome directly recognizing the pathogen effector XopQ. *Science* **370**:eabd9993.

Maruta, N., Burdett, H., Lim, B.Y.J., Hu, X., Desa, S., Manik, M.K., and Kobe, B. (2022). Structural basis of NLR activation and innate immune signalling in plants. *Immunogenetics* **74**:5–26.

Mazo-Molina, C., Mainiero, S., Haefner, B.J., Bednarek, R., Zhang, J., Feder, A., Shi, K., Strickler, S.R., and Martin, G.B. (2020). Ptr1 evolved convergently with RPS2 and Mr5 to mediate recognition of AvrRpt2 in diverse solanaceous species. *Plant J.* **103**:1433–1445.

Mosavi, L.K., Cammett, T.J., Desrosiers, D.C., and Peng, Z. (2004). The ankyrin repeat as molecular architecture for protein recognition. *Protein Sci.* **13**:1435–1448.

Nekrasov, V., Staskawicz, B.J., Weigel, D., Jones, J., and Kamoun, S. (2013). Targeted mutagenesis in the model plant *Nicotiana benthamiana* using Cas9 RNA-guided endonuclease. *Nat. biotechnol.* **31**:691–3.

Ngou, B.P.M., Jones, J.D.G., and Ding, P. (2022). Plant immune networks. *Trends Plant Sci.* **27**:255–273.

Pan, X., Lührmann, A., Satoh, A., Laskowski-Arce, M.A., and Roy, C.R. (2008).

Ankyrin repeat proteins comprise a diverse family of bacterial type IV effectors. *Science* **320**:1651–1654.

Parry, G., Patron, N., Bastow, R., and Matthewman, C. (2016). Meeting report: GARNet/OpenPlant CRISPR-Cas workshop. *Plant Methods* **12**:6.

Peeters, N., Carrère, S., Anisimova, M., Plener, L., Cazalé, A.-C., and Genin, S. (2013). Repertoire, unified nomenclature and evolution of the type III effector gene set in the *Ralstonia solanacearum* species complex. *BMC Genom.* **14**:859.

Poueymiro, M., Cunnac, S., Barberis, P., Deslandes, L., Peeters, N., Cazale-Noel, A.-C., Boucher, C., and Genin, S. (2009). Two type III secretion system effectors from *Ralstonia solanacearum* GMI1000 determine host-range specificity on tobacco. *Mol. Plant Microbe Interact.* **22**:538–550.

Prior, P., Ailloud, F., Dalsing, B.L., Remenant, B., Sanchez, B., and Allen, C. (2016). Genomic and proteomic evidence supporting the division of the plant pathogen *Ralstonia solanacearum* into three species. *BMC Genom.* **17**:90.

Prokchorchik, M., Pandey, A., Moon, H., Kim, W., Jeon, H., Jung, G., Jayaraman, J., Poole, S., Segonzac, C., Sohn, K.H., et al. (2020). Host adaptation and microbial competition drive *Ralstonia solanacearum* phylotype I evolution in the Republic of Korea. *Microb. Genom.* **6**:mgen000461

Qi, D., DeYoung, B.J., and Innes, R.W. (2012). Structure-function analysis of the coiled-coil and leucine-rich repeat domains of the RPS5 disease resistance protein. *Plant Physiol.* **158**:1819–1832.

Robatzek, S., Chinchilla, D., and Boller, T. (2006). Ligand-induced endocytosis of the pattern recognition receptor FLS2 in *Arabidopsis*. *Genes Dev.* **20**:537–542.

Sabbagh, C.R.R., Carrere, S., Lonjon, F., Vailleau, F., Macho, A.P., Genin, S., and Peeters, N. (2019). Pangenomic type III effector database of the plant pathogenic *Ralstonia* spp. *PeerJ* **7**:e7346.

Sang, Y., Wang, Y., Ni, H., Cazalé, A.-C., She, Y.-M., Peeters, N., and Macho, A.P. (2018). The *Ralstonia solanacearum* type III effector RipAY targets plant redox regulators to suppress immune responses. *Mol. Plant Pathol.* **19**:129–142.

Sang, Y., Yu, W., Zhuang, H., Wei, Y., Derevnina, L., Yu, G., Luo, J., and Macho, A.P. (2020). Intra-strain elicitation and suppression of plant immunity by *Ralstonia solanacearum* type-III effectors in *Nicotiana benthamiana*. *Plant Commun.* **1**:100025.

Schultink, A., Qi, T., Lee, A., Steinbrenner, A.D., and Staskawicz, B.J. (2017). Roq1 mediates recognition of the *Xanthomonas* and *Pseudomonas* effector proteins XopQ and HopQ1. *Plant J.* **92**:787–795.

Seong, K., Seo, E., Witek, K., Li, M., and Staskawicz, B.J. (2020). Evolution of NLR resistance genes with noncanonical N-terminal domains in wild tomato species. *New Phytol.* **227**:1530–1543.

Takken, F.L., Albrecht, M., and Tameling, W.I. (2006). Resistance proteins: molecular switches of plant defence. *Curr. Opin. Plant Biol.* **9**:383–390.

Tameling, W.I.L., Vossen, J.H., Albrecht, M., Lengauer, T., Berden, J.A., Haring, M.A., Cornelissen, B.J.C., and Takken, F.L.W. (2006). Mutations in the NB-ARC domain of I-2 that impair ATP hydrolysis cause autoactivation. *Plant Physiol.* **140**:1233–1245.

Thomas, N.C., Hendrich, C.G., Gill, U.S., Allen, C., Hutton, S.F., and Schultink, A. (2020). The immune receptor Roq1 confers resistance to the bacterial pathogens *Xanthomonas*, *Pseudomonas syringae*, and *Ralstonia* in tomato. *Front. Plant Sci.* **11**:463.

van Ooijen, G., Mayr, G., Kasiem, M.M.A., Albrecht, M., Cornelissen, B.J.C., and Takken, F.L.W. (2008). Structure–function analysis of the NB-ARC domain of plant disease resistance proteins. *J. Exp. Bot.* **59**:1383–1397.

Walker, J.E., Saraste, M., Runswick, M.J., and Gay, N.J. (1982). Distantly related sequences in the alpha- and beta-subunits of ATP synthase, myosin, kinases and other ATP-requiring enzymes and a common nucleotide binding fold.

EMBO J. **1**:945–951.

Wang, J., Hu, M., Wang, J., Qi, J., Han, Z., Wang, G., Qi, Y., Wang, H.-W., Zhou, J.-M., and Chai, J. (2019). Reconstitution and structure of a plant NLR resistosome conferring immunity. *Science* **364**:eaav5870.

Wang, J., Chen, T., Han, M., Qian, L., Li, J., Wu, M., Han, T., Cao, J., Nagalakshmi, U., Rathjen, J.P., et al. (2020). Plant NLR immune receptor Tm-2^2 activation requires NB-ARC domain-mediated self-association of CC domain. *PLoS Pathog.* **16**:e1008475.

Weber, E., Engler, C., Gruetzner, R., Werner, S., and Marillonnet, S. (2011). A modular cloning system for standardized assembly of multigene constructs. *PLoS One* **6**:e16765.

Wróblewski, T., Spiridon, L., Martin, E.C., Petrescu, A.-J., Cavanaugh, K., Truco, M.J., Xu, H., Gozdowski, D., Pawłowski, K., Michelmore, R.W., et al. (2018). Genome-wide functional analyses of plant coiled–coil NLR-type pathogen receptors reveal essential roles of their N-terminal domain in oligomerization, networking, and immunity. *PLoS Biol.* **16**:e2005821.

Wu, C.-H., Abd-El-Haliem, A., Bozkurt, T.O., Belhaj, K., Terauchi, R., Vossen, J.H., and Kamoun, S. (2017). NLR network mediates immunity to diverse plant pathogens. *Proc. Natl. Acad. Sci. U.S.A.* **114**:8113–8118.

Xie, Y., Zheng, Y., Li, H., Luo, X., He, Z., Cao, S., Shi, Y., Zhao, Q., Xue, Y., Zuo, Z., et al. (2016). GPS-Lipid: a robust tool for the prediction of multiple lipid modification sites. *Sci. Rep.* **6**:28249.

Yu, W., and Macho, A. (2021). A fast and easy method to study *Ralstonia solanacearum* virulence upon transient gene expression or gene silencing in *Nicotiana benthamiana* leaves. *Bio Protoc.* **11**:e4116.

Yu, G., Xian, L., Xue, H., Yu, W., Rufian, J.S., Sang, Y., Morcillo, R.J.L., Wang, Y., and Macho, A.P. (2020). A bacterial effector protein prevents MAPK-mediated phosphorylation of SGT1 to suppress plant immunity. *PLoS Pathog.* **16**:e1008933.

Zheng, X., Huang, M., Tan, X., Wang, B., Li, Y., Xue, H., Cheng, D., Qiu, H., Li,

W., Song, B., et al. (2023). A toxic ankyrin cysteine protease effector RipBH of brown rot triggered autophagy-associated cell death. *BioRxiv* https://doi.org/10.1101/2023.03.08.531657.

ABSTRACT IN KOREAN

풋마름병균 (*Ralstonia pseudosolanacearum*) 은 경제적으로 중요한 가지과 작물인 감자, 토마토, 고추를 비롯하여 많은 작물에 풋마름병을 유발하여 생산에 심각한 영향을 미친다. 풋마름병에 대해 저항성 반응을 유도할 수 있는 소수의 식물면역수용체가 발견되었지만, 풋마름병균의 유전적 다양성으로 인해 안정적인 지속가능저항성 (Durable resistance) 을 가진 작물의 육종은 여전히 어려운 과제이다. 이를 위해서는 다양한 유전자원에서 식물 면역수용체를 발현시킬 수 있는 여러 저항성 유전자를 발굴하여 집적하는 것이 필요하다. 식물의 선천적 면역수용체 (Innate immune receptor) 중 하나인 Nucleotide-binding leucine-rich repeat receptor (NLR) 는 병원균이 병원성 증진을 위해 식물체 내의 III 형 분비 장치 (Type III secretion system, T3SS) 를 이용하여 숙주 세포에 직접 주입되는 세균단백질인 이펙터 (Type III effector, T3E) 를 인식할 수 있다. NLR의 활성화는 일련의 세포신호전달을 통해 식물의 면역반응을 유도한다. 그 중 강력한 면역반응인 과민성반응 (Hypersensitive response, HR) 은 병원균이 침입한 세포에 세포사멸을 일으켜 병원균의 증식을 억제시킨다. 따라서 병 저항성에 핵심 역할을 하는 NLR을 발현하는 유전자들은 풋마름병 저항성작물을 육종하는데 유용한 자원이다. 담배 근연종 *Nicotiana benthaiana* (*Nb*) 은 다양한 기

능유전체학 도구를 활용할 수 있는 가지과 모델 식물이며, 수 백여개의 NLR을 암호화하는 유전자를 가지고 있다고 알려져 있어 가지과 병 저항성 육종에 유용한 식물 유전자원으로 활용할 수 있다. 본 논문은 *N. benthamiana*에 풋마름병균의 이펙터를 인식하여 면역반응을 활성화 하는 NLR을 탐색하고, 더 나아가 면역반응 활성화 기작에 대한 연구를 진행하였다.

제 1 장에서는 *N. benthamiana*에서 풋마름병균이 분비하는 이펙터를 인식할 수 있는 NLR를 탐색하였다. 풋마름병균의 이펙터 단백질인 RipE1 (*Ralstonia*-injected protein RipE1) 과 RipY는 *N. benthamiana*에서 발현시켰을 때, 강력한 세포사멸 반응과 더불어 과민성반응 마커 유전자 발현의 활성화 및 병원성 세균 증식의 억제와 같은 면역반응을 활성시키는 비병원성 이펙터임을 확인하였다. 더 나아가 바이러스 매개 유전자 침묵 기법 (Virus-induced gene silencing, VIGS)을 통해 현재까지 보고된 면역신호전달인자들이 RipE1과 RipY에 의해 유도된 면역반응에 관여하지 않음을 관찰하였다. 최근에 개발된 NbNLR-VIGS 라이브러리를 활용하여 345개의 *N. benthamiana* NLR에 대한 스크리닝을 진행하였다. 이를 통해 *N. benthamiana*에서 RipE1과 RipY를 인식하는 NLR인 NbPtr1 (토마토 근연종에서 발견된 PSEUDOMONAS TOMATO RACE 1의 오솔로그) 과 RESISTANCE TO RALSTONIA SOLANACEARUM RIPY (RRS-Y) 을 구명하였다.

제 2 장에서는 NbPtr1의 RipE1인식을 통한 풋마름병균에 대한 면역반응이 숙주세포의 세포막에서 활성이 된다는 것을 밝혔다. 유전적 상보 (Genetic complementation) 실험을 통해 NbPtr1이 *N. benthamiana*에서 RipE1을 인식하는데 필수적인 역할을 한다는 것을 증명하였다. 또한, RipE1이 발현된 식물 조직에서는 NbPtr1 매개 면역에 의해 병원성 풋마름병균의 증식이 억제되는 것을 관찰하였다. 이는 NbPtr1이 풋마름병에 대한 저항성에 기여한다는 것을 보여준다. 공초점 현미경을 통해 형광단백질이 함께 발현되는 RipE1이 식물 세포의 세포막에 존재한다는 것을 관찰하였고, RipE1의 돌연변이체를 이용하여 RipE1의 세포막의 위치가 NbPtr1인식에 필요하다는 것을 확인하였다. 최근 연구에 의하면 RipE1은 단백질분해효소의 기능을 가지는 것으로 보고되어, 면역블롯분석을 통해 RipE1이 식물 세포내의 단백질의 발현에 영향을 미치는지 분석하였다. 흥미롭게도 RipE1은 세포막에 존재하는 단백질인 RPM1-INTERACTING PROTEIN 4 (RIN4) 의 단백질의 발현에 영향을 미치는 것을 관찰하였다. 따라서, NbPtr1은 RipE1의 RIN4 단백질에 대한 생화학적 변화를 인식하여 면역반응이 유도될 수 있다는 것을 시사한다.

제 3 장에서는 새롭게 발견된 NLR인 RRS-Y의 RipY인식을 통해 유도된 풋마름병균에 대한 면역반응분석과 RRS-Y의 특성 및 활성화 기작에 대해 연구를 진행하였다. 본 연구를 통해 확보한 *RRS-Y* 유전자

녹아웃 식물체에서 RRS-Y는 *N. benthamiana*에서 RipY를 인식하는데 직접적으로 관여한다는 것과, 풋마름병균에 대해 면역반응을 유도한다는 것을 확인하였다. RRS-Y는 ATP결합에 의해 활성화가 조절되는 기능적 NLR로 RipY와 동일하게 식물 세포 내 세포막에 위치했다. RRS-Y을 구성하는 도메인 중에 아미노기 말단에 존재하는 코일-코일 (Coiled-coil, CC) 도메인은 면역신호전달과 RRS-Y의 세포 내 세포막 위치의 연관성 조절에 중요한 역할을 하고 있었고, 공동면역침강법을 통해 RRS-Y는 RipY의 존재와 상관없이 독립적으로 식물 세포에서 self-association 을 형성할 수 있었다. 그리고 RRS-Y는 넓은 범위의 RipY인식 특이성을 보였는데, 풋마름병균의 다른 종인 *R. solanacearum*와 *R. syzygii*에 존재하며 단백질 서열에 다형성을 보이는 다양한 RipY를 인식할 수 있었다. 또한, RipY의 카르복실기 말단이 RRS-Y에 의해 인식되는 중요 부위임을 확인하였다. 이를 통해 본 논문에서 새롭게 발견된 RRS-Y와 RipY 상호작용은 식물의 면역시스템에서 NLR의 활성화에 대한 기본원리를 탐구하는데 새로운 모델을 제시할 수 있다.

본 논문을 통해 *N. benthamiana*에서 풋마름병에 대한 면역반응을 유도하는 두 개의 NLR을 발굴함으로서, 가지과 작물의 풋마름병 지속가능저항성의 유전적 자원으로의 활용 가능성을 확인할 수 있었다. 또한, 새로운 NLR-effector pair 시스템을 제공함으로서 NLR 저항성 단백질에 의한 면역 활성화 기작을 분자적인 측면에서 심도 있게 이해하는데

기여할 것으로 기대한다.